

AMERICAN UNIVERSITY OF BEIRUT

Collective Behaviour of Active Matter:  
Transition between States and Cone of Vision  
Effects

by

Amara Adham Al-Sayegh

A Dissertation

submitted in partial fulfillment of the requirements  
for the degree of Doctor of Philosophy  
to the Department of Physics  
of the Faculty of Arts and Sciences  
at the American University of Beirut

Beirut, Lebanon  
May 2016

# AMERICAN UNIVERSITY OF BEIRUT

## Collective Behaviour of Active Matter: Transition between States and Cone of Vision Effects

by

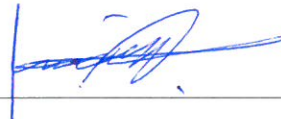
Amara Adham Al-Sayegh

Approved by:

---

Dr. Jihad Touma, Professor  
Physics Department

Advisor



---

Dr. Leonid Klushin, Professor  
Physics Department

Co-advisor



---

Dr. Khalil Bitar, Professor  
Physics Department

Chair of Committee



---

Dr. Kolbjorn Tunstrom, Assistant Professor  
Complex System Group, Chalmers University of Technology

Member of Committee



---

Dr. Sara Najem, Post-Doctoral Research Associate  
Graduate Aerospace Laboratories, California Institute of Technology

Member of Committee



Date of thesis defense: May 6, 2016

# AMERICAN UNIVERSITY OF BEIRUT

## THESIS, DISSERTATION, PROJECT RELEASE FORM

Student Name: Al Sayegh Amara Adham  
Last First Middle

Master's Thesis       Master's Project       Doctoral Dissertation

I authorize the American University of Beirut to: (a) reproduce hard or electronic copies of my thesis, dissertation, or project; (b) include such copies in the archives and digital repositories of the University; and (c) make freely available such copies to third parties for research or educational purposes.

I authorize the American University of Beirut, **three years after the date of submitting my thesis, dissertation, or project**, to: (a) reproduce hard or electronic copies of it; (b) include such copies in the archives and digital repositories of the University; and (c) make freely available such copies to third parties for research or educational purposes.

Amara Sayegh May, 10, 2016  
Signature Date

# Acknowledgements

Firstly, I would like to express my sincere gratitude to my co-advisors Prof. Leonid Klushin and Prof. Jihad Touma for their continuous support throughout my Ph.D study. Prof. Klushin with his patience, immense knowledge and realistic approach to problems managed to put me back on track whenever I'm overwhelmed with the difficulties. Prof. Touma, on the other hand, challenged me, taught me how to be curious and passionate about what I do, and showed me an inspiring example of a scientist who's not limited to his science but have something useful to say about life, society, politics, culture, religion and much more. I cannot imagine having a better combination of mentors for my Ph.D study and who ended up as mentors for life.

Besides my co-advisors, I would like to thank the rest of my thesis committee: Prof. Khalil Bitar, Prof. Kolbjorn Tunstrom, and Dr. Sara Najem, for their insightful comments and encouragement.

My sincere thanks also goes to all professors at the physics department especially Prof. Ali Chamseddine, Prof. Malek Tabbal and Prof. Samih Isber for their continuous support through out my undergraduate, masters and Ph.D studies at AUB.

Speaking of my long stay at AUB, I can't but thank Ms. Jumana Abi Fallah, the dedicated administrative assistant at physics department, not only for the technical support she provided, reminding me of deadlines, procedures and forms, but also for being a good listener and a friend.

I thank my fellow friends at the physics department for the stimulating discussions, for the sleepless nights we were working together before deadlines, and for all the fun we have had. I will not have enough space here to name all the friends I made in the department, but I'd like to mention Sara Abu Diab, Lama Tannoury, Antranik Selfian and Rodrigue Badr for being around in the last year.

Last but not the least, I would like to thank my family: Adham, Hoda, Sulieman and Osama for their unconditional love and spiritual support all over the stages of my life.

# An Abstract of the Dissertation of

Amara Adham Al Sayegh for Doctor of Philosophy  
Major: Physics

Title: Collective Behaviour of Active Matter:  
Transition between States and Cone of Vision Effects

Examples of collective behavior are everywhere around us, from birds flocking, fish schooling, fireflies synchronizing, ants colonizing, crowds flowing, to individuals self-organizing into neighborhoods in cities. How does this all come about? Are these forms of collective behavior governed by unifying principles, and can one apprehend them through mathematical models, with insights, physical? I exhibit serious attempts at dealing with such similar questions, the way a physicist, armed with computational resources would. Working with agent-based models, I studied two dimensional swarms, explored emergent self-organized states at low energies, their stability, their basins of attraction and the transitions between them. My experiments identify key ingredients for any future first principles theory of such behavior. Then, I shift settings and take a deep look at leader-follower dynamics, with cone-of-vision type coupling. My work here is motivated by studies of shoals of fish in tanks. But rather than focusing on leadership behavior (which is fashionable in this field), I identify leader-avoiding states, which have as much to say about conditions of effective leadership, as they do about robots in formation, and/or paradoxical regimes of human behavior in confinement.

# Contents

<b>Acknowledgements</b>	<b>v</b>
<b>Abstract</b>	<b>vi</b>
<b>1 Introduction</b>	<b>1</b>
<b>2 Low-energy States in Swarms of Self-Propelled Particles</b>	<b>10</b>
2.1 Introduction . . . . .	10
2.2 The Model . . . . .	13
2.3 Bound States and Basins of Attraction . . . . .	16
2.3.1 Coherent Flock . . . . .	17
2.3.2 Rigid Rotation . . . . .	18
2.3.3 Random Droplet . . . . .	18
2.3.4 Basins of attraction and transient state lifetimes . . . . .	20
2.3.5 Linear Stability . . . . .	23
2.4 Transition mechanisms . . . . .	26
2.4.1 Case 1: Slow Gradual Transition . . . . .	28
2.4.2 Case 2: Sharp Transition . . . . .	29
2.4.3 Potential of mean force . . . . .	30
2.5 Summary and Discussion . . . . .	36
<b>3 Leader-Follower Dynamics in a Confined Space</b>	<b>39</b>
3.1 Background . . . . .	39
3.2 The Model . . . . .	44
3.3 The Attractors . . . . .	46
3.3.1 Vertical Attractor . . . . .	47
3.3.2 Eight-shaped Attractor . . . . .	50
3.3.3 Head-Phone Attractor . . . . .	55
3.3.4 Periodic Solutions . . . . .	57
3.3.5 Phase diagram . . . . .	61
3.4 Robustness To Model Variations . . . . .	62
3.4.1 Initial Conditions/Model Parameters . . . . .	63
3.4.2 The Leader as a group . . . . .	64

3.4.3	Leader along the rim . . . . .	64
3.4.4	Sharp Follower Response . . . . .	68
3.5	Summary and Discussion . . . . .	70
<b>4</b>	<b>Future Work</b>	<b>79</b>
	<b>Appendices</b>	<b>82</b>
<b>A</b>	<b>Non-Dimensionalizing the equation of motion of the Linear model</b>	<b>83</b>
<b>B</b>	<b>Linear stability analysis of the coherent flock</b>	<b>86</b>
<b>C</b>	<b>Linear stability of the rigid rotation state</b>	<b>90</b>
<b>D</b>	<b>Derivation of mean-field equation</b>	<b>93</b>
<b>E</b>	<b>Details of the Computational Scheme of Leader-Follower Model</b>	<b>97</b>

# List of Figures

2.1	<b>Coherent flock.</b> (a)Velocity vectors superimposed on the positions of particles in a snapshot;(b) lattice positions in a snapshot. ( $\gamma_1 = 40$ ) . . . . .	17
2.2	<b>Rigid rotation.</b> (a)Configuration with velocity vectors superimposed on positions; (b) distribution of order parameter M which has a non-zero width rather than being peaked, indicating that the rigid rotation state is not a perfect state;(c) radial density of particles showing six rings;(d) distribution for the fluctuation-averaged velocity as a function of radius in the center of mass frame as a function of radius, showing a linear dependence for the first three rings after which the velocity saturates at the terminal velocity.( $\gamma_1 = 25$ ) . . . . .	19
2.3	<b>Random droplet.</b> (a)Configuration with velocity vectors superimposed over positions; (b) distribution of order parameter P fitted with a Rayleigh distribution (Maxwell speed distribution in 2d); (c) distribution of parameter M fitted with a Gaussian with zero mean;(d) superimposed single particle trajectories; the particles spend most of the time close to rings that pass through the lattice points of the Lagrangian configuration.( $\gamma_1 = 80$ ). . . . .	21
2.4	<b>Probability of obtaining each of the three organized states as a function of <math>\gamma_1</math>.</b> (a)The linear model; (b)the cubic model. The length of the trajectory is $t_{final} = 100t_{kinetic}$ . Statistics is based on 50 runs with different random initial conditions at fixed control parameters. . . . .	22
2.5	<b>First passage times for transition from a random initial condition to a final steady state vs. the velocity relaxation rate <math>\gamma_1</math>.</b> (a)Mean of first passage time for the linear model with the number of particles $N = 50$ ; (b)the maximum, the minimum,and the mean values of first passage times obtained from a set of 50 independent runs for the cubic model are shown by dashed green, dashed-dotted red and solid blue curves, respectively. The inset displays the same data on a log scale indicating relative broadening of the first passage time distribution with the increase in $\gamma_1$ . . . . .	24



2.6	<b>Flock stability.</b> (a) Largest non-zero eigenvalue versus $\gamma_1$ for the coherent flock state; (b) all 400 eigenvalues vs $\gamma_1$ for the stability matrix of a coherent flock of 100 particles. . . . .	25
2.7	<b>Largest eigenvalue versus <math>\gamma_1</math> for the rigid rotation state.</b> The relationship is linear and the graph passes through the origin; i.e. for arbitrarily small $\gamma_1$ the largest positive eigenvalue which represents the linear growth of perturbations of the perfect rigid rotation becomes very small. . . . .	26
2.8	<b>Growth of perturbations of the perfect rigid rotation state for <math>\gamma_1 = 0.08</math> and <math>\gamma_2 = 83</math>.</b> (a) Speed of a single particle as a function of time; (b) radial position of a single particle as a function of time. Linear instabilities grow exponentially, but are then stabilized by non-linear terms. . . . .	27
2.9	<b>Slow gradual transition to flock.</b> (a) Typical single particle trajectory with each color representing a part of the trajectory and the order in time is: cyan,red, green, magenta and blue; (b)time evolution of the flocking order parameter P as the swarm transits gradually from a random initial condition to a coherent flock. ( $\gamma_1 = 9$ ) . . . . .	28
2.10	<b>Slow gradual transition to rigid rotation.</b> (a)Typical single particle trajectory, see Fig. 2.9 for the color scheme; (b) time evolution of the order parameter M as the swarm transits gradually from a random initial condition to a rigid rotation.( $\gamma_1 = 7$ ) . . . . .	29
2.11	<b>Mean first passage time to an organized steady state vs. the velocity relaxation time <math>t_{rel} = \frac{1}{\gamma_1}</math>.</b> The range displayed corresponds to $\gamma_1$ between 2 and 20. . . . .	30
2.12	<b>Sharp transition to flock.</b> (a)Typical single particle trajectory for the long-lived random state with each color representing a part of the trajectory, see Fig. 2.9 for color scheme; (b) time evolution of the flocking order parameter P as the swarm transits from a random initial condition to a coherent flock. ( $\gamma_1 = 70$ ) . . . . .	31
2.13	<b>Sharp Transition to rigid rotation.</b> (a) Typical single particle trajectory for the long-lived random state,see Fig. 2.9 for the color scheme; (b)time evolution of the order parameter M as the swarm transits from a random initial condition to a rigid rotation. ( $\gamma_1 = 75$ ) . . . . .	31
2.14	<b>Average value of the order parameter s for the 3 organized states as a function of <math>\gamma_1</math>.</b> . . . . .	33

2.15 **Instantaneous Forces and Potentials of mean force as a function of  $s$  at  $\gamma_1 = 30$  and  $\gamma_1 = 75$ .** Panels (a) and (c) give the instantaneous forces as a function of  $s$  for  $\gamma_1 = 30$  and  $\gamma_1 = 75$  respectively. The noise is dependent on  $s$ , it is zero at  $s = 0$  (coherent flock state) and very small around  $s = 0.9$  (rigid rotation state). Panels (b) and (d) give the corresponding potentials of mean forces which have two distinct minima characterizing the coherent flock ( $s = 0$ ) and the rigid rotation state ( $s = 0.9$  for  $\gamma_1 = 30$  and  $s = 0.99$  for  $\gamma_1 = 75$ ) and a flat maxima characterizing the random droplet state ( $s = 0.63$  for  $\gamma_1 = 30$  and  $s = 0.77$  for  $\gamma_1 = 75$ ). . . . . 34

3.1 **Model Description.** The position, orientation, and velocity of fish  $i$  are given by  $\vec{r}_i$ ,  $\theta_i$ , and  $\vec{v}_i$  respectively.  $\phi_i$  is the angle between  $\vec{v}_i$  and the  $x$ -axis, while the relative position between fish  $i$  and  $j$  is given by  $d_{ij}$ . 44

3.2 **Definition of COV.** Two symmetric rays are cast from the position of the  $i$ -th fish; its *COV* is defined as the angle between the ray and its velocity vector on either sides; fish  $j$  is perceived while  $k$  is not. . . . . 44

3.3 **Basins of attraction of steady states as a function of the cone of vision (COV).** For small and large COV the dominant state is the vertical attractor. For intermediate values of COV the head-phone and the eight-shaped attractors are obtained with different probabilities as a function of COV. . . . . 47

3.4 **Vertical Attractor.** (a) For small *COV*, the Follower hits the boundary at different angles before getting attracted to the Leader, *COV* = 0.4; (b) for Large *COV*, the Follower aligns with the Leader and moves parallel to it after a very short transient. At each reflection, the Follower gets closer and closer to the vertical attractor. The inset enlarges the bounces at the boundary, *COV* = 2. . . . . 48

3.5 **Phase space  $(\theta, p)$  for trajectories approaching the vertical attractor.** The boxes highlights the fact that the last part of the trajectory is along 2 straight lines of equations  $p = -\theta + \frac{\pi}{2}$  and  $p = -\theta - \frac{\pi}{2}$  respectively. *COV* = 2.1 . . . . . 49

3.6	<b>Left Eight-shaped Attractor.</b> The Follower reflects at point 1 to find that the Leader is moving upward, and thus get turned counter-clockwise upward to hit the boundary. Each time the Follower reflects from the boundary it sees the Leader and get turned upward again. The Follower bounces off the boundary between points 1 and 2 (as shown in the inset). At point 2 the Follower reflects to find that the leader is moving downward and thus gets turned clockwise downwards. As it turns downwards the Leader falls outside its COV and thus it continues to move in a straight line to hit point 3. As the Follower reflects at point 3, it finds that the Leader is still moving downwards and thus get turned clockwise to hit the boundary. The Follower undergoes another series of bounces off the boundary between points 3 and 4. At point 4, it reflects to find the Leader moving up and thus it gets turned counter-clockwise until the Leader falls outside its <i>COV</i> so it continues in a straight line to reach point 1. The vertical diameter is the trajectory of the Leader. <i>COV</i> =1.7. . . . .	50
3.7	<b>Variation of the angular positions of the 4 vertices of the left eight-shaped attractor (shown in Fig. 3.6) for consequent hits n.</b> (a) Angular position of vertex 1;(b) angular position of vertex 2;(c) angular position of vertex 3;(d) angular position of vertex 4. . . . .	51
3.8	<b>Evolution of the eight-shaped attractor at different values of COV.</b> We observe that it becomes thinner and wider as COV increases. . . . .	52
3.9	<b>Characteristics of Eight-figure.</b> The angular position of vertex 1 of the Eight-figure is almost constant for all COV (blue), that of vertex 2 decreases (red). The thickness of the arm holding vertex 1 is always larger than that holding vertex 2, but they both decrease as COV increases. . . . .	52
3.10	<b>Transition from the vertical attractor to Eight shape.</b> The eight shape is stable for <i>COV</i> > 1.34, for values of <i>COV</i> between 1.3 and 1.34 the follower jumps between left and right eight-shaped attractors and nearly central back and forth before ending up at the vertical attractor. . . . .	53

- 3.11 **An Order Parameter for the Eight-figure.** The orbit averaged angular separation  $A_{12}$  between vertices 1 and 2 of Fig.1c provides a clean order parameter with which to map the eight-figure phase with increasing  $COV$ . We display the mean value of  $A_{12}$  over all cycles in a given trajectory, and over 50 trajectories with varying initial conditions, and the same  $COV$ . Near zero values of  $A_{12}$  indicate that the follower is hitting the upper (hence the lower) part of the circular tank at neighboring points, and that the follower is thus approaching the vertical attractor. Increasingly larger values of  $A_{12}$  indicate an increasingly well defined eight-figure attractor. Transition in and out of the eight-figure attractor is evident at  $COV \sim 1.3$  and  $COV \sim 2$  respectively. . . . . 54
- 3.12  **$(\theta, p)$  phase space for eight-shaped attractors.** The transients are removed and the trajectories on the eight-shaped attractor are drawn in the  $(\theta, p)$  phase space for the subset of the 50 initial conditions that lead to the eight-figure for each value  $COV \in [1.5, 1.55, 1.6, 1.65, 1.7]$ . Points 1(1'), 2(2'), 3(3') and 4(4') represent the vertices on the right(left) eight-shaped attractor. . . . . 55
- 3.13 **Head-phone attractor.** Starting at a point on the upper left part of the circular boundary, the Follower bounce off down the boundary until it reaches point 1. When the Follower is at point 1, the Leader reflects from the boundary switching its direction of motion and thus causing the Follower to rotate counterclockwise. As the Follower rotates the Leader is no more in its cone of vision and thus the former moves in a straight line towards point 2. At point 2, the Follower reflects from the boundary and is rotated counter-clockwise by the Leader which is now in its  $COV$  and is still moving up. Soon the Leader switches direction and starts moving down at this instant it is out  $COV$  of the follower which is grazing the boundary with nearly tangent bounces. When the follower gets to the lower part of the circle, the Leader falls back into its  $COV$  and this causes it to rotate counterclockwise every time it bounces off the boundary. When the Follower is at point 3, the Leader switches direction up thus causes the former to rotate clockwise. As the Follower rotates, the Leader is no more in its  $COV$  and so it continues in a straight line towards point 4. At point 4, the Follower reflects and is then rotated clockwise since the Leader is still moving up, the inset shows the reflection at point 4. Soon the Leader switches direction and start moving down. The Follower, which is now in the lower part on the circle, bounces off the boundary and is rotated clockwise at each reflection until it reaches point 1. The cycle repeats itself. The red and the blue curves represent the trajectories of the leader and the follower respectively.  $COV = 0.85$ . . . . . 56

3.14	<b>Transition into and out of the Head-phone attractor.</b> The follower lingers between upper and lower headphone attractors and nearly central trajectories are favored around transitions into and out of headphone state. . . . .	58
3.15	<b>Evolution of the Head-phone attractor at different values of <math>COV</math>.</b> It becomes thinner and wider as $COV$ increases. . . . .	58
3.16	<b>An Order Parameter for the head-phone attractor.</b> The orbit averaged angular separation $S_{24}$ between vertices 2 and 4 of Fig.3.13 provides a clean order parameter with which to map the head-phone attractor with increasing $COV$ . We display the mean value of $S_{24}$ over all cycles in a given trajectory, and over 50 trajectories with varying initial conditions, and the same $COV$ . $S_{24}$ increases linearly with $COV$ , until it disappears at $COV = 1.1$ . . . . .	59
3.17	<b><math>(\theta, p)</math> phase space head-phone attractors.</b> The transients are removed and the trajectories on the head-phone attractor are drawn for 50 initial conditions for $COV \in [0.85, 0.9, 0.95, 1]$ . Note that the curves intersect the $p=1$ and $p=-1$ lines, which are the trajectories tangent to the boundary. Points 1(1'), 2(2'), 3(3') and 4(4') represent the vertices on the upper(lower) head-phone attractor. . . . .	59
3.18	<b>Relaxation time to Vertical attractor.</b> The logarithmic scale of the time required to get to the vertical attractor as a function of $COV$ . Three prominent peaks are observed at $COV$ values corresponding to transitions between attractors. . . . .	60
3.19	<b>Variation of model parameters.</b> $C_2$ is changed to 0.01 instead of 0.006 and $C_1 = 1$ is unaltered. The obtained states are the same but the occur over different ranges of $COV$ . (a) Head-phone attractor obtained at $COV = 0.9$ ;(b) eight-shaped attractor $COV = 1.6$ . . . . .	63
3.20	<b>Cohesion of a group started at the diameter.</b> 100 particles are initially started at the bottom of the diameter heading up. The initial positions are chosen such that the particles are symmetric with respect to the vertical diameter and are within a distance 0.0001 units of length. (a) At $t_f = 10000$ units of time the group keeps its cohesion around the vertical diameter and all the 100 particles are still within the same distance of 0.0001 units of length; (b) zoom out of the trajectories of the 100 particles shown in (a). . . . .	65
3.21	<b>Probabilities of being attracted to or escaping the Leader for the leader on the rim variation of the model.</b> The follower can escape the Leader in two ways: moving on a polygon (same as circular billiards with no interaction) or being trapped to the eight-like attractor described in Fig. 3.24. . . . .	66

3.22	<b>Straying attractors for the leader on the rim variation.</b> This is part of the trajectory, only few hits are shown to illustrate the behaviour, a complete trajectory is given in Fig. 3.23. Note that the follower is trapped in trajectories where it moves nearly tangent for some time and then moves in straight line to hit the other side of the boundary. This is similar to the eight-shaped attractor of the initial model, with rotation superimposed. The angular distance which the follower covers nearly tangent to the boundary changes with <i>COV</i> and is given in Fig. 3.25. . . . .	67
3.23	<b>Irregular rotating variant of Eight-shaped attractor obtained in the case of the leader on the rim variation.</b> . . .	68
3.24	<b>Example of a Typical state of the leader on the rim variation.</b> At point 1, the follower hits the boundary in front of the leader which is at point 3 (red and black arrows give the direction of motion of the leader and follower respectively) and is in the COV of the follower. The angle between the directions of motion of the Leader and the Follower $\phi_L - \phi$ is less than 180 and thus $\omega^*$ is positive and the follower rotates counterclockwise. As the follower reflects from the boundary the Leader is no more in its COV, but $\omega$ which doesn't drop immediately to zero is still positive and the follower will rotate counterclockwise again and thus move in the opposite direction of motion of the Leader to hit the boundary. As it reflects from the boundary the follower will not see the Leader but it already has a positive $\omega$ and thus will rotate counter-clockwise. This process is repeated until the Follower reflects and finds the leader in its COV (points 2 and 4), here the angle between the Leader and the Follower is larger than 180 and thus the follower rotates clockwise. Soon the Leader will no more be in the COV of the Follower which will continue to move in a straight line to hit the boundary in front of the Leader and the process repeats again.	69
3.25	<b>An order parameter for the irregular rotating variant of eight-figure.</b> The follower bounces off the boundary between the landing and the taking off points. The angular displacement along the boundary decreases as the <i>COV</i> increases. The landing and taking off points rotate along the circle. . . . .	70
3.26	<b>Straying Attractors for the sharp response variation of the model.</b> (a) 2-periodic (diameter) attractor obtained at <i>COV</i> = 1.51; (b) sharper version of Head-phone attractor obtained at <i>COV</i> = 1.57; (c) nearly eight-shaped attractor obtained at <i>COV</i> = 1.8 (the follower jumps between the two right and left attractors on both sides of the vertical diameter) . . . . .	71

3.27	<b>Probabilities of being attracted to and escaping form the Leader as a function of <math>COV</math> for the sharp response model variation of the model.</b> The blue and red lines give the probability of being attracted to or escaping from the Leader respectively. Note that at the beginning of the interval of escape from the Leader the follower has the highest probability of ending up in the nearly diameter attractor, for intermediate values it has highest probability of ending up in the nearly headphone attractor, and in the last part in the nearly eight-shaped attractor. . . . .	71
------	---	----

# Chapter 1

## Introduction

The philosophy of physics since its inception has been linked to the notion of reductionism: that the world around us can be understood in terms of properties of simple blocks. The other fundamental notion at the heart of this philosophy is determinism. This framework which was clearly formulated by Isaac Newton, has allowed scientists to perceive the world as being the product of cause and effect interactions between isolated objects, that can be represented by mathematical equations. This approach has achieved tremendous successes in the mechanical and industrial sectors, but started to get questioned in the beginning of the twentieth century with the revolutionary discoveries of relativity and quantum mechanics. These discoveries gave mankind a new outlook on matter, time, space, life and the universe, and also paved the road to technological physics including nuclear energy, semi-conductors, lasers, and new materials superconductive one. These technologies have changed the methods of our industrial production and our ways of life. Soon after, around mid-century, the urge to understand non-linear problems escalated and led to the development of a new type of physics, computational physics. It has gained its popularity after the great progress it



achieved in developing chaos theory [1], in discovering solitons [2] and in exploring the long-time tail [3]. Moreover, with significant advances in the computational power, the trend spread among various fields such as biology, economics, neural science and much more.

The world is becoming more and more complex. Globalization, technology and Big Data present us with new challenges of understanding, designing and managing systems -classified as complex systems- that are highly interacting, interconnected, interdependent and non-linear. Few examples are swarms of fish or birds, ant colonies, ecosystems, brains, crowds, cars and financial markets. The complexity doesn't come from the large number of constituents, rather from the complicated interactions between them. We understand systems with avogadro's number of particles ( $10^{23}$ ), yet we are not able to fully comprehend such systems with few hundreds to few billions agents. Moreover, the fact that they are out of equilibrium systems makes their study even more perplexing and necessitates the development of new tools and theories. I can't agree more with physicists R. B. Laughlin and D. Pines who stated in their paper entitled "The Theory of Everything" that:

*The central task of theoretical physics in our time is no longer to write down the ultimate equations, but rather to catalogue and understand emergent behavior in its many guises, including potentially life itself. We call this physics of the next [21st] century the study of complex adaptive matter. For better or worse, we are now witnessing a transition from the science of the past, so intimately linked to reductionism, to the study of complex adaptive matter, firmly based in experiment, with its hope for providing a jumping-off point for new discoveries, new concepts, and new wisdom.*

The search for alternative scientific methods better suited to research in

these complex systems, supported by the paradigm that sees the world as interconnected elements whose interactions give rise to the patterns we observe, necessitated the emergence of specialized research institutes and departments in universities around the world that bring together researchers from natural sciences, social sciences and even humanities. Thanks to the generous support of FAS Dean's Office, I got the chance to take a summer course at one of the leading institutes in the field, "Santa Fe Institute", Santa Fe, New Mexico, USA. There, I learned about different tools implemented in the field such as: agent based models, cellular automata, genetic algorithms, non-linear dynamics and far-from-equilibrium thermodynamics. I implemented some of these tools during my research, and I am curious to explore others in the future.

Collective behaviour of complex systems is fascinating as well as puzzling for both scientists and layman. Examples include systems with varying scales such as: human crowds [4], traffic [5], and autonomous robots [6], in addition to biological systems ranging from molecular scale such as actin and tubulin filaments [7], up to microscopic such as bacteria [8], up to fish, birds flocks [9] and herds. One asks how can local interactions among agents give rise to ubiquitous emergent patterns and phenomena? Models are devised to understand and replicate observations, and to make predictions about these systems' behavior. These models provide the ground for the exploration of the most important issues encountered in artificial life, of the continuous phase transitions observed in biological systems, and of the behavioral criteria leading to collective behavior in social organisms. On the other hand, physicists are mainly concerned with building a basic theory for these systems as new state of matter and classifying the generic types of behaviors in terms of non-equilibrium phases and phase transitions, characteristic instabilities, correlations and responses.

Models ranging from agent-based, to kinetic, to hydrodynamic were developed and principles of non-equilibrium statistical mechanics were applied to a collection of active particles [10, 11, 41, 13, 14, 15, 16, 17, 18, 19, 20, 21]. A living system termed "active matter" can be thought of as new kind of material in a fundamentally new non-equilibrium regime. It is new in the sense that: 1) the input of energy which drives the system out-of-equilibrium takes place locally and is thus homogeneously distributed through the bulk of the system, unlike sheared fluids or three dimensional bulk granular matter, where forcing is applied at the boundaries; 2) the system is force free and the direction of self-propelled motion is set by the orientation of the particle itself rather than being imposed by external fields (although some models study the effect of external field on swarms, nonetheless the latter does not have a major contribution in inducing the motion). In the following sections we discuss of the models studied in literature as well as the attempts to find equilibrium thermodynamic analogies.

**Agent-based models.** In contrast to the field view of traditional fluid dynamics, agent-based models consider rule-based interactions among individual agents. They have some advantage over the continuum approach for two reasons: a- they are closer to the mental models people have for these systems and b- experimental data maybe more directly mapped onto agents' behavioral rules than onto system level equations. Moreover, complex boundary conditions are much easier to implement in agent based models than in continuum models with partial differential equations. They are also more appropriate for studying small populations which cannot be approximated by continuous distributions. In simulations, agents have different initial conditions and thus different conditions in their local environments and this makes them more realistic.

The most general ingredients of agent-based models are self-propulsion, dis-

sipation and three behavioral mechanisms: attraction, repulsion and alignment. Different models select few or all of the above components and thus they produce various self-organized states. The first model to report collective behavior is the Viscek's model ([13]), which is very basic and uses alignment as the only ingredient. Each agent is associated with a velocity vector of fixed magnitude. At each time step, the orientation of each agent is updated to match the mean direction of its neighbors in the presence of some noise. Different variations of the model are studied in literature and it is found that the Viscek family of models displays a well defined transition from a disordered phase to a coherent flock as the noise level is decreased or the number density is increased. The particle model proposed by Cucker-Smale ([15]) also considers only alignment mechanism to obtain flocking. Here each individuals adjust their relative velocities with all others in the swarm, but the strength of this averaging process depends on the mutual distance; closer individuals have more influence than the far distance ones.

Another family of models is that of systems of self-propelled particles (SPPs), which includes most of the ingredients mentioned above; i.e the particles are self-propelled, they interact according to an attractive-repulsive pairwise potential ([17, 18, 19, 20]) and they are subject to a drag force. This family produces a rich variety of states such as coherent flock, single-mill, double-mills, rigid rotation and droplet. Levine et al. introduced this type of models in [17] and showed that these simple rules lead to coherent localized self-organizing states that are stable in the presence of noise and disorder in one- and two-dimensions. They focus on the single mill (vortex) state, which appeared for the first time without the need of a confining boundary or of a rotational chemo-taxis. Through a systematic numerical exploration of the parameter space of the same model, Touma et al. identified in [18] different types of collective behavior and summarized results

in a phase diagram where regions over which each state occur and the transition lines between the states are specified. The analysis of phase-transitions between ordered and disordered states which are driven by self-propulsion to viscosity ratio, is supported by a thermodynamic analogy with temperature-driven transitions between liquid and gaseous states. In [20], another member of the family that implements the same Morse potential but different propulsion and friction is introduced.

Agent-based models discussed above are able to catch the essence of certain behavior observed in nature, but they are clearly far from being realistic in their basic form. There are various attempts to make these models more realistic by: adding stochasticity, implementing cone of vision, imposing external fields or/and adding non-markovian terms. On the other hand, agent-based models are faced with the limitations of speed or memory of current computers as the number of members in the swarm increases, so continuum models come to rescue.

**Continuum approaches.** Instead of tracking trajectories and velocities of individual agents, kinetic models, following the strategy from kinetic theory of gases, describe the collective behavior encoded by the density distribution whose evolution is governed by partial differential equation. In the traditional language of stochastic processes this amounts to using the Fokker-Planck equation instead of the Langevin equations for individual particle trajectories. The change in time of the density distribution depends on transport (agents moving freely) and interactions with others.

The connection between Langevin and Fokker-Planck equations was used to obtain an analytic solution to a restricted type of open out-of-equilibrium swarming systems, namely the canonical-dissipative systems [22]. The basic assump-

tion on both the conservative and the dissipative elements of the dynamics of such systems, is that they are determined by invariants of motion. The complex dynamics is mapped to analytically tractable model. The equations of motion of a tractable model with Hamiltonian  $H$  is extended by adding the propulsion-dissipation term (which is only a function of  $H$  or some other invariant of motion). Langevin equations are then obtained by adding a white noise terms and eventually the corresponding Fokker-Plank equation for the probability distribution of many-particle system is written. It is proved in [22] that the obtained Fokker-Plank equation has an exact stationary solution which turns out to be a direct extension of the equilibrium canonical ensemble. This approach is very clean but the basic restriction that the propulsion-friction terms must be expressed only in terms of the constants of motion of the underlying Hamiltonian system it is too strong to cover realistic swarming models.

We close the discussion of continuum models by introducing the hydrodynamic ones. They are obtained by coarse-graining the equations of motion of individual agents and studying the flow of the swarm in terms of velocity moments of the particle distribution function. The system is now represented by the coupled fields of the density and momentum density governed by the continuity equations and momentum equation. This approach presents a computational advantage for simulations but is less illuminating in deciphering the basic interaction mechanisms in natural settings.

**H-stable and catastrophic potentials.** The notion of H-stability was introduced in the classical equilibrium statistical mechanics in connection with the thermodynamic limit definitions [23]. A system of  $N$  interacting particles is said to be H-stable if the potential energy per particles is bounded below by a constant which is independent of the number of particles present; thus the average

potential energy per particle remains finite in the limit of  $N \rightarrow \infty$ . H-stability is necessary and sufficient for the existence of the thermodynamic limit. Potentials that are not H-stable are called catastrophic. H-stability was discussed in connection to the agent-based models of swarms in [19, 20]. It was shown that the majority of the self-organized states are observed when the interaction potential is catastrophic. Vortex states with small number of particles can exist for H-stable potentials but do not survive when the number of particle increases beyond a certain value. Thus the existence of self-organized dynamic states precludes the "normal" thermodynamic behavior and vice versa. H-stability criterion is also linked to the validity of the continuum kinetic theory approach. As shown in [20] the continuum model does not approximate the particle dynamics when interaction potential is H-stable and it does when the potential is catastrophic.

**My work.** The work which is to be presented in this thesis is solely based on agent-based models and it is split into two parts. In the first part, I study two closely related agent-based models of self-propelled particles in the low energy regime and find the generic characteristics common to both. Besides, I classify the obtained states, find their life-times and characterize the transitions between them. Eventually, I derive the potential of the mean force that drives the change in an order parameter characterizing all of the obtained states. In the second part, I develop a minimal model that focuses on two key aspects of collective behavior, namely, visual cues and leader-follower dynamics. On one hand, there is a growing research suggesting that visual cues are the main mechanisms for information transfer in fish schools. On the other hand, there is an increasing interest in understanding the conditions for following the leader in biological and social systems. The unexpected non-monotonic behavior of the follower as a function of one control parameter makes the focus of this study. Although the

constructed model is too simplified to mimic reality closely, it lies at the interface between different interdisciplinary fields and its results might have significant implications in the study of complex systems.



## Chapter 2

# Low-energy States in Swarms of Self-Propelled Particles

### 2.1 Introduction

This chapter studies the generic characteristics of two closely related deterministic models of self-propelled particles (SPPs) that interact according to an attractive/repulsive potential and are subject to a dissipative force [17, 18, 19, 20]. These terms proved to be sufficient to give rise to collective self-organized migration such as the coherent flock, single mill, double mills, ring, droplet and rigid-body rotation. The most common potential used is the attractive/repulsive Morse potential, but other forms of repulsion (hard core) are also checked to produce the same qualitative results [17]. The two models that we study differ in their prescription of particle propulsion and drag. The first, which we refer to as the linear model, has constant self-propulsion and is subject to viscous drag proportional to  $\vec{v}$  [18]. The second, which we refer to as the cubic model, has self propulsion proportional to its speed and is subject to drag opposing its motion

and proportional to  $v^3$  [19, 20]. Here, one asks whether these differences will lead to different self-organized states or not.

Comparing both models, considerable overlap of the states is observed but the differences are also quite noticeable. In particular, the low energy states reported for the cubic model are the coherent flock and the rigid-rotation which have crystalline-like lattice structures. Instead, compact disk states with random velocities are reported for the linear model. The relaxation of the velocity magnitude to the terminal speed is linear and independent of self-propulsion in one model, while it is non-linear with linearized rate proportional to propulsion in the other. In literature, each model is studied using different set of parameters with different physical meanings which makes understanding the discrepancies difficult. Although phase diagrams representing different cross-sections of the entire parameter space are constructed, the picture is still not complete because of the complexity of the parameter space. It is not clear whether the reported differences between the two models observed at low energies have physical origins or are just the result of looking at different regions of the parameter space.

There are several questions that motivated our work, starting with the simplest ones: why would a state appear in one model but not in the other? What is the role played by the velocity dependence of the the dissipative force in approaching the final state? More specific questions relate to the possibility of competing self-organized states once the model parameters are fixed: why would the system end up in one state rather than the other for the same set of parameters? What is the probability of ending up in each state? How stable each state is? What types of transitions are involved? Can we deduce the final outcomes based on the transients? Finally, taking a broader view one asks if there is a mechanism for relaxation to the final state which is not model-specific, and whether there

is an appropriate extremal principle for the selection of a final steady state? In other words, is there a natural thermodynamic potential for non-equilibrium self-propelled systems that controls the relaxed phases, in the same way that such potentials operate in equilibrium thermodynamics? This is admittedly a challenging program. Here we report on considerable progress in answering most of the questions, while setting stringent constraints on any further attempts to answering more thorny issues.

The chapter is organized as follows. In section 2.2 we start by comparing the equations of motion and the resultant steady states for the two models under study. We employ the re-scaled dimensionless parameters that are equally applicable to both models. The re-scaled form provides a solid basis for comparing the models and allows a natural mapping between two sets of original parameters. We limit our investigations to the high-viscosity regime characterized by the existence of three competing low-energy states, namely the coherent flock, the rigid rotation, and the random droplet. In section 2.3 we characterize the properties of each state and attempt to quantify their respective basins of attraction. We also address the question of their stability and conclude that the random droplet is a transient state, although possibly a long-lived one. We report the first-passage time from the random droplet to either of the two true steady states, and demonstrate that both models are very close both in terms of the attraction basins and the lifetimes of the random droplet transient. In section 2.4 we investigate the transition from disordered to ordered states, both by following single particle trajectories, and studying the evolution of relevant order parameters with time. We present the equation of motion for a composite scalar order parameter and interpret it as a Langevin-type equation containing the mean force and a rapidly fluctuating noise. We evaluate the potential of mean force numerically and ad-

dress the question of meta-stability of the random droplet. In section 2.5, we discuss and summarize our results.

## 2.2 The Model

We consider  $N$  agents as point particles with masses  $m_i$ , position vectors  $\vec{r}_i$ , and velocity vectors  $\vec{v}_i$ . In the following we discuss the re-scaling procedure taking the cubic model as example. The particles interact with each other according to the Morse potential. The Newtonian equations for the  $i^{\text{th}}$  particle are given by:

$$\begin{aligned} \frac{d\vec{r}_i}{dt} &= \vec{v}_i \\ m_i \frac{d\vec{v}_i}{dt} &= (\alpha - \beta|\vec{v}_i|^2)\vec{v}_i - \vec{\nabla}_{\vec{r}_i} U_i \end{aligned} \quad (2.1)$$

where,

$$U_i = \sum_{i \neq j} \left( -C_a e^{-\frac{|\vec{r}_i - \vec{r}_j|}{l_a}} + C_r e^{-\frac{|\vec{r}_i - \vec{r}_j|}{l_r}} \right) \quad (2.2)$$

is the Morse potential,  $C_a$  and  $C_r$  specify the respective strengths of attraction and repulsion while  $l_a$  and  $l_r$  specify their respective length scales. Competition between the self-propulsion and drag term forces the speeds to relax to their terminal value ( $v_t = \sqrt{\frac{\alpha}{\beta}}$ ), while the Morse potential in biologically relevant cases combines shorter-range repulsion with a longer-range attraction. In [19] the final patterns obtained were classified according to the dimensionless ratios  $C = \frac{C_r}{C_a}$  and  $l = \frac{l_r}{l_a}$ . As discussed in [19], the biologically relevant range,  $C > 1$  and  $l < 1$ , is split in two parts: H-stable for  $Cl^2 > 1$  and catastrophic for  $Cl^2 < 1$ , the latter being particularly important for self-organized states. Following [24],

we introduce the rescalings:

$$\begin{aligned}\vec{r}_i &= l_a \vec{r}'_i \\ \vec{v}_i &= v_t \vec{v}'_i \\ t &= t^* t'\end{aligned}$$

where  $v_t = \sqrt{\frac{\alpha}{\beta}}$  is the terminal speed,  $l_a$  is the characteristic length of attraction and  $t^*$  is to be defined later. Substituting in Eqs. (2.1) we obtain:

$$\begin{aligned}\frac{d\vec{r}'_i}{dt'} &= \frac{t^*}{l_a} \sqrt{\frac{\alpha}{\beta}} \vec{v}'_i = t^* \frac{v_t}{l_a} \vec{v}'_i \\ \frac{d\vec{v}'_i}{dt'} &= \frac{\alpha t^*}{m} (1 - |\vec{v}'_i|^2) \vec{v}'_i - \frac{C_a t^*}{m l_a} \sqrt{\frac{\beta}{\alpha}} \vec{\nabla}_{\vec{r}'_i} U'_i\end{aligned}\quad (2.3)$$

where

$$U'_i = \sum_{i \neq j} \left( -e^{-|\vec{r}'_i - \vec{r}'_j|} + C e^{-\frac{|\vec{r}'_i - \vec{r}'_j|}{l}} \right) \quad (2.4)$$

Writing the equations in the dimensionless form above, three characteristic times appear: 1)  $t_{kin} = \frac{l_a}{v_t}$  is the time required to cover the characteristic distance of a swarm by a freely moving particle, 2)  $t_{rel} = \frac{m}{\alpha}$  is the time of relaxation to terminal speeds due to the propulsion/ friction terms, and 3)  $t_{pot} = \frac{m l_a}{C_a} v_t$  is the characteristic time for a noticeable momentum change due to the Morse potential forces. The choice of  $v_t$  as the unit speed and  $l_a$  as the unit length makes  $t^* = t_{kin}$  the unit time. Dropping the prime, Eq. 2.3 is given by:

$$\begin{aligned}\frac{d\vec{r}_i}{dt} &= \vec{v}_i \\ \frac{d\vec{v}_i}{dt} &= \gamma_1 (1 - |\vec{v}_i|^2) \vec{v}_i - \gamma_2 \vec{\nabla}_{\vec{r}_i} U_i\end{aligned}\quad (2.5)$$

where  $\gamma_1 = \frac{t_{kin}}{t_{rel}}$  and  $\gamma_2 = \frac{t_{kin}}{t_{potential}}$  are the corresponding rates of the change of momentum. In this way the initial seven parameters of the model ( $N, l_a, l_r, C_a, C_r, \alpha, \beta$ ) are reduced to two characteristic time ratios  $\gamma_1$  and  $\gamma_2$ , a length ratio  $l = \frac{l_r}{l_a}$ , an energy ratio  $C = \frac{C_r}{C_a}$ , and  $N$ . For the linear model, the equation of motion of the  $i^{th}$  particle is given by:

$$m_i \frac{d\vec{v}_i}{dt} = a \frac{\vec{v}_i}{|\vec{v}_i|} - b\vec{v}_i - \vec{\nabla}_{\vec{r}_i} U_i \quad (2.6)$$

Here the terminal velocity and speed relaxation time are given by different expressions:  $v_t = \frac{a}{b}$  and  $t_{rel} = \frac{m}{b}$ , while the other two characteristic times  $t_{kin}$  and  $t_{pot}$  are defined as before in the cubic model. Eventually, the reduced equations of motion take a very similar form (see appendix A for details):

$$\begin{aligned} \frac{d\vec{r}_i}{dt} &= \vec{v}_i \\ \frac{d\vec{v}_i}{dt} &= \gamma_1(1 - |\vec{v}_i|) \frac{\vec{v}_i}{|\vec{v}_i|} - \gamma_2 \vec{\nabla}_{\vec{r}_i} U_i \end{aligned} \quad (2.7)$$

where  $\gamma_1 = \frac{t_{kin}}{t_{rel}}$  and  $\gamma_2 = \frac{t_{kin}}{t_{potential}}$  have exactly the same physical meaning as in the case of the cubic model. We are interested in studying high viscosity limit with low kinetic energy states. High viscosity implies large relaxation rate  $\gamma_1$ , while large potential forces imply large rate  $\gamma_2$ . The values of the parameters used in this study are as follows:  $C = 2$  and  $l = 0.25$  corresponding to the catastrophic part of the biologically relevant region;  $N = 100$ , and  $\gamma_2 = 112$ . The last parameter,  $\gamma_1$ , serves as the relevant control parameter and is varied in the range  $\gamma_1 \in [1, 90]$  i.e. with  $\gamma_2 > \gamma_1$ . We solve Eqs. (2.5) and (2.7) in two dimensions numerically using (4,5) Runge-Kutta time discretization solver in Matlab R2014b. Initial  $x$ - and  $y$ - components of positions and velocities are

chosen randomly from uniform distributions in the range:  $-1 < x_i < 1$ ,  $-1 < y_i < 1$ ,  $-1 < v_{xi} < 1$  and  $-1 < v_{yi} < 1$ . For each value of the control parameter  $\gamma_1$ , 50 trajectories with different initial conditions are generated. The trajectory length is typically  $t_{final} = 100$  (in units of  $t_{kin}$ ) although longer trajectories up to  $t_{final} = 500$  are studied in some relevant cases.

## 2.3 Bound States and Basins of Attraction

Low energy states for the model with Morse potential were identified in [20] as a coherent flock and a rigid rotation state, while the flock and a random droplet were observed in [18]. Although both papers study Morse potential models, the exact form of the self-propulsion and friction terms differed. We demonstrate here that all three low energy states emerge irrespective of the specific form of the propulsion/friction term and their basins of attraction vary with the change in the control parameter in a very similar way. In the following subsections we initially characterize each of these states using two order parameters  $P$  and  $M$  defined as:

$$\begin{aligned}
 P &= \frac{|\sum_i \vec{v}_i|}{\sum_i |\vec{v}_i|} \\
 M &= \frac{(\sum_i \vec{r}_i \times \vec{v}_i) \cdot \vec{k}}{\sum_i |\vec{v}_i| |\vec{r}_i|}
 \end{aligned}
 \tag{2.8}$$

For the coherent flock  $P = 1$  and  $M = 0$ , for the perfect rigid rotation  $P = 0$  and  $M = \pm c$  where  $c$  is a constant close to 1, while for the random droplet both  $P$  and  $M$  are consistent with the notion of Maxwellian particle velocities as discussed later.

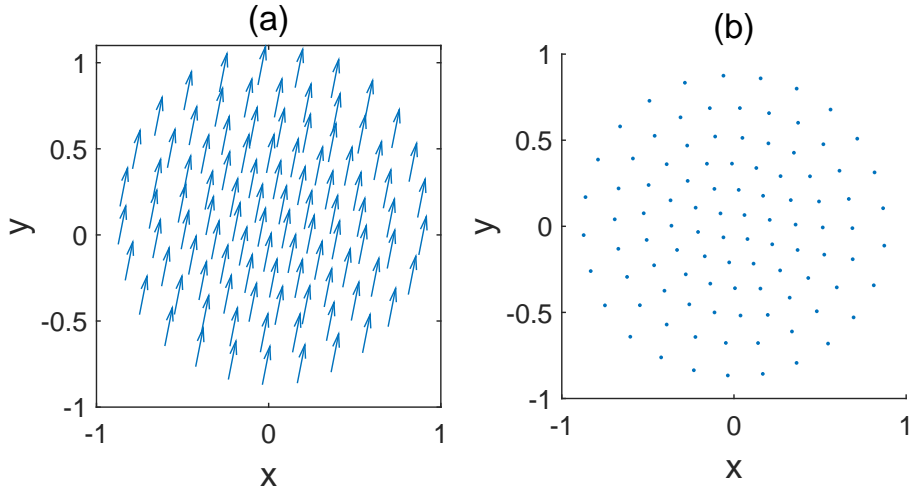


Figure 2.1: **Coherent flock.**(a)Velocity vectors superimposed on the positions of particles in a snapshot;(b) lattice positions in a snapshot. ( $\gamma_1 = 40$ )

### 2.3.1 Coherent Flock

The coherent flock has a ring-like lattice structure corresponding to the Lagrangian configuration with  $\nabla U = 0$  so that the net potential force acting on each particle sums up to zero. Once the particles reach these lattice positions and their velocities are aligned they move together with a constant terminal velocity (self-propulsion and friction terms cancel up), all relative distances being fixed. Figure 2.1 shows the configuration of a coherent flock and the vectors are the velocity vectors in a fixed frame of reference (panel a), and the lattice positions in the co-moving frame of reference (panel b). Note that the flock is a perfect state with a  $\delta$ - peak distributions of the translational order parameter  $P = 1$  and the rotational order parameter  $M = 0$ ; there are no fluctuations in either positions or velocities. This is true for both linear and cubic models.



### 2.3.2 Rigid Rotation

A perfect rigid rotation state is a frozen-configuration state where particles rotate all together at a constant angular velocity  $\omega$  about the center of mass. In a co-rotating frame the configuration would be static with the particles fixed at positions slightly deformed from the non-rotating Lagrangian configuration to compensate for the centrifugal forces and unbalanced propulsion/friction terms. Rotating Lagrangian configurations can be obtained numerically from the stationarity conditions as discussed in appendix C. However, our dynamic simulations produce rigid rotation states that are not perfect. Particles are found to rotate around the center of mass with small non-linear oscillations about mean positions and velocities while the angular velocities are not exactly equal. This imperfection is reflected in the distribution of the rotational order parameter  $M$ , see panel (b) of Fig. 2.2, which has a pronounced width rather than being sharply peaked. As is the case of the coherent flock state, the particles are also arranged in 6 rings (panel (c) of Fig. 2.2). The mean speed of particles as a function of the radial position is shown in panel (d) of Fig. 2.2. The relation is linear with constant of proportionality  $\omega$  ( $v = \omega r$ ) for the first 3 rings with saturation at the unit terminal speed for the outer rings. It is also observed that the rotating states become more and more distorted for larger values of the control parameter  $\gamma_1$  transforming into a single mill with empty center for large  $\gamma_1$ .

### 2.3.3 Random Droplet

The random droplet state turns out to be not quite random, at least as far as particle positions are concerned. A snapshot of the configuration with velocity vectors superimposed on the positions of the particles (panel (a) of Fig. 2.3)

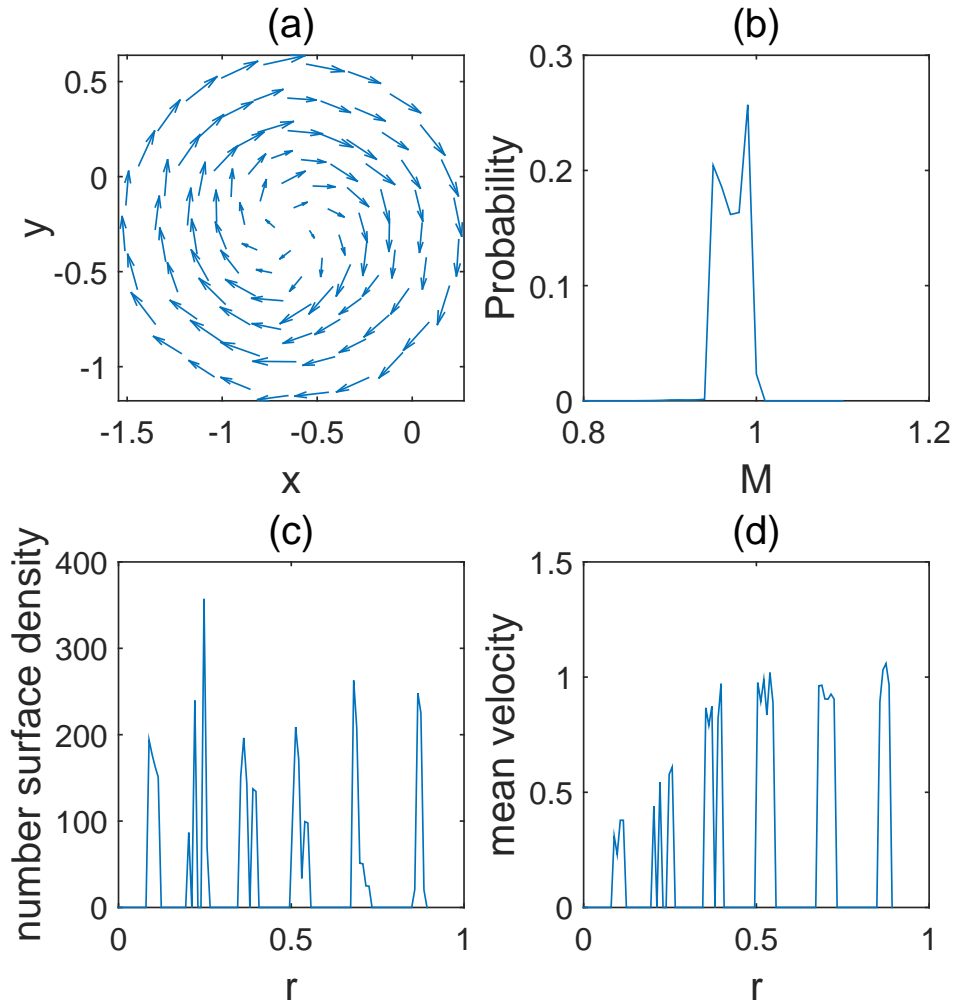


Figure 2.2: **Rigid rotation.**(a) Configuration with velocity vectors superimposed on positions; (b) distribution of order parameter  $M$  which has a non-zero width rather than being peaked, indicating that the rigid rotation state is not a perfect state;(c) radial density of particles showing six rings;(d) distribution for the fluctuation-averaged velocity as a function of radius in the center of mass frame as a function of radius, showing a linear dependence for the first three rings after which the velocity saturates at the terminal velocity. ( $\gamma_1 = 25$ )

indicates that although velocities have random orientations, particles are confined inside a circular drop of radius close to 1 (i.e. attraction length  $l_a$ ). Moreover, following the trajectories of all particles over time indicates that the particles, rather than being randomly distributed, are mostly localized on rings that keep some memory of the Lagrangian configuration (panel(d) of Fig. 2.3). The outer rings are well separated in contrast to the inner ones. The trajectory of a single particle shows that after a short initial transient the particle mostly moves along well defined rings of small thickness with occasional jumps from one ring to another (Fig. 2.3 (d)). The distribution of the rotational order parameter  $M$  is peaked at zero and is well represented by a Gaussian distribution with mean zero and a standard deviation  $\sigma$  that depends on the value of  $\gamma_1$ , see Fig. 2.3), panel (c). On the other hand the distribution density of the flocking order parameter  $P$  is that of a modulus of a two-component Gaussian random variable, similar to a Maxwell speed distribution in 2d, see panel (c) of Fig. 2.3.

### 2.3.4 Basins of attraction and transient state lifetimes

An estimate of the size of the basin of attraction of each of the three states discussed above is obtained statistically by calculating the probability of obtaining a given state at the end of a simulation starting with random initial conditions. The statistics is based on 50 independent simulation runs with random initial conditions for each value of the control parameter  $\gamma_1$  (velocity relaxation rate), displayed in Fig. 2.4 for both the cubic (panel a) and the linear model (panel b). It is clear that the random droplet state dominates at the lowest values of the control parameter  $\gamma_1 = 1, 2$  as well at the largest values starting from  $\gamma_1 = 80$ . At intermediate values of  $\gamma_1$  the share of the random droplet is negligible and

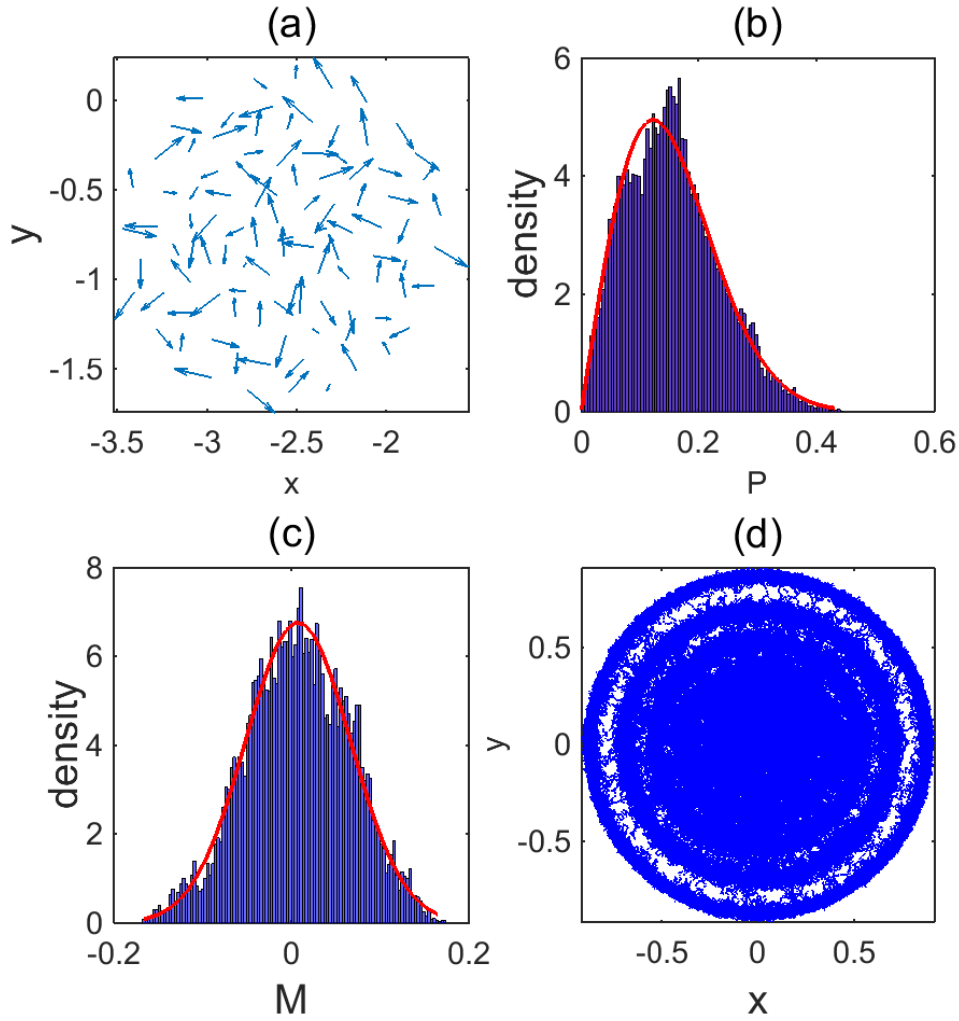


Figure 2.3: **Random droplet.**(a)Configuration with velocity vectors superimposed over positions; (b) distribution of order parameter  $P$  fitted with a Rayleigh distribution (Maxwell speed distribution in 2d); (c) distribution of parameter  $M$  fitted with a Gaussian with zero mean;(d) superimposed single particle trajectories; the particles spend most of the time close to rings that pass through the lattice points of the Lagrangian configuration. ( $\gamma_1 = 80$ ).

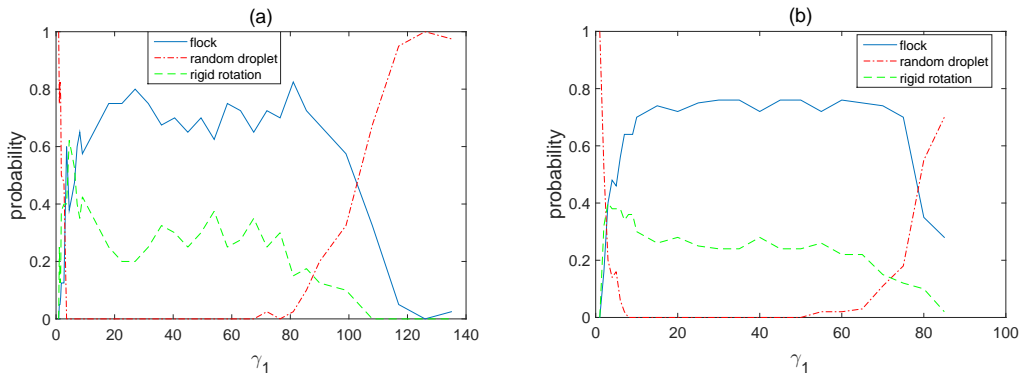


Figure 2.4: **Probability of obtaining each of the three organized states as a function of  $\gamma_1$ .** (a)The linear model; (b)the cubic model. The length of the trajectory is  $t_{final} = 100t_{kinetic}$ . Statistics is based on 50 runs with different random initial conditions at fixed control parameters.

the outcomes are either a flock or a rigid rotation state with probabilities being roughly 2/3 and 1/3, respectively. The data for the cubic and the linear models (panels a and b, respectively) are quite close; the statistical error for 50 distinct trajectories is rather pronounced but better statistics were out of reach with available computational facilities.

The data of Fig. 2.4 are based on trajectories of length  $t_{final} = 100$  in units of  $t_{kin}$ . Longer simulations reveal that the random droplet is a long-lived (possibly meta-stable) state rather than a true stationary state for the system; i.e random droplets are formed relatively fast but if we wait long enough all of them evolve into either a flock or a rotating state. Thus the apparent statistics describing the basins of attraction is strongly affected by the lifetime of the random droplet as compared to the duration of the simulation run, and the observed predominance of the random droplet state at the lowest and highest values of  $\gamma_1$  is of a purely kinetic nature. The waiting time to observe a transition to any of the true stationary states turns out to be strongly dependent on the control parameter  $\gamma_1$ . Note that for the same fixed set of parameters we get a distribution of first

passage times corresponding to different initial conditions. Figure 2.5(a) gives the mean first passage time for the cubic model as a function of  $\gamma_1$  along with the maximum and the minimum waiting times observed in a set of 50 runs. The dependence is strongly non-monotonic with three distinct regimes. For small values  $1 < \gamma_1 < 20$  the mean of the waiting time starts at very large values and drops with the increase in  $\gamma_1$ . In the intermediate range  $20 < \gamma_1 < 60$ , the mean of the waiting time is more or less constant and much smaller than the trajectory length. For  $\gamma_1 > 60$  the mean waiting time increases dramatically with increasing  $\gamma_1$ . For comparison, a similar graph for a linear model is shown in panel (b). Here, only the mean first passage time is displayed. Taken together, Figs. 2.4 and 2.5 demonstrate that the behavior of the two models (linear and the cubic) in the high viscosity, low-energy regime is essentially the same. So, in the more detailed analysis presented below we discuss only the cubic model as a representative the class of Morse potential swarms.

### 2.3.5 Linear Stability

The droplet state turns out to be a transient, albeit a long-lived one in some range of the control parameter. Together, Figs. 2.4 and 2.5 show that the linear and the cubic models are qualitatively and even semi-qualitatively very close once they are characterized in terms of the re-scaled parameters  $\gamma_1$  and  $\gamma_2$ . The fact that random droplet and rigid rotation were reported differently in the literature can be readily understood. Since only relatively small parts of the parameter space were explored it was easy not to notice the random droplet in the range  $20 < \gamma_1 < 60$  where its lifetime is quite short, and conversely, to overlook the rigid rotation for  $\gamma_1 > 80$  when the sampling trajectories were not long enough.

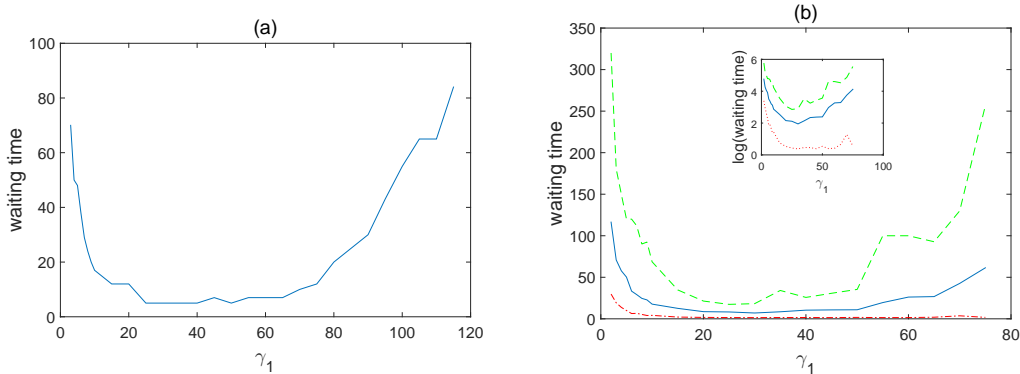


Figure 2.5: **First passage times for transition from a random initial condition to a final steady state vs. the velocity relaxation rate  $\gamma_1$ .** (a) Mean of first passage time for the linear model with the number of particles  $N = 50$ ; (b) the maximum, the minimum, and the mean values of first passage times obtained from a set of 50 independent runs for the cubic model are shown by dashed green, dashed-dotted red and solid blue curves, respectively. The inset displays the same data on a log scale indicating relative broadening of the first passage time distribution with the increase in  $\gamma_1$ .

To understand better the properties of the two true stationary states we present their linear stability analysis. Phase space configurations, linearized equations of motion, and the relevant eigenvalue problem for the cubic model are described in appendix B. The main results are qualitatively similar for both models and can be summarized as follows.

**Coherent flock** The flock is stable at any values of the control parameters  $\gamma_1$  and  $\gamma_2$ . The stability matrix has 4 zero-eigenvalue modes representing 2 independent uniform translations, one virtual rigid-rotation displacement for coordinates and one uniform rotation for velocity vectors. All the other eigenvalues have negative real parts as displayed in Fig. 2.6 (b) vs. the control parameter,  $\gamma_1$ . The real parts ( $\lambda_r$ ) are confined between two lines:  $\lambda_r = 0$  and  $\lambda_r = -2\gamma_1$  where the latter is the line of the mode with fastest relaxation. The largest real-part eigenvalue describes the relaxation of the slowest mode and is shown in Fig. 2.6 (a) as a function of the control parameter. The curve actually consists of two branches,

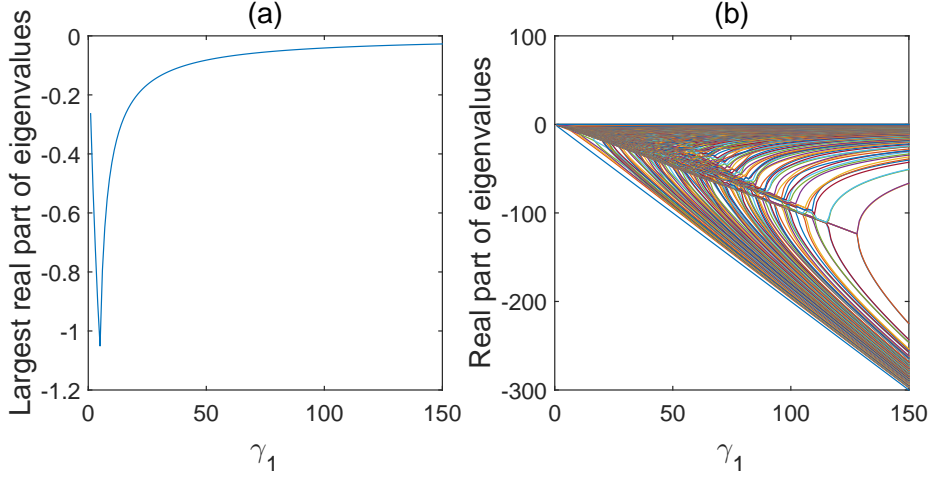


Figure 2.6: **Flock stability.** (a) Largest non-zero eigenvalue versus  $\gamma_1$  for the coherent flock state; (b) all 400 eigenvalues vs  $\gamma_1$  for the stability matrix of a coherent flock of 100 particles.

the first one being linear in  $\gamma_1$  and the other branch appearing as a result of a bifurcation in a pair of complex-conjugate eigenvalues. A more detailed analysis of the eigenvalues and their bifurcations falls outside the scope of this paper.

**Rigid Rotation** A perfect rigid rotation state can be constructed by deforming a Lagrangian configuration as described in the appendix C. In the limit of  $\gamma_2 \gg 1$  and  $\gamma_2 \gg \gamma_1$  these deformations can be arbitrarily small. There are 3 zero-value eigen-modes (compared to the flock state, the uniform rotation in the velocity space is missing). However, the state turns out to be always linearly unstable. The real part of the eigenvalue describing the fastest growing perturbation is displayed in Fig. 2.7 as a function of  $\gamma_1$ . Small deviations from the perfect rotating state in either coordinates or velocities grow exponentially with time but eventually saturate due to non-linearities in the full equations of motion, as illustrated in Fig. 2.8 panels (a) and (b). With the increase in  $\gamma_1$  the linear instability becomes more pronounced which is consistent with the shrinking basin of



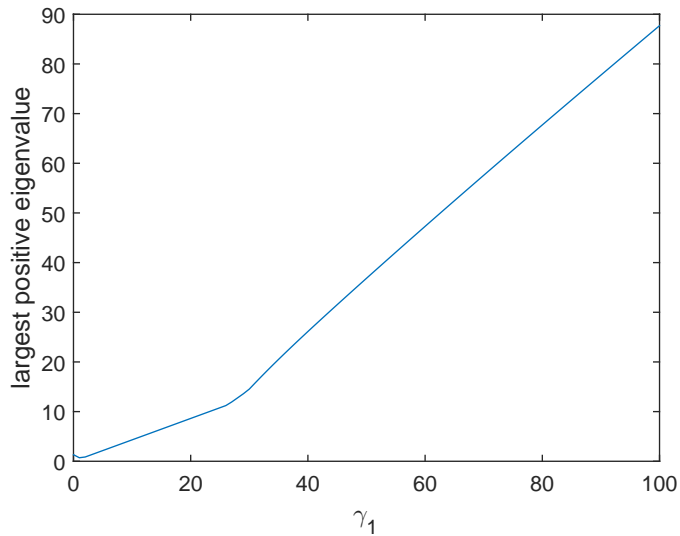


Figure 2.7: **Largest eigenvalue versus  $\gamma_1$  for the rigid rotation state.** The relationship is linear and the graph passes through the origin; i.e. for arbitrarily small  $\gamma_1$  the largest positive eigenvalue which represents the linear growth of perturbations of the perfect rigid rotation becomes very small.

attraction of the rigid rotation state as seen in Fig. 2.4, and stabilization occurs with larger deviations from the perfect rigid rotation. As the viscous velocity relaxation rate  $\gamma_1$  approaches the velocity change rate due to potential forces  $\gamma_2$  the rotating states becomes closer to a mill with all speeds maintained close to the terminal value.

## 2.4 Transition mechanisms

Above, we noted a marked difference in the mean waiting time to observe a transition to one of the two steady states (flock or rigid rotation), and studying the dependence of this transition time with  $\gamma_1$ . Here, we point out that the transition mechanism itself is different for different values of  $\gamma_1$ . Indeed, two types of transitions are observed and discussed in the following subsections: 1) Gradual

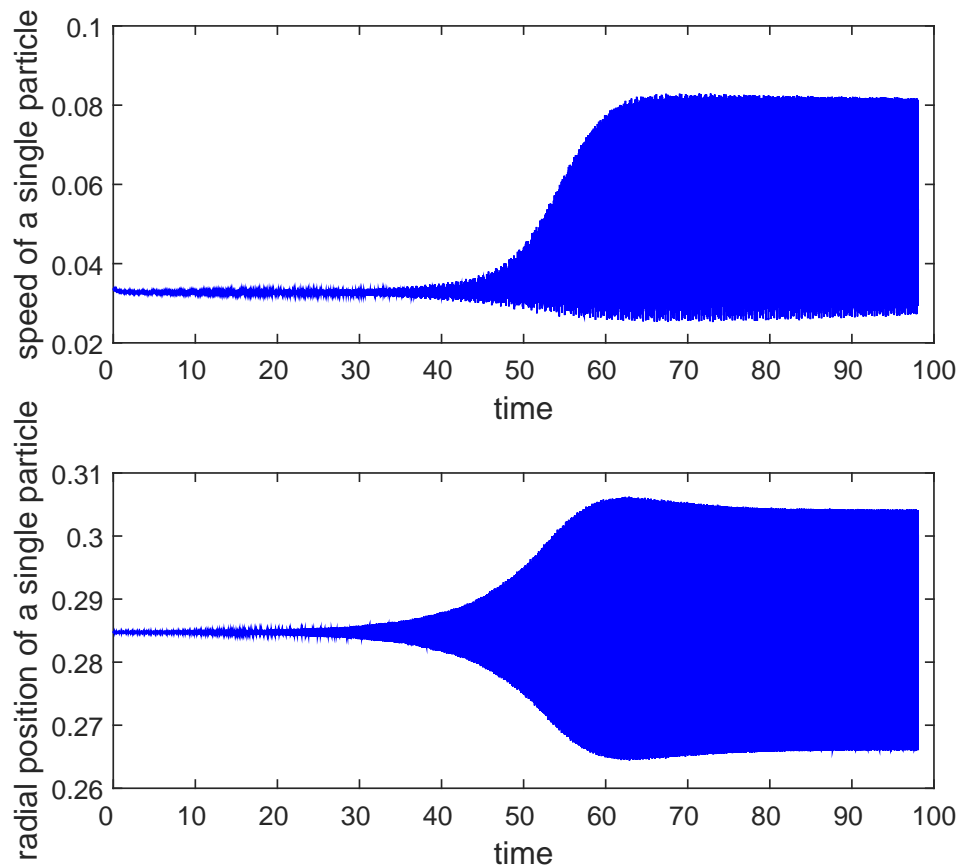


Figure 2.8: **Growth of perturbations of the perfect rigid rotation state for  $\gamma_1 = 0.08$  and  $\gamma_2 = 83$ .**(a) Speed of a single particle as a function of time; (b) radial position of a single particle as a function of time. Linear instabilities grow exponentially, but are then stabilized by non-linear terms.

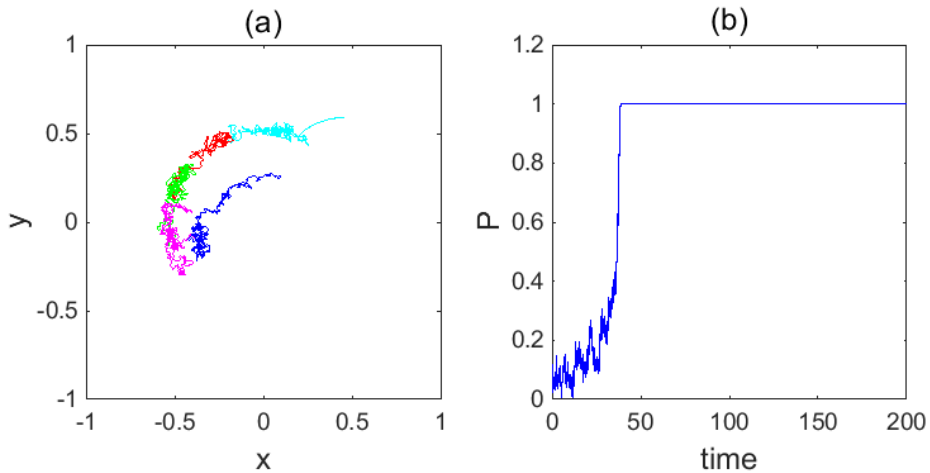


Figure 2.9: **Slow gradual transition to flock.**(a) Typical single particle trajectory with each color representing a part of the trajectory and the order in time is: cyan,red, green, magenta and blue; (b)time evolution of the flocking order parameter  $P$  as the swarm transits gradually from a random initial condition to a coherent flock. ( $\gamma_1 = 9$ )

slow transition for very small values of  $\gamma_1$  and 2) sharp transition following the long-lived random state for large values of  $\gamma_1$ .

### 2.4.1 Case 1: Slow Gradual Transition

The transition is studied by following the time evolution of the order parameters  $P$  and  $M$  for the coherent flock and the rigid rotation respectively. We observe that for small values of  $\gamma_1$  ( $2 < \gamma_1 < 20$ ), the transition to the final state is quite slow and proceeds gradually. The relevant order parameter grows in a quasi-monotonic way from a typically low initial value to the final value characterizing the steady state, as illustrated in Fig. 2.9 for a transition to a flock and in Fig. 2.10 for a transition to a rigid rotation state. Initial stage is accompanied by some noise but deterministic evolution dominates. Single-particle trajectories in panels (a) are mostly confined to rings with a few ring-to-ring jumps due to collisions.

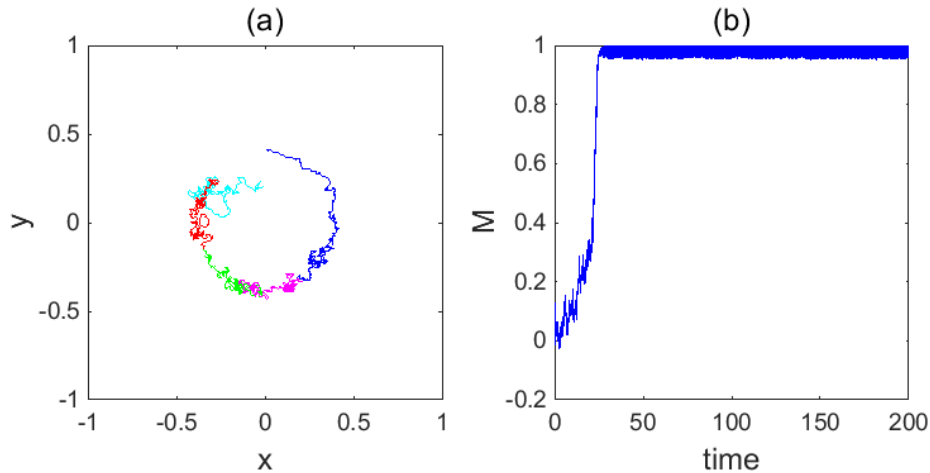


Figure 2.10: **Slow gradual transition to rigid rotation.** (a) Typical single particle trajectory, see Fig. 2.9 for the color scheme; (b) time evolution of the order parameter  $M$  as the swarm transits gradually from a random initial condition to a rigid rotation. ( $\gamma_1 = 7$ )

An important characteristic of this transition mechanism is the proportionality of the mean first passage time to the velocity relaxation time  $t_{relaxation} = \frac{1}{\gamma_1}$ , as displayed in Fig. 2.11.

## 2.4.2 Case 2: Sharp Transition

For intermediate and large values of  $\gamma_1$  we observe that the system resides in the random droplet state described earlier for a long time before undergoing an abrupt jump-wise transition to the final state. The jump itself occurs over a very short time interval. Typical graphs representing the evolution of the relevant order parameter as well as single-particle trajectories are shown in Figs. 2.12 and 2.13. The most prominent feature of the evolution curves is their strongly stochastic nature as compared to much smoother evolution demonstrated in the previous sub-section. A standard approach in analyzing stochastic evolution in-

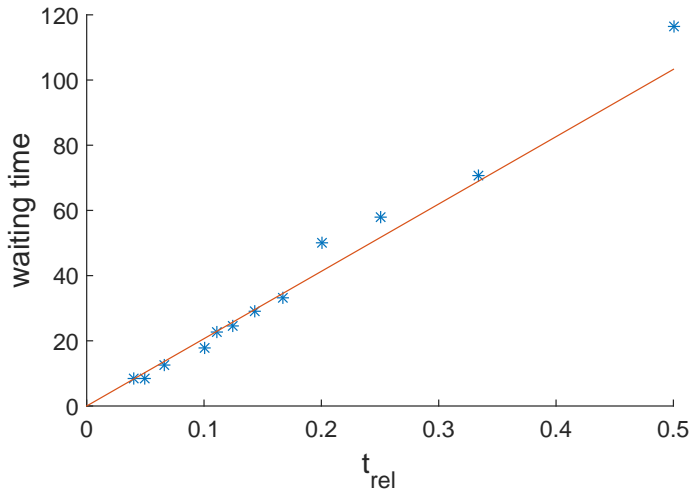


Figure 2.11: **Mean first passage time to an organized steady state vs. the velocity relaxation time**  $t_{rel} = \frac{1}{\gamma_1}$ . The range displayed corresponds to  $\gamma_1$  between 2 and 20.

volves filtering out the noise to define the mean force. If the mean force can be described by a potential, certain conclusions may be made about the transition dynamics. In particular, the question of whether a long-lived transient state is actually meta-stable can be addressed.

### 2.4.3 Potential of mean force

In an attempt to understand the transition mechanisms and the broad variation of the lifetimes we consider the potential of mean force as a function of the order parameter borrowing an analogy from the non-equilibrium free energy first introduced by Landau in his theory of phase transitions. From a dynamical point of view, this is also related to the approach whereby the order parameter is treated as a "slow" variable and the conjugate net force is split into a systematic component causing deterministic drift and a rapidly fluctuating zero-mean component related to much faster dynamic variables. Our original choice of two order pa-

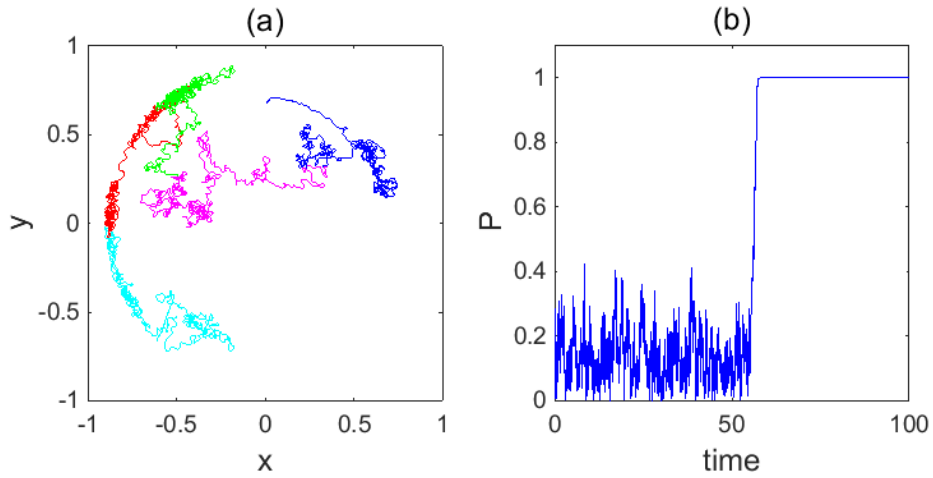


Figure 2.12: **Sharp transition to flock.** (a) Typical single particle trajectory for the long-lived random state with each color representing a part of the trajectory, see Fig. 2.9 for color scheme; (b) time evolution of the flocking order parameter  $P$  as the swarm transits from a random initial condition to a coherent flock. ( $\gamma_1 = 70$ )

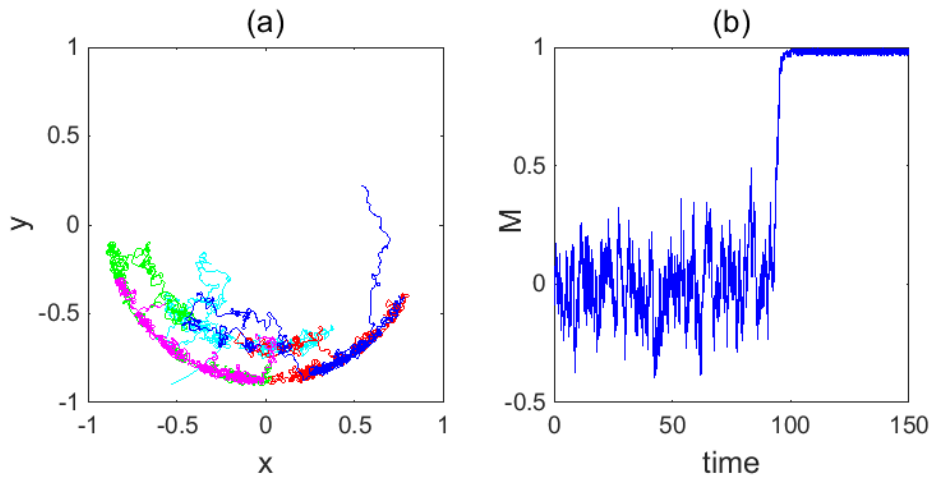


Figure 2.13: **Sharp Transition to rigid rotation.**(a) Typical single particle trajectory for the long-lived random state, see Fig. 2.9 for the color scheme; (b) time evolution of the order parameter  $M$  as the swarm transits from a random initial condition to a rigid rotation. ( $\gamma_1 = 75$ )

rameters,  $P$  and  $M$ , presents a big challenge for carrying out this program: a function of two variables is quite difficult to quantify reliably based on numerical data especially if a noise-filtering stage is involved. An additional (though not a principal) complication is that the mean force defined as a function of two variables would be generally non-potential. To overcome these difficulties, we introduce a new scalar order parameter,  $s$ , able to discriminate between the flock, the rigid rotation state and the random droplet. It is defined as the particle velocity dispersion in the center-of-mass reference frame,

$$s = \frac{\sum_i \tilde{v}_i^2}{N} \quad (2.9)$$

where  $\tilde{v}_i = \vec{v}_i - \frac{\sum_i \vec{v}_i}{N}$ . Clearly, in the coherent flock,  $s = 0$ ; simulation data show that for the rigid rotation state  $s$  take values in the range  $[0.87, 0.99]$ , while the random droplet is characterized by  $s \in [0.55, 0.80]$ . Figure 2.14 gives the equilibrium value of the order parameter at the three states studied as a function of model parameter  $\gamma_1$ . Simulations are done at different values of  $\gamma_1$  and it is observed that  $s$  for the rigid rotation and the droplet states increase with  $\gamma_1$  within the ranges mentioned above. The generalized force conjugate to the chosen order parameter is defined on the basis of the evolution equation for  $s$ :

$$\begin{aligned} \frac{ds}{dt} &= \frac{2}{N} \sum \left( \gamma_1(1 - v_i^2)\vec{v}_i - \gamma_2\vec{\nabla}_i U \right) \cdot \vec{v}_i \\ &- 2\gamma_1 \left( 1 - \frac{\sum_i \tilde{v}_i^2}{N} - 2\frac{\tilde{v}_i^2 \cos^2(\theta_i)}{N} \right) m^2 \\ &+ 2\gamma_1 \frac{|\tilde{v}_i|^3 \cos(\theta_i) m}{N} + 2\gamma_1 m^4 \\ &= \frac{-2\gamma_1}{N} \sum_i \left( \tilde{v}_i^4 + (3\tilde{v}_i^3 \cos\theta_i - 2\tilde{v}_i \cos\theta_i) m + 2\tilde{v}_i^2 \cos^2\theta_i m^2 \right) \\ &- \frac{2\gamma_1}{N} \left( \sum_i 4\tilde{v}_i \cos\theta_i m^3 + 2\gamma_1(1 - m^2)s + \sum_i \gamma_2 \tilde{v}_i \cdot \vec{\nabla}_i U \right) \end{aligned} \quad (2.10)$$

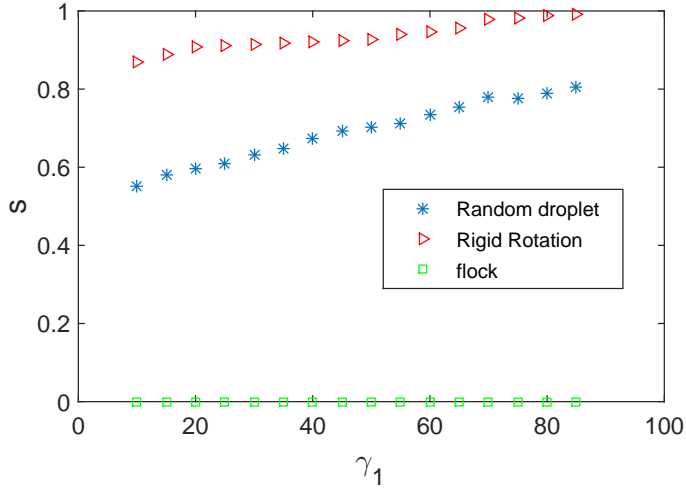


Figure 2.14: **Average value of the order parameter  $s$  for the 3 organized states as a function of  $\gamma_1$ .**

where  $\vec{m} = \frac{\sum_i \vec{v}_i}{N}$  and  $\theta_i$  is the angle between  $\tilde{v}_i$  and  $\vec{m}$ . This can be interpreted as a Langevin-type equation for motion,  $s$  representing a slow degree of freedom and the right-hand side representing the conjugate force,  $f$ , which contains a smooth deterministic contribution representing the mean force  $f_{mean}$ , and a rapidly varying noise-like contribution with zero mean. In contrast to a standard Langevin equation for a Brownian particle, the noise is not thermal but is generated by intrinsic swarm dynamics. Filtering out the noise is achieved by the following procedure: the net force  $f$  is evaluated along the trajectory in the course of simulation along with the instantaneous values of the order parameter  $s$ . This gives an implicit function  $f(s)$  parameterized by time. The values of the force at fixed  $s$  are averaged within a single simulation trajectory, and then over 50 trajectories with random initial conditions at fixed control parameter value. The averaged data for  $f_{mean}(s)$  is then integrated to give the potential of mean force,  $V(s)$  satisfying  $\frac{dV}{ds} = -f_{mean}$ .



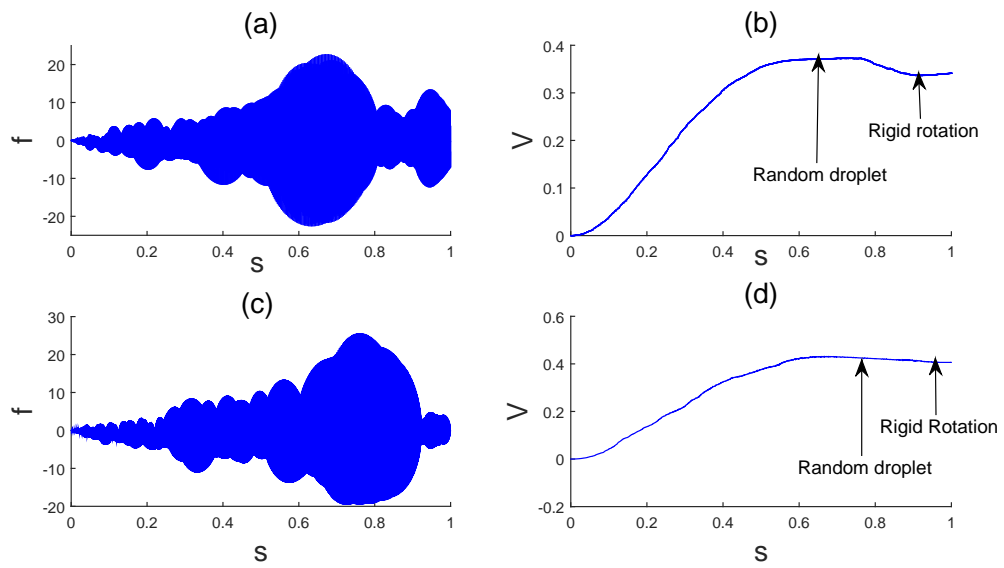


Figure 2.15: **Instantaneous Forces and Potentials of mean force as a function of  $s$  at  $\gamma_1 = 30$  and  $\gamma_1 = 75$ .** Panels (a) and (c) give the instantaneous forces as a function of  $s$  for  $\gamma_1 = 30$  and  $\gamma_1 = 75$  respectively. The noise is dependent on  $s$ , it is zero at  $s = 0$  (coherent flock state) and very small around  $s = 0.9$  (rigid rotation state). Panels (b) and (d) give the corresponding potentials of mean forces which have two distinct minima characterizing the coherent flock ( $s = 0$ ) and the rigid rotation state ( $s = 0.9$  for  $\gamma_1 = 30$  and  $s = 0.99$  for  $\gamma_1 = 75$ ) and a flat maxima characterizing the random droplet state ( $s = 0.63$  for  $\gamma_1 = 30$  and  $s = 0.77$  for  $\gamma_1 = 75$ ).

Figure 2.15 displays the numerical data for the potential of mean force  $V(s)$  (panels (b) and (d)), and the instantaneous random force as a function of  $s$  (panels (a) and (c)) for two values of the control parameter,  $\gamma_1 = 30$  and  $\gamma_1 = 75$ , representing the cases of a short-lived and a long-lived state, correspondingly. The most important result of this approach is the appearance of the three states discussed in this paper. The potential of mean force has two distinct minima, representing the coherent flock (at  $s = 0$ ) and the rigid rotation state (near  $s = 0.9$  for  $\gamma_1 = 30$  and  $s = 0.99$  for  $\gamma_1 = 75$ ) consistent with their stationarity. On the other hand, the random droplet range (indicated by the relevant arrow) does not show any pronounced minimum which makes it difficult to classify this state as meta-stable. Indeed, in the panel (b) of Fig. 2.15 the random droplet range corresponds to a clear maximum. Certain change in the shape of the mean force potential can be seen with the increase in the control parameter  $\gamma_1$  which leads to a longer-living transient state (panel (d)). First, the rigid rotation minimum grows more shallow, which is consistent with stronger velocity fluctuations mentioned above. Second, in the random droplet range of  $s$  the curvature of the potential decreases suggesting a very small mean force in a relatively broad range of  $s$  values. Panels (a) and (c) indicate that the magnitude of the noise component in the force is by itself strongly  $s$ -dependent. In particular, in the range corresponding to the droplet state, the noise amplitude is a maximum while upon approaching either of the steady states the noise goes down dramatically vanishing completely at the flocking state minimum. This behavior makes a marked difference in comparison to a more familiar thermal noise. We propose that the evolution of the order parameter is governed by an advection-diffusion type equation. At low values of the control parameter  $\gamma_1$  the diffusive mechanism is relatively unimportant, and the evolution is predominantly deterministic. On the other hand, at large  $\gamma_1$  the

mean force is much smaller, and the evolution of the order parameter is mostly diffusive. This results not only in a sharp increase in the mean first passage time but also in a broader distribution of the first passage times as seen in the inset of Fig. 2.5 with its logarithmic scale.

## 2.5 Summary and Discussion

Simulations of swarms with Morse potential interactions between particles were reported for two related models [18, 19] differing in the exact form of the self-propulsion and friction terms which we referred to as the linear and the cubic models. The self-organized states reported for these models coincided only partially. A more systematic comparison was difficult since the parameters defining the self-propulsion and friction strength in the two models differed even dimensionally. However, parametrization in terms of the three characteristic times  $t_{kin}$ ,  $t_{rel}$ ,  $t_{pot}$  introduced in [24] and utilized in the present paper in the form of the dimensionless rates  $\gamma_1$  and  $\gamma_2$  allows a unique mapping between the models. With this model-free parametrization, the observed low-energy states, their relative basins of attraction, stability, and the lifetimes of the transient random droplet state are essentially the same for the two models. One is tempted to consider this behavior as generic pertaining to a class of SPP models with Morse potential interaction.

Our linear stability results, when coupled to our extensive numerical simulations of swarms and their relaxed states, make for nonlinear stability statement on flocks and rigid rotation states: our coherent flock states appear linear and nonlinearly stable with a broad basin of attraction; rigid rotation states are linearly unstable, but saturate into neighboring nonlinearly stable states, which have

a reduced though still significant basin of attraction. The mathematical literature on this aspect of our work is extensive. Noteworthy is a rigorous result [25] on the nonlinear stability of flocking states under generic interaction potentials (Morse-type interactions included): it is shown that, under conditions which are satisfied by our flocking states, linearly stable flocks are also non-linearly stable over a broad range of perturbations, in the sense that a perturbed flocking state will relax to a neighboring flocking state (with say a displaced center of mass, or differing orientation of the mean velocity). Beyond certain limits, the authors note that perturbations can lead the system into a chaotic state (our random droplet state) where the mathematics is inconclusive about the relaxed state. Our numerical experiments provide implicit confirmation of the nonlinear stability results as they map out channels for relaxation of swarms when significantly perturbed away from the flocking states. They also set stringent conditions on the saturated states of unstable rigid rotation regimes which we hope will inspire equally rigorous mathematical treatments. Dynamical modeling that would cleanly map out our observed basins of attraction and the behavior in and around them is of course the ultimate desired goal.

It was mentioned that the stochastic dynamics of the order parameter resembles an advection-diffusion equation in the Langevin form. An important difference is related to the nature of the noise. Whereas the thermal noise is completely defined by the fluctuation-dissipation theorem which is rooted in the equilibrium statistical mechanics, the noise properties in the case of the swarm evolution are very poorly understood. The noise cannot be properly referred to as thermal, and there is no known equivalent of the fluctuation-dissipation theorem. The observed amplitude of the noise term depends rather strongly on the order parameter,  $s$ , but not on the control parameter  $\gamma_1$ . Further understanding of the

noise properties would require an evaluation of its time correlation function but this program falls outside the scope of the present work.

A question which is commonly posed in the context of self-organized dynamic systems concerns the existence of a general extremal principle that would allow one to predict the steady states. Starting from the early works of Prigogine and his school the rate of entropy production was proposed as a suitable candidate [26]. In the context of linear non-equilibrium thermodynamics minimum entropy production principle was shown to be consistent with Onsagers relations. Recently, Vicsek et al [27] proposed the use of this principle to explain the self-organized states in driven and self-propelled systems including flocking phenomena. On the other hand, the maximum entropy production principle was also proposed and used successfully in a broad range of out-of-equilibrium situations [28, 29]. It is understood that the two principles are not incompatible but rather refer to different types of additional constraints [29]. In our case, it is not clear what would serve as an analogue of constraints (fixed forces or fixed fluxes) appearing in a general non-equilibrium thermodynamics formulation. The entropy production is easily evaluated as the power dissipated by the friction forces, so one can test which principle is applicable by following the time evolution of the entropy production over the simulation trajectory. Interestingly, during the first short stage of the evolution starting from random initial conditions, the entropy production generally drops and stabilizes once the droplet state is formed. However, when at much longer times the droplet transits to one of the true steady states, the entropy productions goes up. In this sense, both principles are alternatively at work at different stages of self-organization.

# Chapter 3

## Leader-Follower Dynamics in a Confined Space

### 3.1 Background

In the previous chapter we have studied a class of agent based models of self-propelled particles (SPP-models). We have investigated the characteristics of the emerging steady states. These and other models studied in the literature [13, 12, 16, 18, 30], have achieved their initially set goal of reproducing typical patterns of collective behavior observed in nature. They also succeeded in proposing the necessary ingredients to achieve cohesion and coordinated motion. From the point of view of a physicist, these models are attractive out-of-equilibrium systems that do not satisfy the fluctuation-dissipation theorem ("active matter"). They form the ground for building new tools with predictive power or at least finding relevant approximations that make the problem solvable using the well-developed tools of equilibrium thermodynamics [22, 31, 32]. However, the validity of the assumptions of these models remains unclear, both from the

behavioural point of view and in terms of quantitative agreement between outcomes and empirical data. With the tremendous technological developments in tracking and recording positions and velocities of agents, the recent trend is to re-examine these assumptions through experimentally based-behavioural analysis and modeling.

Observations of species that exhibit schooling tendencies have started in 1927 with Parr [33]. Later, pelagic fish of the Baltic Sea and Atlantic Ocean [34], coral-fish in the Californian Gulf [35] and many fresh water fish have been investigated addressing the questions of which/why schooling patterns emerge in natural conditions. Nowadays, increasingly accurate sonar techniques, such as the multi-beam sonar, the advent of ocean acoustic wave-guide remote-sensing technique and high-frequency sonar imaging technique, are being implemented to track the behaviour of species in a wide range of natural environments [36, 37, 38, 39]. On the other hand, different sorts of controlled experiments on fish, insects, bacteria, pedestrians in crowds and many others are now plausible and are added to a rich tradition of observational techniques deployed in the subject [8, 40, 9, 41]. Although, laboratory experiments cannot capture the full diversity of the behaviour seen under natural conditions, it allows experimentalists to isolate key features of collective behaviour [42, 43, 44, 45]. They wish to understand both the collective structures that obtain and the mechanisms that drive it with an increasing focus on behavioral zones of interaction and on notions of leadership within the collection of involved organisms. Does each agent interact with every other agent in the group all the time? What minimum number of interacting neighbors the model must allow for to guarantee cohesion? Are there informed agents in the group that lead change?

The range of interaction of a given agent and the number of agents it in-

teracts with, have been modified in accordance with experiments and real life observations. For example, the biologically relevant blind sensory zone is added to existing models [46]. Several hypotheses of interaction zones, namely metric [47, 48] (individuals interact only with others within some fixed distance  $R$ ), topological [49, 50] (individuals interact with nearest neighbours) or dynamic neighbourhood [51] (based on visual and other sensory perception cues) are competing for validation. The metric neighbourhood fails the first test of keeping cohesion in swarms with low density. The topological neighbourhood, which may be achieved either by considering fixed number of neighbours according to their proximity, or by using the first shell of Voronoi tessellation [42, 52], remains invariant with respect to density changes and has proved to lead to robust cohesion of school under predation. However, some observations and experiments have verified that neither metric, nor topological interactions correctly account for the visual information employed when making movement decisions, and thus may overestimate the local redundancy in the group [53, 54]. A simple justification for using visual perception of neighbours in schools of fish is that schools of fish are observed to break down at night. More robust justifications come from ecological and physiological studies that prove vision to be the main sensory channel involved in schooling [55, 56]. There is growing evidence that visual models outperform topological and metric models when it comes to explaining data, but they increase the mathematical complexity of the problem by explicitly including discontinuous interactions. The number of neighbors with which a given agent interacts differs drastically over time allowing for interesting dynamics.

On the other hand, there is growing research trying to understand various aspects of leadership within animal groups. How are the members of a swarm affected by an informed Leader? How is an informed Leader distracted by the



social influence from other agents? How many informed agents are required to orient a group of a given size and properties? Various leader-following variations of models existing in literature are studied. In [57], the original Viscek model is modified by adding what they call a 0-agent which has a fixed direction of motion and acts as a Leader. It is proved that the members of the n-agents group all eventually follow their Leader under certain conditions. In [58], using a simple model, it is revealed that the larger the group the smaller the number of informed agents required for guiding the group. On the other hand, in [59] it is experimentally demonstrated that decision making in groups of animals is collectively built from individual choices that balances between personal information (based on their past experience) and social information (based on the behavior of other individuals). Yet another intriguing problem thought to be related to the notion of a leader is the intermittent behavior of fish schools whereby the group suddenly switches between near-steady states of motion without any apparent change in the external environmental parameters. The interplay between following and non-following the Leader and the numerous factors influencing the final outcomes have remarkable importance in many interdisciplinary fields related to human behavior like psychology, politics, sociology and others.

With all of the above in mind we propose a model, that is too simplified to be realistic, but which considers realistic components of the interaction mechanisms favored by controlled experiments on groups of fish. Namely it implements the biologically relevant field of vision interactions, confines the fish inside a closed boundary and studies the Leader-Follower dynamics. In contrast with the model studied in the first chapter in which each agent interacts with all other agents in the swarm, here we restricted the interactions to be with agents that fall in the field of vision of the agent under consideration. Moreover, the agents here

are confined to move inside a circular rim with harsh reflective boundary conditions (angle of incidence=angle of reflection). We further split members of the group into Leader/mean field of the organized school, and a single follower responding to the (mean)-field of the Leader. The model functions at the interface between mathematical billiards [60, 61, 62, 63], now generalized to allow for interactions between multiple particles, event driven dynamical systems, discontinuous dynamical systems [64, 65] and the sociology of human control in confinement [66, 67, 68, 69, 70]. The upshot of the results of this study is the seeming inevitability of straying from the Leader for a specific range of values of the control parameter, in the presence of confinement and a persistent drive for alignment. The Follower falls into interesting unexpected attractors away from the Leader. What are the properties of these attractors? Are they chaotic attractors or integrable limit cycles? Over what range of values of the control parameter is every attractor defined? What happens at transition points between attractors? Is the observed behavior robust under model variations? What is the relevance of the obtained results on various interdisciplinary fields of study? This chapter addresses these and other questions and is organized as follows: the first section describes the model, the second gives the characteristics and the basins of attraction of the emerging states, and the third tests robustness of the results under variations to the model. Eventually we close with a section summarizing basic conclusions, their relevance to different fields and insights for future work. A detailed description of the numerical experiments performed is given in the appendix.

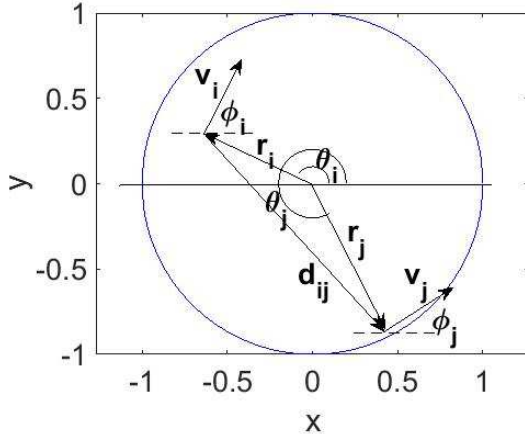


Figure 3.1: **Model Description.** The position, orientation, and velocity of fish  $i$  are given by  $\vec{r}_i$ ,  $\theta_i$ , and  $\vec{v}_i$  respectively.  $\phi_i$  is the angle between  $\vec{v}_i$  and the  $x$ -axis, while the relative position between fish  $i$  and  $j$  is given by  $d_{ij}$ .

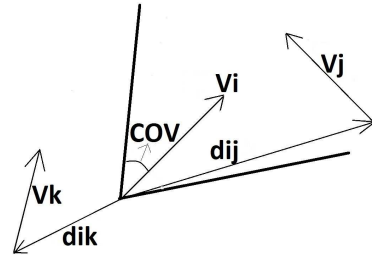


Figure 3.2: **Definition of COV.** Two symmetric rays are cast from the position of the  $i$ -th fish; its  $COV$  is defined as the angle between the ray and its velocity vector on either sides; fish  $j$  is perceived while  $k$  is not.

## 3.2 The Model

Fish in our model are point particles with coordinates  $(r_i, \theta_i)$ , moving with a velocity vector  $\vec{v}_i$ , of constant magnitude  $v$ , and varying direction  $\phi_i$  measured from the positive, horizontal  $x$ -axis (Fig. 3.1). They move inside a tank with an elastic reflective circular boundary. A fish interacts and tries to align only with fish that are in its Cone of Vision (COV)(Fig. 3.2), a biologically motivated alternative to topological interaction with Voronoi neighbors considered in [42]. A fish's angular velocity  $w_i$  is adjusted according to the average behavior of members of the collective who happen to be in its cone of vision:

$$\frac{dw_i}{dt} = -\frac{v}{\xi} (w_i(t) - w_i^*(t)), \quad (3.1)$$

where,

$$w_i^* = \frac{1}{N_i} \sum_{j \in COV_i} \kappa \sin(\phi_j - \phi_i). \quad (3.2)$$

Here  $\xi$  is a persistence length scale,  $COV_i$  the cone of vision of fish  $i$ ,  $w_i^*$  is the angular velocity that drives alignment with the neighbors for a given coupling strength  $\kappa$ . The present model is a radically simplified variant of the model in [42], having dropped attraction and noise from the picture. Now comes a critical feature of our exercise which consists of further quenching dynamics down to two entities interacting in Leader-Follower configuration. The Leader moves along the vertical diameter of the circular boundary where it reflects elastically and is not affected by the Follower. The Follower tries to align with the Leader whenever it is in its cone of vision and also reflects elastically from the walls. The motion of the Follower satisfies Eq. 3.1 and 3.2 with the Leader being the only other particle it interacts with. We express these equations in dimensionless form, with the characteristic timescale  $\tau = \frac{\xi}{v}$  (the time taken by the fish to adjust its angular velocity) and length scale  $R$  (the radius of the tank). Thus the non-dimensional update equations for the angular velocity and the position of the Follower  $\omega(t)$  are now given by:

$$\begin{aligned}
\frac{dw}{dt} &= -(w(t) - w^*(t)) \\
\frac{d\phi}{dt} &= w(t) \\
\frac{dx}{dt} &= C_2 \cos(\phi(t)) \\
\frac{dy}{dt} &= C_2 \sin(\phi(t))
\end{aligned} \tag{3.3}$$

with

$$w^* = \begin{cases} C_1 \sin(\phi_L(t) - \phi(t)) & \text{if Leader is inside COV} \\ 0 & \text{otherwise} \end{cases}$$

where  $C_1 = \tau\kappa$  (ratio of time taken by the fish to change its orientation to the time it takes the Follower to get affected by the leader),  $\phi_L(t) = \pm\frac{\pi}{2}$  and  $\phi(t)$  are the orientations of the velocity vectors of the Leader and the Follower

respectively, and  $C_2 = \frac{v\tau}{R}$  (ratio of the time needed to change orientation to the time needed to cross the radius  $R$ ). The space of parameters is thus reduced to  $COV$ ,  $C_1$  and  $C_2$ . In the rest of this paper, we consider  $C_1 = 1$  and  $C_2 = 0.006$  consistent with the values of  $\xi$ ,  $R$  and  $v$  favored in [42], and we vary the cone of vision (COV).

### 3.3 The Attractors

Within this greatly reduced phase and parameter space, we were surprised by the rich, unfamiliar, and deeply significant behavior that remains possible. We had left ourselves with one single parameter (COV) with which to map out the dynamical evolution of one single member which is seeking reunion with the group, while bouncing from the boundary of their mutual confinement. Varying that parameter, we explored random initial conditions for the follower on the boundary (the leader in these experiments is initially set at the base of the vertical diameter heading up), noting steady state behavior, to the best of our computational abilities and resources.

In the following subsections we describe each of the obtained states, their characteristics and their basins of attraction. To do so we borrow tools from “billiards” literature; namely we consider the bounces with the circular boundary rather than tracing the actual trajectories. The  $n^{th}$  bounce is represented by its angular position ( $\theta_n$ ) and by the tangential momentum  $p_n = \cos(\alpha_n)$ , where  $\alpha_n$  is the angle between the direction of the velocity vector after impact ( $\phi_n$ ) and the forward tangent to the boundary and is given by:  $\alpha_n = \phi_n - \theta_n - \frac{\pi}{2}$ . In billiards literature obtained orbits are classified into: 1) Closed orbits where the

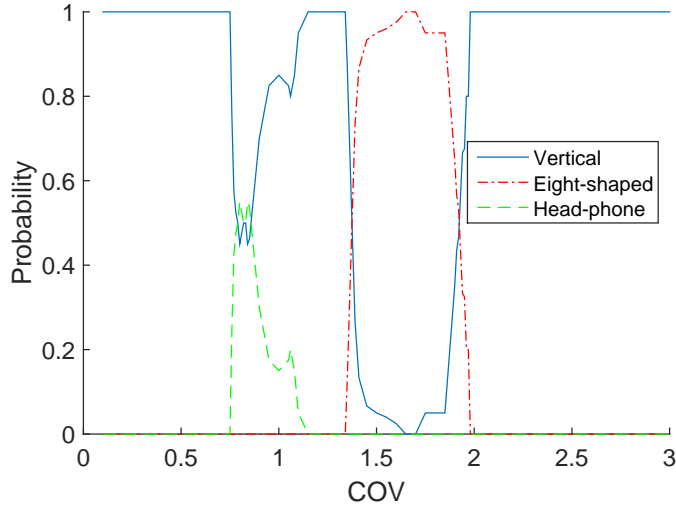


Figure 3.3: **Basins of attraction of steady states as a function of the cone of vision (COV).** For small and large COV the dominant state is the vertical attractor. For intermediate values of COV the head-phone and the eight-shaped attractors are obtained with different probabilities as a function of COV.

trajectory repeats itself after  $N$  bounces. These orbit are represents by  $N$  points in  $(\theta, p)$  phase space and they can be stable, neutrally stable or neutrally stable; 2) orbits that correspond to invariant curves in phase space and which occur only when the dynamics is governed by a constant of motion  $F(\theta, p)$ ; 3) orbits that fill an area in phase space, and this occurs when the motion in unrestricted by a constant of motion, and there is chaotic behavior with sensitive dependence on initial conditions. We use this classification to discuss soe of the properties of the attractors we obtain.

### 3.3.1 Vertical Attractor

In this case and after a series of bounces off the boundary, the follower gradually approaches the leader on its diameter. Full alignment with the leader is achieved asymptotically. While such an alignment is naturally expected for large enough

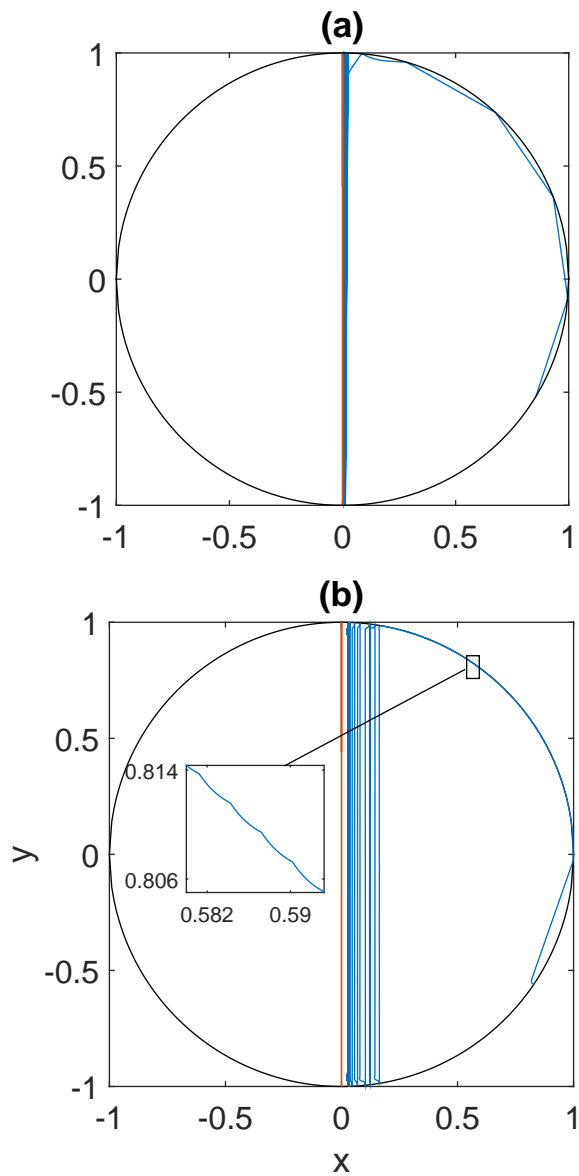


Figure 3.4: **Vertical Attractor.** (a) For small  $COV$ , the Follower hits the boundary at different angles before getting attracted to the Leader,  $COV = 0.4$ ; (b) for Large  $COV$ , the Follower aligns with the Leader and moves parallel to it after a very short transient. At each reflection, the Follower gets closer and closer to the vertical attractor. The inset enlarges the bounces at the boundary,  $COV = 2$ .

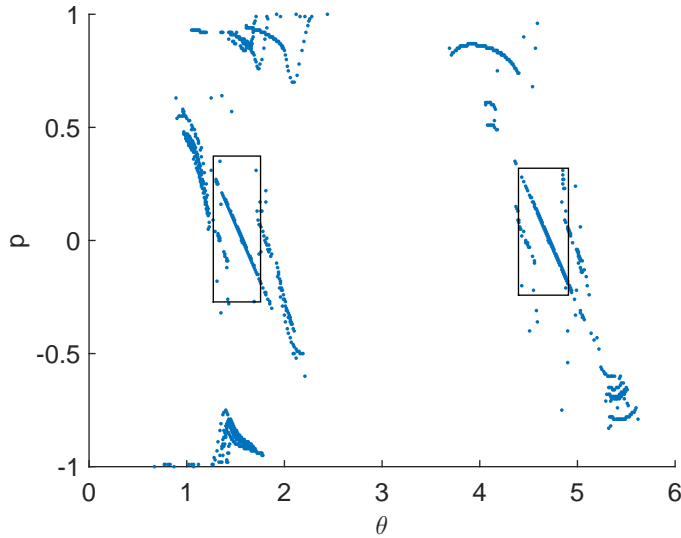


Figure 3.5: **Phase space  $(\theta, p)$  for trajectories approaching the vertical attractor.** The boxes highlights the fact that the last part of the trajectory is along 2 straight lines of equations  $p = -\theta + \frac{\pi}{2}$  and  $p = -\theta - \frac{\pi}{2}$  respectively.  $COV = 2.1$

cones of vision, it is quite surprising that it is also achieved for blindly small ones. Indeed alignment with the Leader is the favored outcome for  $COV < 0.75$ ,  $1.1 < COV < 1.3$  and  $COV > 2$  (Fig. 3.3). For narrow  $COV$ , the Follower hits the boundary at a spread of angles before it aligns with the Leader and eventually gets attracted to it (Fig. 3.4a). For large  $COV$ , the Follower directly aligns with the Leader and asymptotically approaches the vertical diameter with each reflection at the wall (Fig. 3.4b). The trajectories in  $(\theta, p)$  phase space approach two points  $(\frac{\pi}{2}, 0)$  and  $(\frac{3\pi}{2}, 0)$  along straight lines of equations  $p = -\theta + \frac{\pi}{2}$  and  $p = -\theta - \frac{\pi}{2}$  respectively (Fig. 3.5). Thus, transients aside, this attractor is approached along the second type of orbits discussed above; i.e. along an invariant curve in phase space with the dynamics governed by a constant of motion  $(p + \theta)^2 = (\frac{\pi}{2})^2$  which is verified in the appendix.



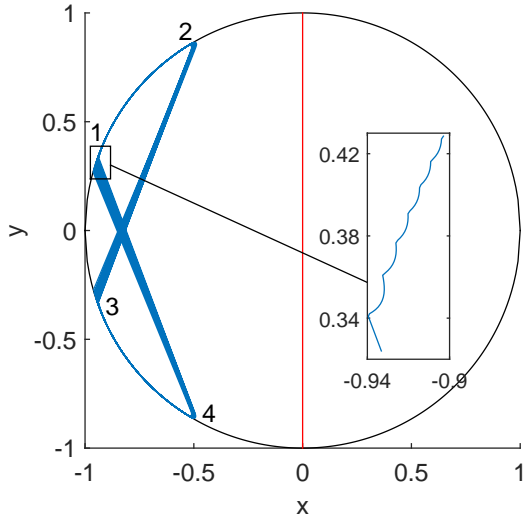


Figure 3.6: **Left Eight-shaped Attractor**. The Follower reflects at point 1 to find that the Leader is moving upward, and thus get turned counter-clockwise upward to hit the boundary. Each time the Follower reflects from the boundary it sees the Leader and get turned upward again. The Follower bounces off the boundary between points 1 and 2 (as shown in the inset). At point 2 the Follower reflects to find that the leader is moving downward and thus gets turned clockwise downwards. As it turns downwards the Leader falls outside its COV and thus it continues to move in a straight line to hit point 3. As the Follower reflects at point 3, it finds that the Leader is still moving downwards and thus get turned clockwise to hit the boundary. The Follower undergoes another series of bounces off the boundary between points 3 and 4. At point 4, it reflects to find the Leader moving up and thus it gets turned counter-clockwise until the Leader falls outside its COV so it continues in a straight line to reach point 1. The vertical diameter is the trajectory of the Leader.  $COV=1.7$ .

### 3.3.2 Eight-shaped Attractor

A sample is shown in Fig. 3.6; it obtains for  $1.3 < COV < 2$  and is dominant for  $1.5 < COV < 1.7$  (Fig. 3.3). After a short transient, the Follower is eventually trapped in an eight-figure, which interleaves numerous short bounces off the boundary (with the Leader in sight after each bounce) with long range flights at points where the Leader reverses direction at the the boundary. Take-off and landing points (4 in total, making for the anchors of the eight-figure see Fig. 3.6)

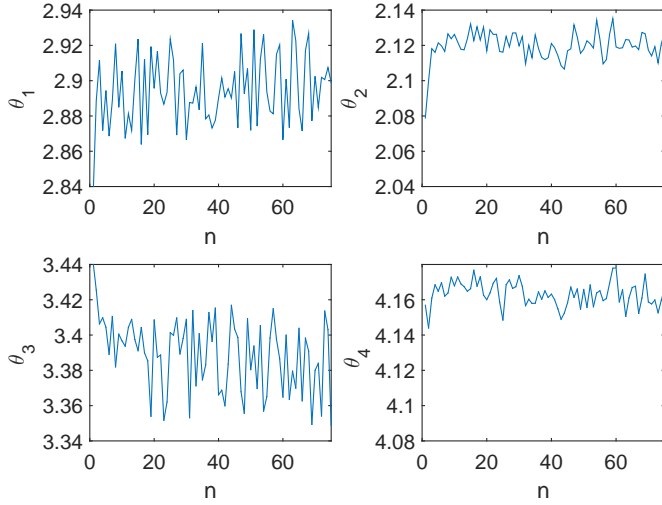


Figure 3.7: **Variation of the angular positions of the 4 vertices of the left eight-shaped attractor (shown in Fig. 3.6) for consequent hits  $n$ .** (a) Angular position of vertex 1;(b) angular position of vertex 2;(c) angular position of vertex 3;(d) angular position of vertex 4.

fluctuate about mean vertices (Fig. 3.7), with the cycle replaying while never exactly repeating. The magnitude of these fluctuations decreases as COV increases (Figs. 3.8 and 3.9). The obtained eight-shape is symmetric with respect to the x-axis and can occur either on the right or on the left of the vertical diameter. Therefore, and without any loss of generality, it can be characterized by the two neighboring anchors (1 and 2). Note that the follower approaches anchor 1 in a straight line and is curved after reflection, while it leaves anchor 2 smoothly after moving tangent to the boundary for a short time. The smoothness or sharpness of the turns at 2 is a function of the ratio of  $C_1$  to  $C_2$  which we fix in our simulations (unless otherwise indicated). As COV increases anchor 1 moves closer to the x-axis while anchor 2 doesn't move much (Fig. 3.9).

In the proximity of  $COV = 1.34$  (smallest  $COV$  for which a steady eight-shaped attractor appears), the Follower lingers between right and left eight-

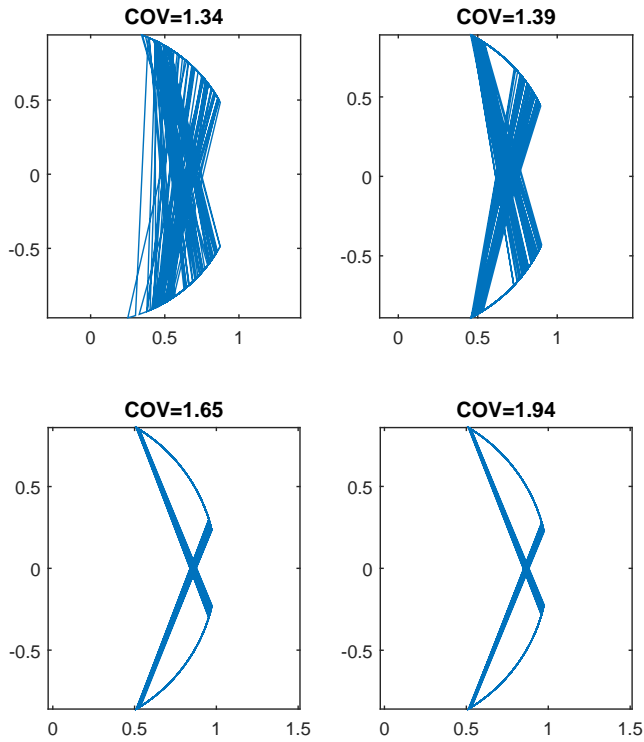


Figure 3.8: **Evolution of the eight-shaped attractor at different values of COV.** We observe that it becomes thinner and wider as COV increases.

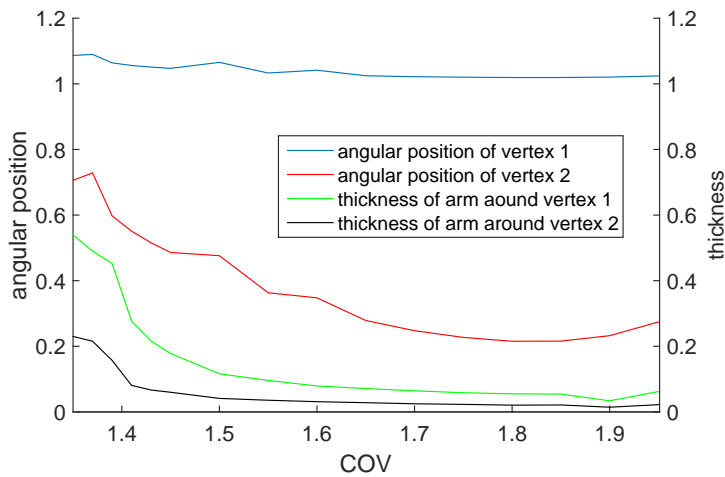


Figure 3.9: **Characteristics of Eight-figure.** The angular position of vertex 1 of the Eight-figure is almost constant for all COV (blue), that of vertex 2 decreases (red). The thickness of the arm holding vertex 1 is always larger than that holding vertex 2, but they both decrease as COV increases.

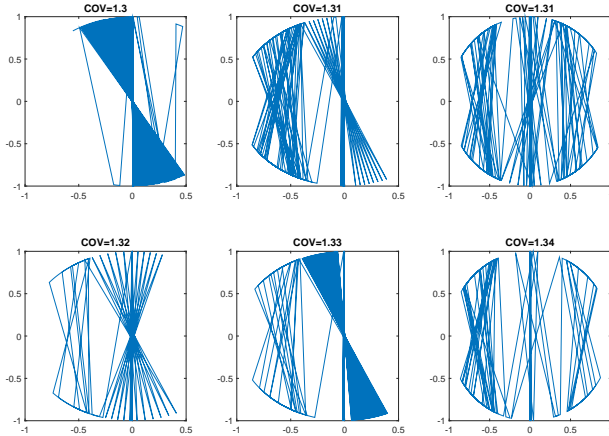


Figure 3.10: **Transition from the vertical attractor to Eight shape.** The eight shape is stable for  $COV > 1.34$ , for values of  $COV$  between 1.3 and 1.34 the follower jumps between left and right eight-shaped attractors and nearly central back and forth before ending up at the vertical attractor.

shaped attractors and jumps along nearly central paths before ending up on the vertical attractor (Fig. 3.10). The transition in and out of this trap with varying  $COV$  is mapped by following the angular separation between the mean position of neighboring anchors (1 and 2, or their symmetric counter-parts, 3 and 4) as function of  $COV$ . Shown in Fig. 3.11 is the mean angular separations  $A_{12}$  (between 1 and 2) as a function of the cone of vision ( $COV$ ), averaged over all cycles in a given trajectory, and over the subset of the 50 different trajectories that belongs to this particular attractor with different initial conditions, and the same ( $COV$ ). Near zero value of  $A_{12}$  (or  $A_{34}$ ) means that the follower is hitting the upper (or lower) part of the circular tank at very close points, and that the follower is approaching the vertical attractor. For small enough cones of vision  $A_{12}$  is small; with increasing  $COV$ , a transition point is hit beyond which  $A_{12}$  increases smoothly. The vertical attractor has now given way to an increasingly well defined eight-shaped attractor. The latter dominated with increasing  $COV$

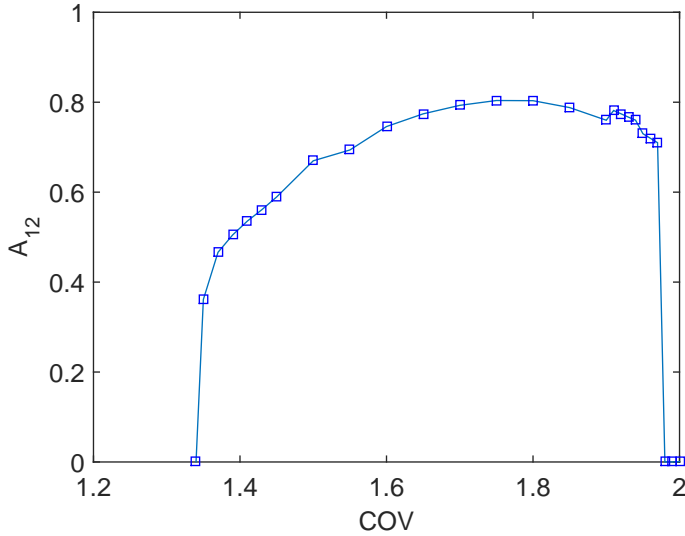


Figure 3.11: **An Order Parameter for the Eight-figure.** The orbit averaged angular separation  $A_{12}$  between vertices 1 and 2 of Fig.1c provides a clean order parameter with which to map the eight-figure phase with increasing  $COV$ . We display the mean value of  $A_{12}$  over all cycles in a given trajectory, and over 50 trajectories with varying initial conditions, and the same  $COV$ . Near zero values of  $A_{12}$  indicate that the follower is hitting the upper (hence the lower) part of the circular tank at neighboring points, and that the follower is thus approaching the vertical attractor. Increasingly larger values of  $A_{12}$  indicate an increasingly well defined eight-figure attractor. Transition in and out of the eight-figure attractor is evident at  $COV \sim 1.3$  and  $COV \sim 2$  respectively.

till another sharp transition is hit, now resulting in a sudden drop in  $A_{12}$ : the follower now has a broad enough cone of vision to escape the eight-figure trap, and find its way to the leader on the vertical attractor. The curve reflects the change in the properties of the eight-shaped attractor by itself and the abrupt transition doesn't include coexistence effects. The value of  $COV$  at which this drop occurs is a critical value since beyond it the Follower is bound to get attracted to the Leader. This critical value depends on the parameters  $C_1$  and  $C_2$ , and can be used as an indication for the minimum field of vision needed to be always attracted to the mean field guaranteeing no stray fish.

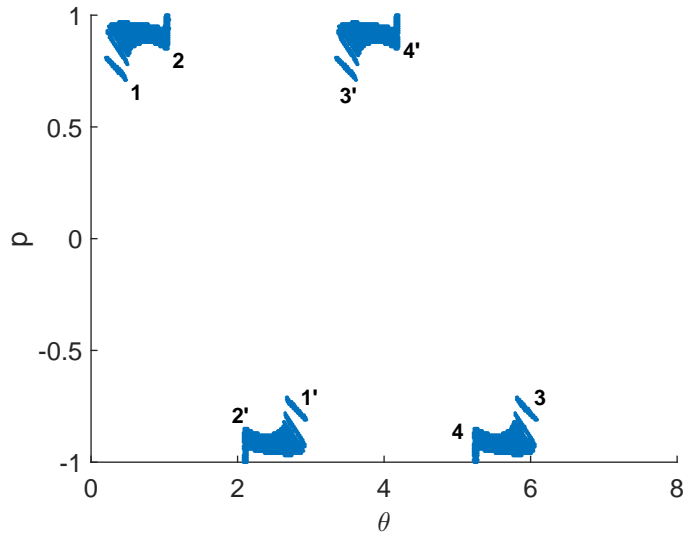


Figure 3.12:  $(\theta, p)$  phase space for eight-shaped attractors. The transients are removed and the trajectories on the eight-shaped attractor are drawn in the  $(\theta, p)$  phase space for the subset of the 50 initial conditions that lead to the eight-figure for each value  $COV \in [1.5, 1.55, 1.6, 1.65, 1.7]$ . Points 1(1'), 2(2'), 3(3') and 4(4') represent the vertices on the right(left) eight-shaped attractor.

Trajectories falling into the (right or left) eight-shaped attractor, obtained for  $1.5 < COV < 1.7$ , are drawn in  $(\theta, p)$  phase space shown in Fig. 3.12. We neglect the transients and notice that each eight-shaped attractor is divided in two thick curves in phase space, corresponding to hits with the upper and lower parts of the boundary respectively. The thickness of the trajectory in phase space (consistent with the fact that the orbit is repetitive but no periodic) indicates the presence of chaos.

### 3.3.3 Head-Phone Attractor

The eight-figure attractor is not alone in trapping the follower in an evading behavior. Another even more curious regime of control away from alignment

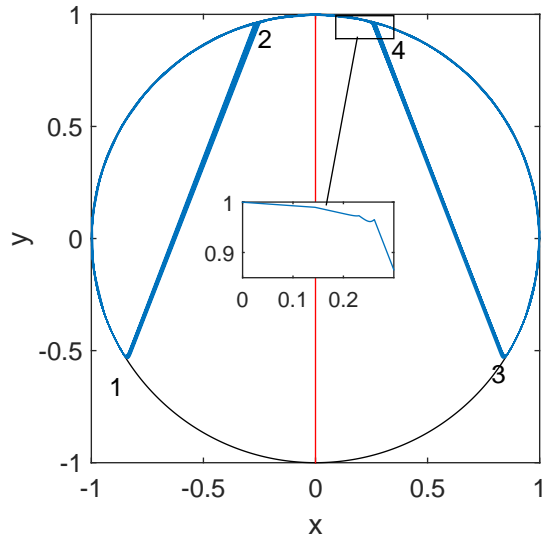


Figure 3.13: **Head-phone attractor**. Starting at a point on the upper left part of the circular boundary, the Follower bounce off down the boundary until it reaches point 1. When the Follower is at point 1, the Leader reflects from the boundary switching its direction of motion and thus causing the Follower to rotate counterclockwise. As the Follower rotates the Leader is no more in its cone of vision and thus the former moves in a straight line towards point 2. At point 2, the Follower reflects from the boundary and is rotated counter-clockwise by the Leader which is now in its *COV* and is still moving up. Soon the Leader switches direction and starts moving down at this instant it is out *COV* of the follower which is grazing the boundary with nearly tangent bounces. When the follower gets to the lower part of the circle, the Leader falls back into its *COV* and this causes it to rotate counterclockwise every time it bounces off the boundary. When the Follower is at point 3, the Leader switches direction up thus causes the former to rotate clockwise. As the Follower rotates, the Leader is no more in its *COV* and so it continues in a straight line towards point 4. At point 4, the Follower reflects and is then rotated clockwise since the Leader is still moving up, the inset shows the reflection at point 4. Soon the Leader switches direction and start moving down. The Follower, which is now in the lower part on the circle, bounces off the boundary and is rotated clockwise at each reflection until it reaches point 1. The cycle repeats itself. The red and the blue curves represent the trajectories of the leader and the follower respectively.  $COV = 0.85$ .

appears for a narrow range of the COV ( $0.76 < COV < 1.1$ ) (Fig. 3.3). We called it the head-phone attractor ( Fig. 3.13 shows an example for  $COV = 0.85$ ) . A distinctive feature of this attractor is that the Follower spends much of its time tangent to the boundary. Similar to the eight-shaped attractor, this attractor is repetitive, without showing signs of relaxation into a periodic limit cycle. A strange attractor of sorts, its full structure remains to be unraveled. Increasing  $COV$  from zero, the head-phone attractor first appears for  $COV = 0.76$  and disappears beyond  $COV = 1.1$ . In the proximity of these two critical values of  $COV$ , central trajectories are favoured (similar to the case of eight-shaped attractor around transition, see Fig. 3.14) and occasionally the Follower jumps between the upper and the lower head-phones before relaxing to one or ending up on the vertical. The shape of this attractor changes as a function of the  $COV$  (Fig. 3.15). We quantify this evolution with the angular separation between vertices 2 and 4 ( $S_{24}$ ), which appears to increase linearly with  $COV$  (Fig. 3.16).

The trajectories of the (upper and lower) head-phone attractor in the  $(\theta, p)$  phase space are shown in Fig. 3.17. They intersect the tangent paths ( $p = \pm 1$ ) and have some thickness indicating chaotic behavior.

### 3.3.4 Periodic Solutions

The periodic solutions are of considerable interest to the billiards problem although they typically contribute a set of measure zero. Here we discuss them for the sake of completeness. It is intuitively clear that strictly periodic trajectories regime keeps the leader forever in the blind zone. If the Follower starts at the circumference with initial velocity heading along the diameter, it can stick to that diameter forever provided its  $COV$  is small enough to keep the Leader



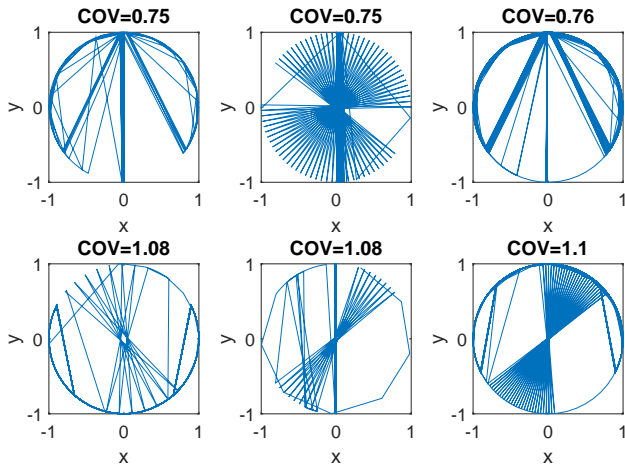


Figure 3.14: **Transition into and out of the Head-phone attractor.** The follower lingers between upper and lower headphone attractors and nearly central trajectories are favored around transitions into and out of headphone state.

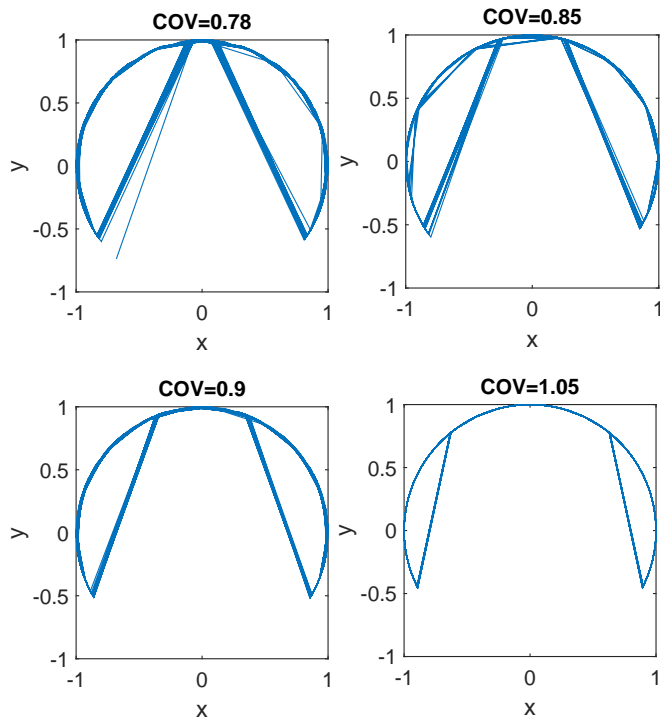


Figure 3.15: **Evolution of the Head-phone attractor at different values of  $COV$ .** It becomes thinner and wider as  $COV$  increases.

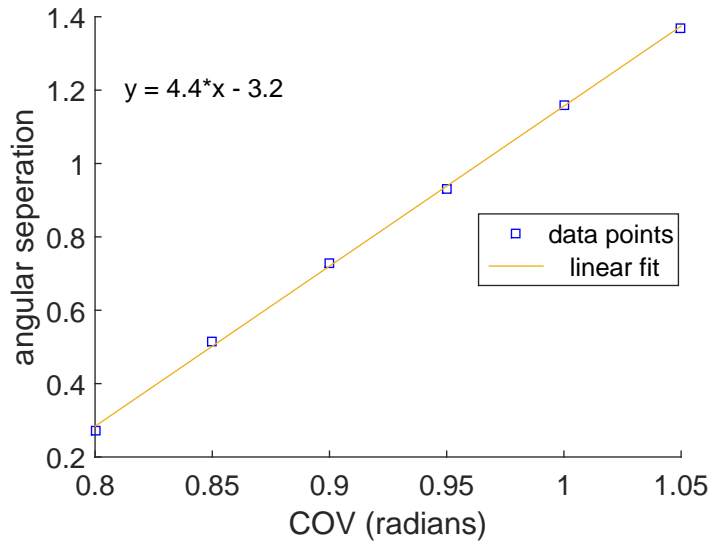


Figure 3.16: **An Order Parameter for the head-phone attractor.** The orbit averaged angular separation  $S_{24}$  between vertices 2 and 4 of Fig.3.13 provides a clean order parameter with which to map the head-phone attractor with increasing  $COV$ . We display the mean value of  $S_{24}$  over all cycles in a given trajectory, and over 50 trajectories with varying initial conditions, and the same  $COV$ .  $S_{24}$  increases linearly with  $COV$ , until it disappears at  $COV = 1.1$ .

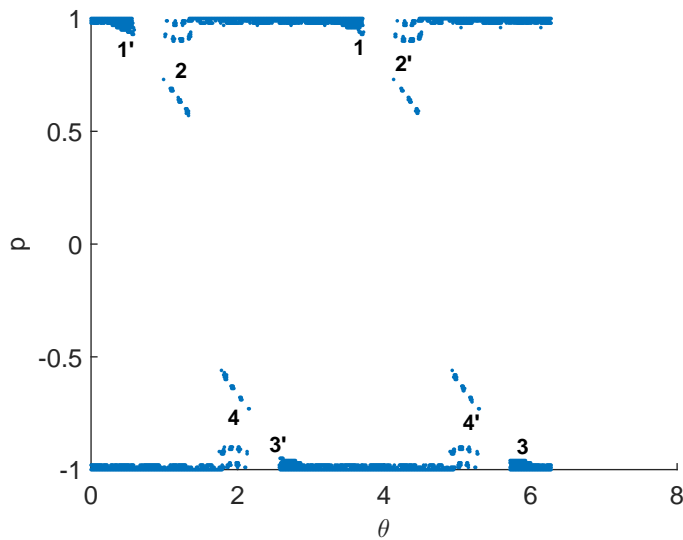


Figure 3.17:  **$(\theta, p)$  phase space head-phone attractors.** The transients are removed and the trajectories on the head-phone attractor are drawn for 50 initial conditions for  $COV \in [0.85, 0.9, 0.95, 1]$ . Note that the curves intersect the  $p=1$  and  $p=-1$  lines, which are the trajectories tangent to the boundary. Points 1(1'), 2(2'), 3(3') and 4(4') represent the vertices on the upper(lower) head-phone attractor.

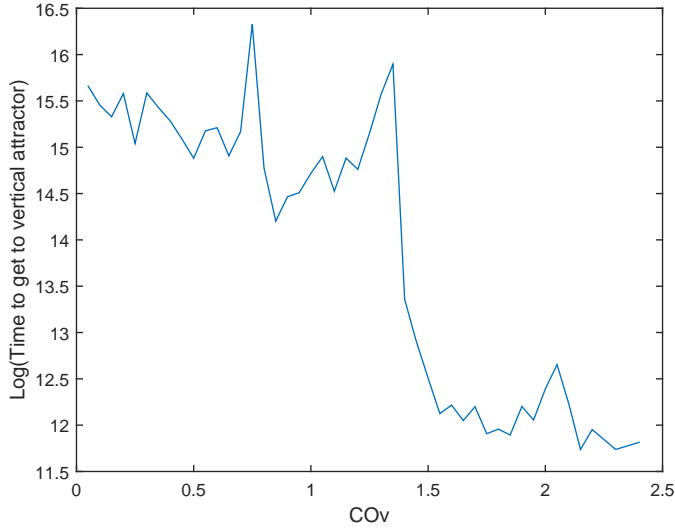


Figure 3.18: **Relaxation time to Vertical attractor.** The logarithmic scale of the time required to get to the vertical attractor as a function of COV. Three prominent peaks are observed at COV values corresponding to transitions between attractors.

permanently out of sight along that particular diameter. The critical angle  $COV_c$  below which the Follower never sees the Leader is given by:

$$COV_c = 2a \cos \left( \frac{\sqrt{1 + y_0}}{\sqrt{2}} \right) \quad (3.4)$$

where  $y_0$  is the initial y-coordinate of the follower on the circumference. For a free particle in a circular billiard, motion along inscribed polygons is stably periodic. Here, and as we argue below, the diameter, a degenerate two-gone, is the only classical periodic orbit that can survive the spell of the Leader. The two conditions to obtain such stable periodic orbits in our case, are to start the Follower along one side of the polygon and to have  $COV$  small enough that the Leader is never in it. While the first condition is easy to satisfy, the second is not, since it requires that the ratio of the side of the inscribed polygon to the radius to be a rational number and that is true only for hexagons (where the

side is equal to the radius of the circumscribing circle). It turns out that even for the hexagon, one cannot find a  $COV$  small enough to avoid the Leader at all times. If the Follower is started with the appropriate initial conditions (i.e make an angle  $\frac{\pi}{6}$  with the tangent), it moves on the hexagonal orbit provided that the Leader is initially outside its  $COV$ . However, before completing the second cycle the Leader will cross the side of the hexagon directly in front of the Follower, and thus the latter will see the former no matter how small  $COV$  is. The only periodic solution that is capable of escaping the Leader is thus the diameter, and it is a closed orbit represented by two points in the  $(\theta, p)$  phase space.

### 3.3.5 Phase diagram

The intervals of  $COV$  over which one state or the other dominates are summarized once more in the phase diagram of Fig. 3.3. There it is apparent that small and large  $COV$  favors the vertical attractor, while the headphone and eight shaped attractors obtain over intermediate values of the cone of vision. Not surprisingly the time needed for alignment with the vertical attractor is longest for the smallest cone of vision and shortest for the larger cone of vision (Fig. 3.18). At transitions between vertical, head-phone and eight-shaped attractors the follower lingers over numerous nearly central trajectories (Figs. 3.10 and 3.14) before settling on one regime or the other, resulting in a local spike in the time for alignment (if and when it obtains). We think that the appearance of nearly central (or diameter) trajectories around transition values of  $COV$ , namely at the interface between total alignment for all initial conditions and non-alignment for some initial condition, plays an important role to understand the dynamics of the obtained attractors.

The periodic nature of the motion of the Leader plays a key role in forming the eight-shaped and the head-phone attractors. The former has the same period as the Leader while the latter has double that of the Leader. Here one asks, is it possible to obtain an attractor whose period is any multiple or maybe any fraction times that of the Leader? Regardless of the existing dynamics, is there a finite set of shapes that are good candidates for being attractors under the given conditions? What are the characteristics of a good candidate? For now we know that a good candidate is symmetric with respect to the y-axis and/or the x-axis, since there is no reason to make one side of the axis different from the other. We can also say that the length of the circumference of a good candidate is a multiple (or a decimal fraction) of the distance crossed by the Leader in one cycle (4 times the radius). Both the head-phone and the eight-shaped attractors are formed of nearly tangent trajectories followed by free flights, is that a common feature for good candidates for attractors? Further investigation is required to fully answer the above questions.

### 3.4 Robustness To Model Variations

The important outcome of the above overview of final states is that, within a rather minimal set of assumptions, non-aligned, non-following, straying states have large basins of attraction over a relatively large range of the control parameter, the COV. Is this result specific to the studied model or is it recurrent in different variations of the model? In this section we overview intra- and inter-model variations, with the aim of answering the above questions of robustness.

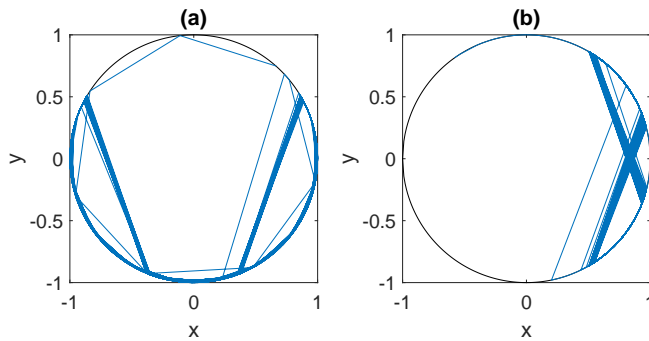


Figure 3.19: **Variation of model parameters.**  $C_2$  is changed to 0.01 instead of 0.006 and  $C_1 = 1$  is unaltered. The obtained states are the same but the occur over different ranges of  $COV$ . (a) Head-phoner attractor obtained at  $COV = 0.9$ ; (b) eight-shaped attractor  $COV = 1.6$ .

### 3.4.1 Initial Conditions/Model Parameters

For the same model parameters, rather than initializing the follower on the boundary, we initialized it at different positions and orientations inside the circle. This amounts to introducing an initial phase shift between the leader and the follower. Transients aside, the same pattern of steady states emerged, as a function of the cone of vision. On the other hand, the model parameters  $C_1$  and  $C_2$  were varied. In some cases the same exact states occurred but with changes in the ranges of  $COV$  over which they obtain, in other cases the shapes of straying attractors changed but the non-aligning behavior was still prevalent. Figure 3.19 gives some of the attractors obtained for different values of  $C_1$  and  $C_2$ . Therefore, non-alignment over a remarkable range of  $COV$  is preserved when varying the initial conditions and the model parameters.

### 3.4.2 The Leader as a group

One asks what exactly is the leader in the context of schooling, then of our model? Naturally, one can think of the leader as the effective mean field of an organized group of fish. Allowing for that, one then asks what is the fate of such a school on the vertical attractor and that of the follower in relation to it? We report that a school bouncing on a diameter maintains its cohesion through bounces provided that its members are initiated close enough to each other and symmetric with respect to the diameter (Fig. 3.20); moreover, that a follower relates to the mean orientation of the school as it would relate to the orientation of the single particle in the position of the Leader.

### 3.4.3 Leader along the rim

A natural periodic alternative to the diameter as a locus for the Leader's path is the basin's circular boundary. The Leader is set in counterclockwise motion along the rim, and the follower is started anywhere on the rim with random orientation. Similar to the case of the Leader on a diameter, the follower ends up following the Leader for small and large enough  $COV$ , and falling into non-aligned states for intermediate  $COV$ . For the same values of parameters  $C_1 = 1$  and  $C_2 = 0,006$ , 50 simulations with different initial conditions for the follower are used to obtain the probability of following or not following the Leader for each value of  $COV$ . Figure 3.21, which gives these probabilities as a function of  $COV$ , is qualitatively similar to its counterpart in the case with Leader on a diameter (Fig. 3.3).

Non-aligned states, include trajectories trapped between a caustic and the circular rim (similar to the case of a classical circular billiards) and irregular ro-

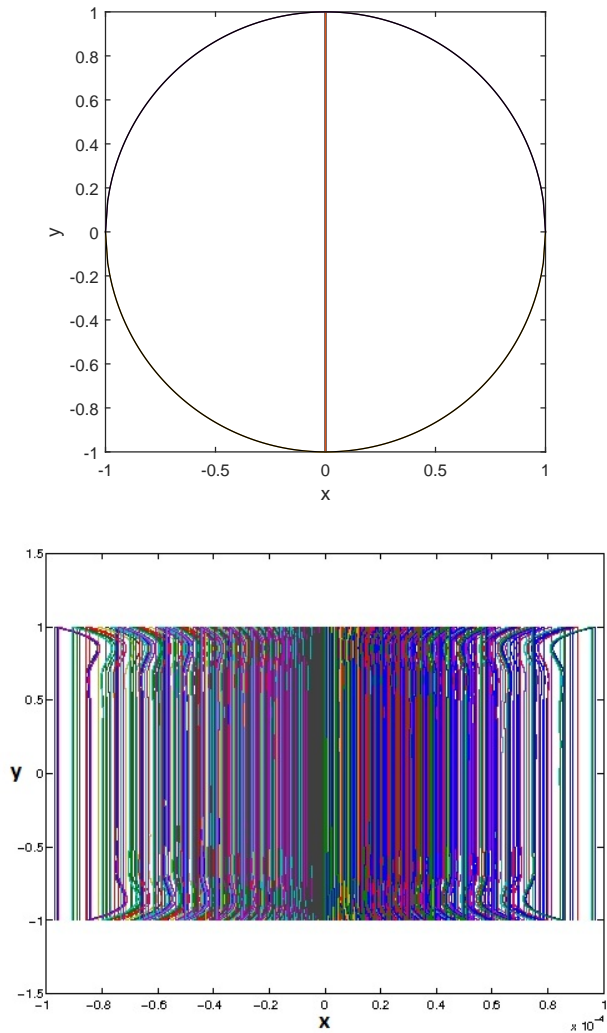


Figure 3.20: **Cohesion of a group started at the diameter.** 100 particles are initially started at the bottom of the diameter heading up. The initial positions are chosen such that the particles are symmetric with respect to the vertical diameter and are within a distance 0.0001 units of length. (a) At  $t_f = 10000$  units of time the group keeps its cohesion around the vertical diameter and all the 100 particles are still within the same distance of 0.0001 units of length; (b) zoom out of the trajectories of the 100 particles shown in (a).



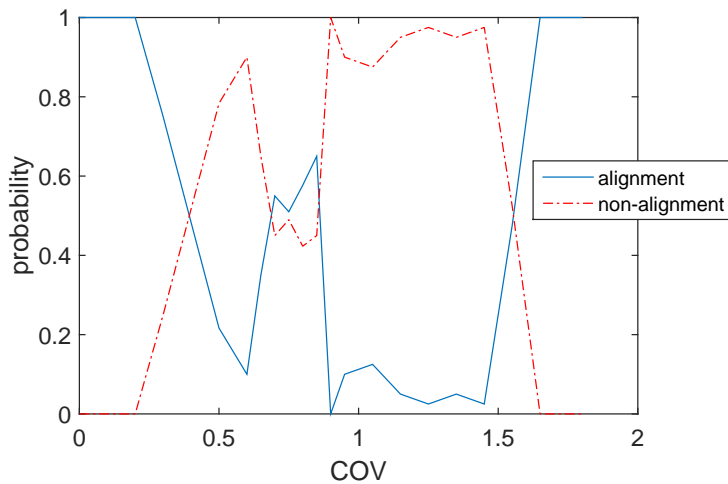


Figure 3.21: **Probabilities of being attracted to or escaping the Leader for the leader on the rim variation of the model.** The follower can escape the Leader in two ways: moving on a polygon (same as circular billiards with no interaction) or being trapped to the eight-like attractor described in Fig. 3.24.

tating variants of the eight-shaped attractor. Figures 3.23 and 3.24 give examples of what we call variants of eight-shaped attractors, they are similar in the sense that they are formed from paths tangent to the circular boundary and straight flights between two points on the boundary. Their shape evolve with  $COV$  as shown in Fig. 3.15 and the length of the tangent trajectory along the rim gets shorter as  $COV$  increases (Fig. 3.25).

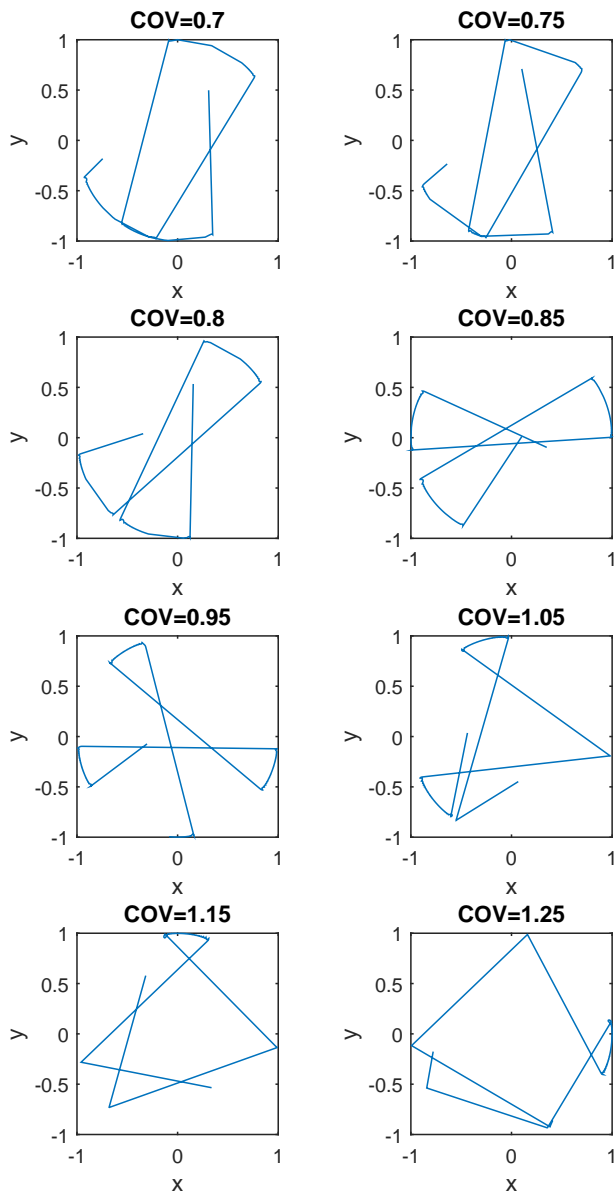


Figure 3.22: **Straying attractors for the leader on the rim variation.** This is part of the trajectory, only few hits are shown to illustrate the behaviour, a complete trajectory is given in Fig. 3.23. Note that the follower is trapped in trajectories where it moves nearly tangent for some time and then moves in straight line to hit the other side of the boundary. This is similar to the eight-shaped attractor of the initial model, with rotation superimposed. The angular distance which the follower covers nearly tangent to the boundary changes with  $COV$  and is given in Fig. 3.25.

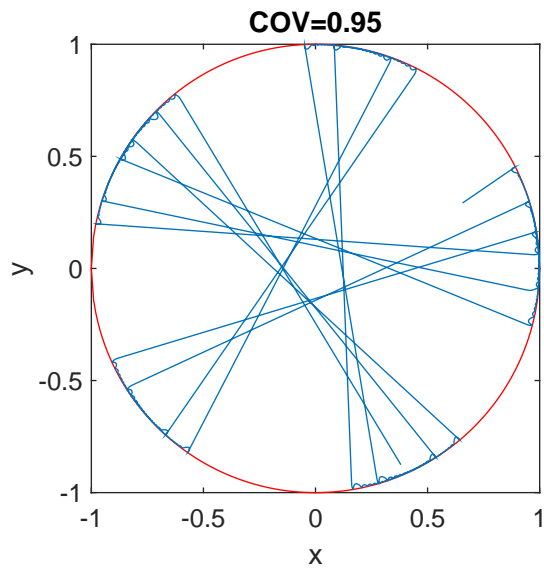


Figure 3.23: **Irregular rotating variant of Eight-shaped attractor obtained in the case of the leader on the rim variation.**

#### 3.4.4 Sharp Follower Response

In this case we perturb the original model drastically by replacing gradual relaxation of angular velocity with instantaneous adjustment to the angular velocity  $\omega^*$  describing the social interaction, i.e. by taking the persistence length  $\xi$  to zero. We expected to lose a number of the observed features in the process, given how the interplay between avoidance and alignment thrives on the gentle curving of the follower's gaze together with sharp turn-around at the boundary. We were surprised to find the same qualitative outcome of the follower landing on straying attractors (sharper versions of the headphone and eight-shaped attractors shown in Fig. 3.26) for intermediate  $COV$  and aligning with the vertical attractor for  $COV$  small or large enough (Fig. 3.27). As one might expect, the range of  $COV$  over which the non-aligned states exist is shorter ( $1.45 < COV < 1.85$  as shown in Fig. 3.27) in this case since the follower instantaneously responds to the Leader's prompts and alignment is in general more probable.

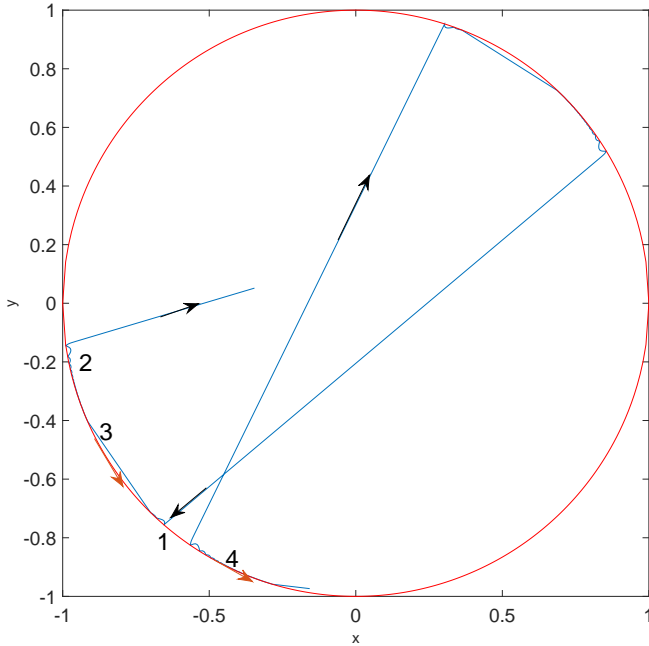


Figure 3.24: **Example of a Typical state of the leader on the rim variation.** At point 1, the follower hits the boundary in front of the leader which is at point 3 (red and black arrows give the direction of motion of the leader and follower respectively) and is in the COV of the follower. The angle between the directions of motion of the Leader and the Follower  $\phi_L - \phi$  is less than 180 and thus  $\omega^*$  is positive and the follower rotates counterclockwise. As the follower reflects from the boundary the Leader is no more in its COV, but  $\omega$  which doesn't drop immediately to zero is still positive and the follower will rotate counterclockwise again and thus move in the opposite direction of motion of the Leader to hit the boundary. As it reflects from the boundary the follower will not see the Leader but it already has a positive  $\omega$  and thus will rotate counter-clockwise. This process is repeated until the Follower reflects and finds the leader in its COV (points 2 and 4), here the angle between the Leader and the Follower is larger than 180 and thus the follower rotates clockwise. Soon the Leader will no more be in the COV of the Follower which will continue to move in a straight line to hit the boundary in front of the Leader and the process repeats again.

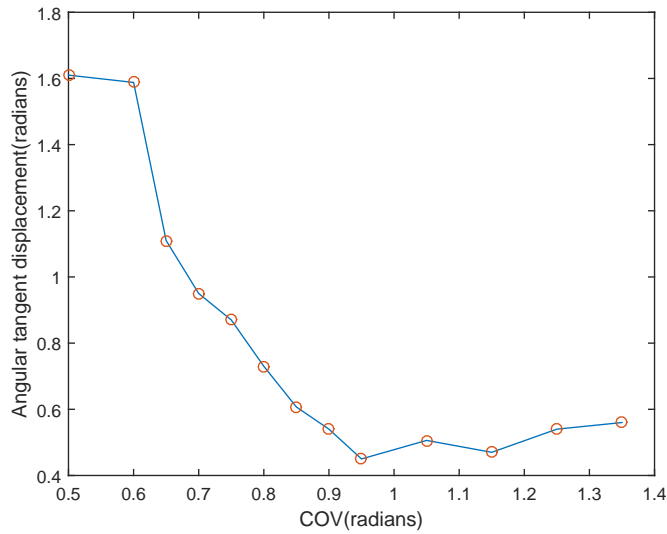


Figure 3.25: **An order parameter for the irregular rotating variant of eight-figure.** The follower bounces off the boundary between the landing and the taking off points. The angular displacement along the boundary decreases as the *COV* increases. The landing and taking off points rotate along the circle.

Thus variations which tested extremes (whether in the leader's trajectory, or the follower response) leave us with a high probability of stray behaviour over a broad range of the *COV*. Try as we may, it seems that a follower confined within a reflecting boundary with a leader dictating alignment when in sight, remains with substantial freedom to stray when the cone of vision is broad enough for the boundary to help structure its motion away from the Leader, and not too broad to find itself overwhelmed by that leader.

### 3.5 Summary and Discussion

Ground breaking studies, both biological/experimental and mathematical, were conducted with a view to exploring the issue of leadership in a schools of fish, rules for group interaction (topological versus metric). Our model is particular in

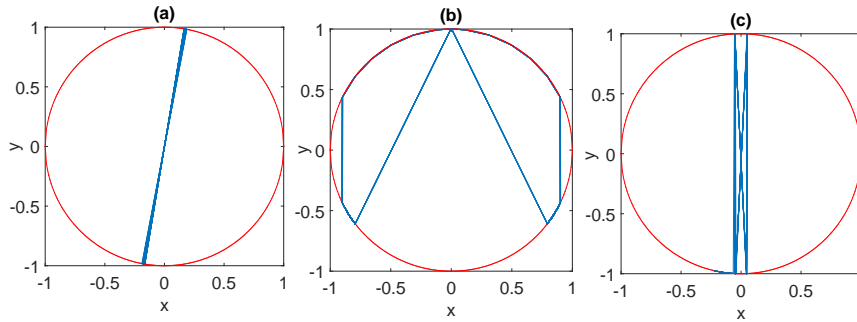


Figure 3.26: **Straying Attractors for the sharp response variation of the model.** (a) 2-periodic (diameter) attractor obtained at  $COV = 1.51$ ; (b) sharper version of Head-phone attractor obtained at  $COV = 1.57$ ; (c) nearly eight-shaped attractor obtained at  $COV = 1.8$  (the follower jumps between the two right and left attractors on both sides of the vertical diameter)

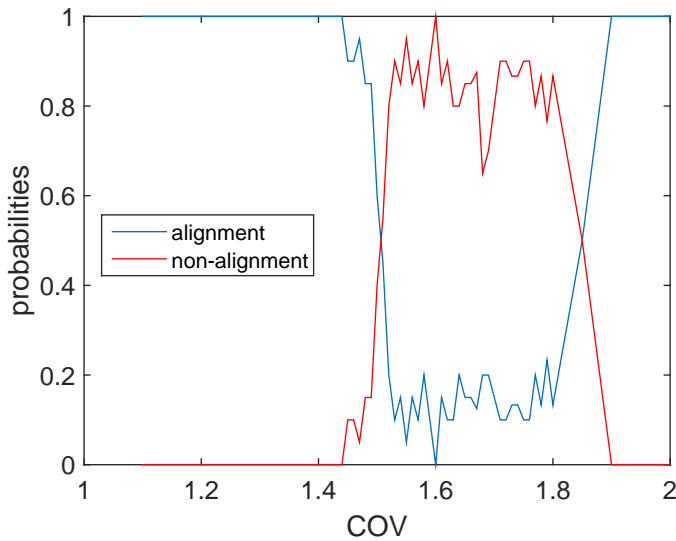


Figure 3.27: **Probabilities of being attracted to and escaping from the Leader as a function of  $COV$  for the sharp response model variation of the model.** The blue and red lines give the probability of being attracted to or escaping from the Leader respectively. Note that at the beginning of the interval of escape from the Leader the follower has the highest probability of ending up in the nearly diameter attractor, for intermediate values it has highest probability of ending up in the nearly headphone attractor, and in the last part in the nearly eight-shaped attractor.

that it leaves room for entrapment away from alignment, this in the presence of a persistent drive to align, and continual encouragement/reinforcement of recurrent encounter with the leader by the impenetrable reflective boundary. Remove the boundary and the behavior outcome is trivial: alignment over a set of measure zero, and otherwise straying for good. Keep the boundary and remove the leader the particle winds around the circle, except for a set of measure zero for which it follows periodic trajectories. Put both leader and boundary together and rich behavior obtains. Boundary and leader provide two recurrent sources of intermittent collisions one sharp (the reflection off the boundary) and the other gentle (relaxing turns in contact with the leader).

The follower is one which has internalized the need to align with controlling field of force. Control is not enforced continuously; rather, as the leader traces its path periodically, the follower which is otherwise free to explore its domain of confinement, bouncing bat-like off its walls, intersects with the leader intermittently. Cone of vision encounters with the leader autonomously incite the follower to alignment. For tight cone of vision, deflection resulting from wish-to-align makes the follower loose track of the leader. Ironically, and following a transient, short lived deflection coupled to reflections at the boundary favor gradual convergence of the follower to the leader, and perfect alignment. In other words, intermittent short impulses with extensive role for boundary adjustment favors alignment, slow though it may be. On the other end, a wide enough cone of vision minimizes the role of the boundary as it enhances fast alignment with the leader, with few long range bounces. Conclusion: Acute, pervasive, ever-present awareness of the leader, makes for fewer bounces, and faster alignment with the leader, as expected. Chaotic, leader-avoiding attractors, arise when the encounter with the leader is long enough to force repression of the follower's free movement,

with the boundary reflecting the follower back into potential contact and eventual alignment with the leader. The nearly balanced interplay between boundary and leader makes for periods of repeated short bounces with long flights of fancy at locations of sharp reversal in the leader's motion, only to engage in repeated short bounces again. The dynamics then encourages trapped states in which the follower is neither totally free nor totally aligned.

One of the initial motivations for this work was the inquiry whether the visual cues inside a closed circular domain can account for the observed temporal alternation between coexisting self-organized phases in shoals of fish. For sure, our model is too simplified to answer this question; however, the special phases obtained and the transitions between them as a function of  $COV$ , encourages further explorations of visual communication networks. In fact, the visual cues are established as the most likely mode of transfer of information in a fish shoal [45, 53] and variations in the  $COV$  can naturally occur whenever the line of sight of a given fish is occluded by some obstacle. Thus, one is tempted to ask: Could temporal variations in the effective  $COV$  of a given fish -variations which may result from the play of shadows and clearings in a shoal- lead to transitions from one self organized state to the other and back? The phase diagram presented above suggests that this could be a possible explanation of the observed intermittency. However, the relatively long time the follower takes to relax to one or the other attractor at critical  $COV$ s around transitions, makes us pause and rethink other possibilities.

As is already apparent from the presentation above, our results also touch the extensive interface between dynamical systems theory, systems control, and ultimately, and most interestingly, the study of human social behaviour. We wish to conclude our exposition by drawing out the connections and implications of



our work in these fields.

**Mathematical vistas** The dynamics of a particle bouncing off a closed curve belongs to the vast field of mathematical billiards. The follower bounces off the boundary but is curved by the mean-field of the Leader instead of moving in straight lines between bounces. Thus we can think of our system as a novel type of billiards, with a special discontinuous force field acting. Classically one particle billiards are regular (integrable), chaotic or mixed. Examples of regular billiards are circular billiards, where orbits are tangent to concentric circles(caustics), and elliptical billiards which have two caustics: conformal ellipses and conformal hyperboli. Dispersing billiards (Sinai and Diamond containers) and billiards with focusing boundaries (stadium) are examples of chaotic billiards. However non-concentric annuli, ovals and mushrooms are examples of billiards with mixed regular-chaotic dynamics. To the best of our knowledge, the only modifications to the one-particle billiards studied are: few particles billiards with head-on particle-particle collisions, and vertical billiards with gravitational field acting on the particle. Therefore there are several novel ways in which our system, and associated results couple to the field: a) classically, a single particle is allowed to bounce off an enclosure of arbitrary shape; here we consider the controlling effect of a perturber/mean field confined with the particle: the resulting dynamics is no longer Hamiltonian, with (chaotic) attractors arising in the process; b) classically, when more than one particle are considered, it is with local collisional interactions in mind; here, we consider long range, intermittent interactions with the controlling agent; c) classically, the departure of the boundary from circular allows hamiltonian chaos and mixing to emerge; here dissipative chaos over attractors emerges within a circular domain. The models we consider, and the behavior they sustain make for open mathematical questions which are best addressed within the

growing field of dynamical systems with discontinuities [65]. There one learns that novel behavior arises when a particle hits the surface of discontinuities along a tangent, so called grazing orbits; here we have preliminary indications that the angle at which the particle encounters the boundary (i.e. how close it is to the normal), plays a role around transitions from one attractor to another. Our exercise is complicated by the coupling between two sources of discontinuities, the basin's boundary, but also the unforeseeable encounters with the leader on its periodic trajectory. Anything more definite will require more experimentation, and careful mathematical analysis, along the lines studied in [65].

**Control Systems** Another interesting class of problems to which our model relates is that of pursuit-evasion type. These problems have fascinated mathematicians for centuries, who succeeded in finding analytic solutions to some while solved the others numerically. In his book "Chases and Escapes", P.J Nahil gives a comprehensive review of problems studied in the literature. Here, we mention one of the problems presented in the book and which is known as "The Lady-in-the-Lake" problem. The original problem as it first appeared in Martins Gardners Mathematical Games column in Scientific American (November and December 1965) is:

*A young lady was vacationing on Circle Lake, a large artificial body of water named for its precisely circular shape. To escape from a man who was pursuing her, she got into a rowboat and rowed to the center of the lake, where a raft was anchored. The man decided to wait it out on the shore. He knew she would have to come ashore eventually; since he could run four times faster than she could row, he assumed that it would be a simple matter to catch her as soon as her boat touched the lakes edge. But the girl, a mathematics major at Radcliffe, gave some thought to her predicament. She*

*knew that on foot she could outrun the man [which does raise the question of why such a smart lady got herself into this situation in the first place by rowing out into a lake!]; it was only necessary to devise a rowing strategy that would get her to a point on shore before he could get there. She soon hit on a simple plan, and her applied mathematics applied successfully. What was the girl's strategy?*

This classical formulation shares some aspects with our model: a- Leader-Follower is analogous to Lady-Man; b- the motion is confined to a circular region including the boundary; c- existence of non-following (Lady escaping) states. Various modifications of the problem can be formulated and studied in connection to the evading regimes discussed above.

In a broader sense, one can ask about strategies for guiding a self propelled particle into a given regime of motion, within confinement. A possible answer suggested by our work: a diametric sentinel which guides a robot through a broad enough cone of vision, can force it into an eight figure or a headphone attractor, without the need for continuous monitoring. Control into eight-shaped trajectories has been studied in relation to grid-tie inverters for photo-voltaic applications ([72]), and quadrotors going around two focal points ([73]).

**Sociological connections** Our model and the non-aligned states which it sustains can be linked to the modeling of opinion dynamics, particularly when a collective is caught between the competing influence of media on one large scale, and that of neighbouring social groups on another more local scale, with the undecided group playing a crucial role in the outcome [66]. In [66] it is shown that for relatively small media pressure and in the presence of enough proportion of un-decided agents, the opinion, which is neither favored by media

nor by the interactions among peers, survives and might even gain the support of the majority. This is another example of non-alignment appearing in systems subject to different kinds of competing pressures.

We close our discussion with a less obvious but more curious tentative connection between our work and the works of Milgram and Goffman on social psychology and the sociology of collective human behavior respectively. The works of both social scientists have already made their way into mathematical modeling of social dynamical phenomena. Milgram's pioneering work on the "small world problem" stimulated extensive studies of network dynamics (e.g. [68]), and Goffman's insights into pedestrian traffic were incorporated in recent work on crowd dynamics in public spaces [40]. Here it is through their independent work on human response to conflicting pressures to conform, that we see them further informing socio-dynamical modeling [69, 70]. This connection is largely stimulated by the explicitly dynamical language employed by both observers, in settings which bear resemblance to ours. In experiments probing "the conditions of obedience and disobedience to authority" [69], Milgram's subject is caught between obedience to authority and compassion with the victim. Milgram notes variations in the subject's response with closeness of authority, and proximity to the victim, describing the two influences as fields of force that weaken with distance. Milgram notes the tension between the two influences, promoting erratic behavior in the subject, all the while being trapped in a conflicting state without the sufficient strength to terminate the experiment. "Similarly", the follower in our experiments is caught between the Leader's normative (but intermittent) influence and the boundary's reflective perturbation, and finds itself with sufficient though not overwhelming presence of authority, trapped in "un-willfull" states of incomplete obedience. One wonders how Milgram's results would have changed

with intermittent rather than persistent intervention by authority, the actual distance being fixed. Equally suggestive is Goffman's extensive treatment of an individual's self as shaped (even constituted) by continuous dynamical interactions with the social environment. Goffman was keenly interested in mapping the force fields (mostly mediated by face-to-face interactions) which couple the individual to authority. A "gathering" is that interactive, compact, confined, space in which a collective is self-regulated through those dynamically shifting force fields. Goffman notes that in a given "gathering", the individual is constrained to maintain a consistent, "viable image in the eyes of others". He further notes that due to the constant, and unexpected shift in local circumstances, adjustments will be continuously necessary, to the point that an individual's sense of him- or her-self emerges as a dynamical byproduct of inter-face with fluctuating social encounters. On a very speculative note, we ponder if the trapping though evading attractors of our follower could re-emerge, in a richer setting, as dynamical analogs of Goffman's "conception of the self as contingent in the sense of being only probabilistic, a theatre run of performances to audiences and critics whose responses are always in play, whose applause is never certain..." [74]?

# Chapter 4

## Future Work

The work presented in this thesis opens the scope for further investigations in different directions. In the discussion of each chapter some directions are included. Here we give a brief description of some of the possible continuations and variations that can be implemented and that were not clearly explained previously.

**Completing the mean field approach of low-energy swarms:** We succeeded in constructing a mean field potential that recovers the three observed low-energy steady states of the swarms of self-propelled particles considered. We averaged over all the noise and studied the dynamics in terms of a single order parameter  $s$ . Consistent with our numerical simulations, the constructed potential has two minima corresponding to the stable states (coherent flock and rigid rotation), and a maximum/plateau corresponding to the long-lived transient state (random droplet). Although the flatness of the potential increases with  $\gamma_1$  and this is consistent with the longer life of the random droplet for larger  $\gamma_1$ , we still don't have a clear explanation of the relatively long time the swarm spends wondering in the random state before transitioning to one of the stable states. We also need to investigate further the necessity that the swarm spends some

time in the random droplet state before jumping into the coherent flock or rigid rotation state. Keeping in mind that the obtained noise cannot be classified as a white thermal noise whose effects are well understood, we intend to explore its properties by computing its correlation function. Furthermore, we think that we might have neglected some aspects of the dynamics by reducing it to a single slow degree of freedom  $s$  and the mean force conjugate to it. Work has already been started in this direction by considering two coupled order parameters ( $s$  and  $m$ ) and looking at the velocity fields in the  $(s, m)$  phase space, where  $s$  is the dispersion of velocities in center of mass frame and  $m$  is the velocity of the center of mass. Preliminary results in this direction encourage more exploration.

**Understanding transitions from random droplet to ordered states:**

One of the remarkable results presented here is that the random droplet is not at all random in configuration space. The directions of the velocity vectors of individual particles are random, but the particles are found to move in something like a random walk on well defined rings while occasionally jumping from one ring to another. We wish to understand the internal dynamics of this state that eventually drives the transition to one of the other ordered states. Separating the radial and angular motions of a given particle and assuming the radial motion to be much slower we obtain a restricted system closely resembling oscillators studied in Kuramoto models. Some progress was achieved in this direction and further analysis is required to complete the picture.

**Exploring Variations of Leader-follower dynamics in confined areas:**

Natural variations of the model introduced in chapter 3 can be explored: first, consider different shapes of confining boundaries such as rectangles, ovals, ellipses and mushrooms (inspired by billiards literature); second, consider different types of interactions between leader and follower (e.g. apply Viscek rules of interaction,

add some noise, add attraction not only alignment); third, add other followers interacting with the leader and between themselves. It is curious to explore all these directions to test for the robustness of non-alignment in the presence of the “will ”to align.

**Searching for ingredients of intermittency** : Swarms of fish are observed to naturally shift between milling and flocking states. This intermittency between states is not recovered by existing swarming models. Here one asks: under what conditions might a given model allow for intermittency? Our leader-follower minimal model gives some insights that the cone of vision ( $COV$ ) might be the missing ingredient that will lead to this observed behaviour if implemented properly. In our model, different attractors were obtained for different values  $COV$  and the latter can naturally change/fluctuate with the change of shadows or in the presence of obstacles. So a promising extension of the model would be to allow for a time varying  $COV$ , coupling strength and/or noise.



# Appendices

# Appendix A

## Non-Dimensionalizing the equation of motion of the Linear model

For the linear model, the Newtonian equations for the  $i^{th}$  particle are given by:

$$\begin{aligned}\frac{d\vec{r}_i}{dt} &= \vec{v}_i \\ m_i \frac{d\vec{v}_i}{dt} &= a \frac{\vec{v}_i}{|\vec{v}_i|} - b\vec{v}_i - \vec{\nabla}_{\vec{r}_i} U_i\end{aligned}\tag{A.1}$$

where,

$$U_i = \sum_{i \neq j} \left( -C_a e^{-\frac{|\vec{r}_i - \vec{r}_j|}{l_a}} + C_r e^{-\frac{|\vec{r}_i - \vec{r}_j|}{l_r}} \right)\tag{A.2}$$

is the Morse potential,  $C_a$  and  $C_r$  specify the respective strengths of attraction and repulsion while  $l_a$  and  $l_r$  specify their respective length scales. Following [24],

we introduce the rescalings:

$$\begin{aligned}\vec{r}_i &= l_a \vec{r}'_i \\ \vec{v}_i &= v_t \vec{v}'_i \\ t &= t^* t'\end{aligned}$$

where  $v_t = \frac{a}{b}$  is the terminal speed,  $l_a$  is the characteristic length of attraction and  $t^*$  is to be defined later. Substituting in Eqs. (A.1) we obtain:

$$\begin{aligned}\frac{d\vec{r}'_i}{dt'} &= \frac{t^* a}{l_a b} \vec{v}'_i = t^* \frac{v_t}{l_a} \vec{v}'_i \\ \frac{d\vec{v}'_i}{dt'} &= \frac{bt^*}{m} (1 - |\vec{v}'_i|^2) \vec{v}'_i - \frac{C_a t^* b}{m l_a a} \vec{\nabla}_{\vec{r}'_i} U'_i\end{aligned}\quad (\text{A.3})$$

where

$$U'_i = \sum_{i \neq j} \left( -e^{-|\vec{r}'_i - \vec{r}'_j|} + C e^{-\frac{|\vec{r}'_i - \vec{r}'_j|}{l}} \right) \quad (\text{A.4})$$

Writing the equations in the dimensionless form above, three characteristic times appear: 1)  $t_{kin} = \frac{l_a}{v_t}$  is the time required to cover the characteristic distance of a swarm by a freely moving particle, 2)  $t_{rel} = \frac{m}{b}$  is the time of relaxation to terminal speeds due to the propulsion/ friction terms, and 3)  $t_{pot} = \frac{m l_a}{C_a} v_t$  is the characteristic time for a noticeable momentum change due to the Morse potential forces. The choice of  $v_t$  as the unit speed and  $l_a$  as the unit length makes  $t^* = t_{kin}$  the unit time. Dropping the prime, Eq. A.3 is given by:

$$\begin{aligned}\frac{d\vec{r}_i}{dt} &= \vec{v}_i \\ \frac{d\vec{v}_i}{dt} &= \gamma_1 (1 - |\vec{v}_i|^2) \frac{\vec{v}_i}{|\vec{v}_i|} - \gamma_2 \vec{\nabla}_{\vec{r}_i} U_i\end{aligned}\quad (\text{A.5})$$

where  $\gamma_1 = \frac{t_{kin}}{t_{rel}}$  and  $\gamma_2 = \frac{t_{kin}}{t_{potential}}$  are the corresponding rates of the change of momentum. In this way the initial seven parameters of the model ( $N, l_a, l_r, C_a, C_r, a, b$ ) are reduced to two characteristic time ratios  $\gamma_1$  and  $\gamma_2$ , a length ratio  $l = \frac{l_r}{l_a}$ , an energy ratio  $C = \frac{C_r}{C_a}$ , and  $N$ .

# Appendix B

## Linear stability analysis of the coherent flock

In the flocking state, all particles are moving parallel to each other with terminal speed. Without loss of generality the direction of motion can be taken along the x-axis. The equations of motion in the co-moving frame are given by:

$$\begin{aligned}\frac{dx_i}{dt} &= v_{xi} \\ \frac{dy_i}{dt} &= 0 \\ \frac{dv_{xi}}{dt} &= \gamma_1 (1 - (v_{xi} + 1)^2) (v_{xi} + 1) - \gamma_2 \frac{\partial U}{\partial x_i} \\ \frac{dv_{yi}}{dt} &= -\gamma_2 \frac{\partial U}{\partial y_i}\end{aligned}\tag{B.1}$$

In the co-moving frame the flock state is a stationary state where the positions of the particles are those of the Lagrangian configuration and  $v_{xi} = v_{yi} = 0$ . A

generic perturbation in the co-moving frame has the form:

$$\begin{aligned}
x'_i &= x_{0i} + \delta x_i \\
y'_i &= y_{0i} + \delta y_i \\
v'_{xi} &= \delta v_{xi} \\
v'_{yi} &= \delta v_{yi}
\end{aligned} \tag{B.2}$$

where  $(x_{0i}, y_{0i})$  specify the positions in the Lagrangian configuration. Time evolution of the perturbation is given by the linearized equations:

$$\begin{aligned}
\frac{d\delta x_i}{dt} &= \delta v_{xi} \\
\frac{d\delta y_i}{dt} &= \delta v_{yi} \\
\frac{d\delta v_{xi}}{dt} &= -2\gamma_1 \delta v_{xi} - \gamma_2 \sum_j C_{1ij} (\delta x_i - \delta x_j) \\
&\quad + \gamma_2 \sum_j C_{2ij} (\delta y_i - \delta y_j) \\
\frac{d\delta v_{yi}}{dt} &= -\gamma_2 \sum_j C_{2ij} (\delta x_i - \delta x_j) \\
&\quad + \sum_j C_{3ij} (\delta y_i - \delta y_j)
\end{aligned} \tag{B.3}$$

where

$$\begin{aligned}
C_{1ij} &= \\
& - \sum_{j \neq i} \frac{1}{r_{0ij}^2} \left( -\frac{C}{l^2} e^{-\frac{r_{0ij}}{l}} + e^{-r_{0ij}} \right) (x_{0i} - x_{0j})^2 \\
& + \sum_{j \neq i} \frac{1}{r_{0ij}^3} \left( -\frac{C}{l} e^{-\frac{r_{0ij}}{l}} + e^{-r_{0ij}} \right) (y_{0i} - y_{0j})^2 \\
C_{2ij} &= \\
& \sum_{j \neq i} \frac{1}{r_{0ij}^3} \left( -\frac{C}{l} e^{-\frac{r_{0ij}}{l}} + e^{-r_{0ij}} \right) (y_{0i} - y_{0j}) (x_{0i} - x_{0j}) \\
& - \sum_{j \neq i} \frac{1}{r_{0ij}^2} \left( -\frac{C}{l^2} e^{-\frac{r_{0ij}}{l}} + e^{-r_{0ij}} \right) (x_{0i} - x_{0j}) (y_{0j} - y_{0j}) \\
C_{3ij} &= \\
& - \sum_{j \neq i} \frac{1}{r_{0ij}^2} \left( -\frac{C}{l^2} e^{-\frac{r_{0ij}}{l}} + e^{-r_{0ij}} \right) (y_{0i} - y_{0j})^2 \\
& + \sum_{j \neq i} \frac{1}{r_{0ij}^3} \left( -\frac{C}{l} e^{-\frac{r_{0ij}}{l}} + e^{-r_{0ij}} \right) (x_{0i} - x_{0j})^2 \tag{B.4}
\end{aligned}$$

and  $x_{0i}, y_{0i}$  and  $r_{0ij}$  are the x-coordinate and the y-coordinate of the  $i^{th}$  particle and the distance between the  $i^{th}$  and the  $j^{th}$  particle in the Lagrangian configuration of the unperturbed flock. In the matrix form

$$\frac{d\delta u}{dt} = A\delta u \tag{B.5}$$

where  $u = (\delta x_i, \delta y_i, \delta v_{x_i}, \delta v_{y_i})$  and A is a  $4N \times 4N$  stability matrix. Note that the only diagonal terms appearing in the evolution matrix are related to the longitudinal velocity perturbation  $\delta v_{x_i}$  and have negative constant value proportional to viscosity  $(-2\gamma_1)$ . Off-diagonal terms originate from perturbing coordinates or velocities that would lead to a deformation of the Lagrangian configuration

causing oscillations. Therefore we conclude that any perturbation of the coherent flock dies out after some oscillations which amounts to absolute linear stability. This is verified numerically by identifying a Lagrangian configuration, building up the stability matrix  $A$  and finding its eigenvalues as functions of the two control parameters,  $\gamma_1$  and  $\gamma_2$ . Matrix  $A$  has 4 zero eigenvalues corresponding to two uniform coordinate translations, a rigid-body coordinate rotation, and a uniform velocity rotation. The other eigenvalues are complex conjugate pairs with negative real parts discussed in the main text.



# Appendix C

## Linear stability of the rigid rotation state

We study the stability of the rigid rotation state in a rotating frame, with equations of motion modified to:

$$\begin{aligned}\frac{d\vec{r}_i}{dt} &= \vec{v}_i \\ \frac{d\vec{v}_i}{dt} &= t_1 (1 - |\vec{v}_i + \vec{\omega} \times \vec{r}_i|^2) (\vec{v}_i + \vec{\omega} \times \vec{r}_i) - t_2 \vec{\nabla}_{\vec{r}_i} U_i \\ &\quad - 2\vec{\omega} \times \vec{v}_i - \vec{\omega} \times \vec{\omega} \times \vec{r}_i\end{aligned}\tag{C.1}$$

where  $\omega$  is the angular velocity of the rotating frame. A perfect rigid rotation state is stationary in a co-rotating frame leading to  $v_{xi} = v_{yi} = 0$  while the positions  $\vec{r}_{0i} = (x_{0i}, y_{0i})$  are expected to be slightly deviating from the nearest Lagrangian configuration. These deviations are necessary to provide forces that balance the fictitious centrifugal force resulting from the rotating frame, as well as maintain most of the particle speeds away from the terminal value. Setting

$v_{xi} = v_{yi} = 0$  and  $r_{0i}^{\vec{}} = (x_{0i}, y_{0i})$  in Eq.(C.1) gives:

$$\vec{F}_{i0} = t_1 (1 - |\vec{\omega} \times \vec{r}_{i0}|^2) (\vec{\omega} \times \vec{r}_{i0}) - \vec{\omega} \times (\vec{\omega} \times \vec{r}_{i0}) \quad (\text{C.2})$$

where  $\vec{F}_{i0} = t_2 \vec{\nabla}_{\vec{r}_i} U_i$  are the potential forces resulting from the deviations from the Lagrangian configuration. The net torque of these potential forces is zero:

$$\sum_i \vec{F}_{i0} \times \vec{r}_{i0} = 0 \quad (\text{C.3})$$

Eqs. (C.2) and (C.3) define the angular velocity of the rotation :

$$\omega = \sqrt{\frac{\sum x_{i0}^2 + y_{i0}^2}{\sum (x_{i0}^2 + y_{i0}^2)^2}} \quad (\text{C.4})$$

Eqs. (C.1) and (C.4) together with the stationarity condition,  $v_{xi} = v_{yi} = 0$ , constitute a set that defines a rotating Lagrangian configuration. Equations are solved numerically by an iterative procedure that starts with a non-rotating Lagrangian configuration as a seed. Once the configuration is found, the angular velocity is given by Eq. (C.4), and the particle velocities in the non-rotating frame are defined by the rigid rotation condition. If a perfect rotation state is taken as initial condition and then evolved in the fixed frame we observe that rigid rotation is not maintained. Particle velocities and coordinates develop oscillations that grow initially but later saturate. This suggests that the rigid-body rotation state may be linearly unstable. Linearised equations of motion for a generic

perturbation are given by:

$$\begin{aligned}
\frac{d\delta x_i}{dt} &= \delta v_{xi} \\
\frac{d\delta y_i}{dt} &= \delta v_{yi} \\
\frac{d\delta v_{xi}}{dt} &= (2\gamma_1 x_{0i} y_{0i} \omega^3 + \omega^2) \delta x_i - \gamma_2 \sum_j C_{1ij} \delta x_j \\
&+ \gamma_1 (x_{0i}^2 \omega^3 + 3y_{0i}^2 \omega^3 - \omega) \delta y_i - \gamma_2 \sum_j C_{2ij} \delta y_j \\
&+ \gamma_1 (1 - x_{0i}^2 \omega^2 - 3y_{0i}^2 \omega^2) \delta v_{xi} + (2\gamma_1 \omega^2 x_{0i} y_{0i} + 2\omega) \delta v_{yi} \\
\frac{d\delta v_{yi}}{dt} &= \gamma_1 (-y_{0i}^2 \omega^3 - 3x_{0i}^2 \omega^3 + \omega) \delta x_i - \gamma_2 \sum_j C_{2ij} \delta x_j \\
&+ (-2\gamma_1 x_{0i} y_{0i} \omega^3 + \omega^2) \delta y_i - \gamma_2 \sum_j C_{3ij} \delta y_j \\
&+ (2\gamma_1 \omega^2 x_{0i} y_{0i} - 2\omega) \delta v_{xi} \\
&+ \gamma_1 (1 - y_{0i}^2 \omega^2 - 3x_{0i}^2 \omega^2) \delta v_{yi}
\end{aligned} \tag{C.5}$$

where  $C_{1ij}$ ,  $C_{2ij}$  and  $C_{3ij}$  are obtained from the positions of the particles rigid rotation state in the co-rotating frame defined earlier. The eigenvalues of the stability matrix are then found numerically as functions of the control parameters.

# Appendix D

## Derivation of mean-field equation

Starting from the single particle equation for the cubic model (Eq. 2.5) we derive the equation of the change with time of the order parameter  $s$  (Eq. 2.10). Below we give the details of this derivation:

$$\frac{d\vec{v}_i}{dt} = \gamma_1(1 - |\vec{v}_i|^2)\vec{v}_i - \gamma_2\vec{\nabla}_{\vec{r}_i}U_i \quad (\text{D.1})$$

let  $\vec{m} = \frac{\sum \vec{v}_i}{N}$  and  $\tilde{v}_i = \vec{v}_i - \vec{m}$  and substitute them in the above equation to get:

$$\frac{d\tilde{v}_i}{dt} + \frac{d\vec{m}}{dt} = \gamma_1(1 - (\tilde{v}_i + \vec{m}) \cdot (\tilde{v}_i + \vec{m}))(\tilde{v}_i + \vec{m}) - \gamma_2\vec{\nabla}_{\vec{r}_i}U_i \quad (\text{D.2})$$

Taking the sum over all  $N$  particles, all potential forces (which are pairwise) cancel out and we are left with:

$$N\frac{d\vec{m}}{dt} = \gamma_1 \sum_i (\tilde{v}_i + \vec{m} - (\tilde{v}_i^2 + 2\tilde{v}_i \cdot \vec{m} + m^2))(\tilde{v}_i + \vec{m}) - \gamma_2\vec{\nabla}_{\vec{r}_i}U_i \quad (\text{D.3})$$

Expanding all terms and substituting  $\sum_i \tilde{v}_i = 0$  we get:

$$N \frac{d\vec{m}}{dt} = \gamma_1 \left( N\vec{m} - \sum_i |\tilde{v}_i|^2 \tilde{v}_i - \sum_i \tilde{v}_i^2 \vec{m} - 2 \sum_i \tilde{v}_i \cdot \vec{m} \tilde{v}_i - Nm^2 \vec{m} \right) \quad (\text{D.4})$$

Taking the dot product of  $\vec{m}$  with both sides of the equation we get:

$$\frac{N}{2} \frac{dm^2}{dt} = \gamma_1 \left( Nm^2 - \sum_i |\tilde{v}_i|^2 \tilde{v}_i \cdot \vec{m} - \sum_i \tilde{v}_i^2 m^2 - 2 \sum_i (\tilde{v}_i \cdot \vec{m})^2 - Nm^4 \right) \quad (\text{D.5})$$

substituting  $\tilde{v}_i \cdot \vec{m} = |\tilde{v}_i| m \cos \theta_i$   $\theta_i$  be the angle between  $\tilde{v}$  and  $\vec{m}$  we get:

$$\begin{aligned} \frac{dm^2}{dt} &= 2\gamma_1 \left( m^2 - \frac{\sum_i |\tilde{v}_i|^3 \cos \theta_i}{N} m - \frac{\sum_i \tilde{v}_i^2}{N} m^2 - \frac{2 \sum_i (|\tilde{v}_i|^2 \cos^2 \theta_i)}{N} m^2 - m^4 \right) \\ \frac{dm^2}{dt} &= 2\gamma_1 \left( 1 - \frac{\sum_i \tilde{v}_i^2}{N} - \frac{2 \sum_i |\tilde{v}_i|^2 \cos^2 \theta_i}{N} \right) m^2 - 2\gamma_1 \frac{\sum_i |\tilde{v}_i|^3 \cos \theta_i}{N} m - 2\gamma_1 m^4 \end{aligned}$$

initially we considered  $q = m^2$  as our order parameter, but  $q$  is equal to one for the coherent flock state and zero for both the random droplet and rigid-rotation state. So  $q$  is not a good enough parameter to describe the rigid rotation state. Therefore, we had to think of another parameter which uniquely describes the three states. A good candidate is  $s = \frac{\sum_i \tilde{v}_i^2}{N}$ , which is zero for the coherent flock, something around 0.6 for the random droplet and something between 0.8 and 1 for the rigid-rotation. Before writing the equation for the change of  $s$  with time,

we write s as:

$$\begin{aligned}
s &= \frac{\sum_i \tilde{v}_i \cdot \tilde{v}_i}{N} \\
&= \frac{\sum_i (\vec{v}_i - \vec{m}) \cdot (\vec{v}_i - \vec{m})}{N} \\
&= \frac{\sum_i (v_i^2 - 2\vec{v}_i \cdot \vec{m} + m^2)}{N} \\
&= \frac{\sum_i v_i^2 - 2Nm^2 + Nm^2}{N} \\
&= \frac{\sum_i v_i^2 - Nm^2}{N}
\end{aligned} \tag{D.7}$$

therefore the change of s with respect to time is given by:

$$\begin{aligned}
\frac{ds}{dt} &= \frac{1}{N} \frac{d \sum v_i^2}{dt} - \frac{dq}{dt} \\
&= \frac{2}{N} \sum_i \vec{v}_i \cdot \frac{d\vec{v}_i}{dt} - \frac{dq}{dt}
\end{aligned} \tag{D.8}$$

evaluating Eqs. D.1 and D.6 we get:

$$\begin{aligned}
\frac{ds}{dt} &= \frac{2}{N} \sum_i \vec{v}_i \cdot \left( \gamma_1 (1 - |\vec{v}_i|^2) \vec{v}_i - \gamma_2 \vec{\nabla}_{\vec{r}_i} U_i \right) - 2\gamma_1 \frac{\sum_i |\tilde{v}_i|^3 \cos \theta_i}{N} m - 2\gamma_1 m^4 \\
&\quad - 2\gamma_1 \left( 1 - \frac{\sum_i \tilde{v}_i^2}{N} - \frac{2 \sum_i |\tilde{v}_i|^2 \cos \theta_i^2}{N} \right) m^2
\end{aligned} \tag{D.9}$$

expanding the first term of the right side of the equation and rearranging terms we get:

$$\begin{aligned}
\frac{ds}{dt} &= \frac{2}{N} \sum \left( \gamma_1(1 - v_i^2)\vec{v}_i - \gamma_2\vec{\nabla}_i U \right) \cdot \vec{v}_i \\
&- 2\gamma_1 \left( 1 - \frac{\sum_i \tilde{v}_i^2}{N} - 2\frac{\tilde{v}_i^2 \cos^2(\theta_i)}{N} \right) m^2 \\
&+ 2\gamma_1 \frac{|\tilde{v}_i|^3 \cos(\theta_i) m}{N} + 2\gamma_1 m^4 \\
&= \frac{-2\gamma_1}{N} \sum_i \left( \tilde{v}_i^4 + (3\tilde{v}_i^3 \cos\theta_i - 2\tilde{v}_i \cos\theta_i) m + 2\tilde{v}_i^2 \cos^2\theta_i m^2 \right) \\
&- \frac{2\gamma_1}{N} \left( \sum_i 4\tilde{v}_i \cos\theta_i m^3 + 2\gamma_1(1 - m^2)s + \sum_i \gamma_2 \tilde{v}_i \cdot \vec{\nabla}_i U \right) \quad (D.10)
\end{aligned}$$

$s$  and the right hand side of this equation ( $f(s)$ ) are evaluated simultaneously at different points in time of the trajectory and are stored in columns 1 and 2 respectively of a matrix. We collect results from 50 trajectories for a given value of  $\gamma_1$ , combine all matrices in one huge matrix of two columns. Then we sort the second column ( $f(s)$ ) according to the first one (increasing order of  $s$ ). Plotting the second column versus the first gives the dependence of the conjugate force  $f(s)$  as a function of  $s$  (Figs. 2.15a and 2.15c). The range of  $s$  which between 0 and 1 is separated into 1000 equal bins, and the values of  $f$  are averaged over each bin. The averaged data  $f_{mean}(s)$  is then integrated, using the trapezoid built in integrator of matlab, to give the potential of the mean force  $V(s)$  satisfying  $\frac{dV}{ds} = -f_{mean}(s)$ .

# Appendix E

## Details of the Computational Scheme of Leader-Follower Model

Equations 3.3 were solved using an Euler scheme with time step  $\delta t = 0.001$ : the position and orientation of the follower are integrated forward in time, while the leader moves unaffected along the vertical diameter, with the same speed as the follower. The leader's position relative to the follower's cone of vision is tracked in order to update  $\omega^*$  in Eq.3.3. The *COV* is defined as the angle between the follower's velocity vector and the clockwise and counterclockwise rays cast from its position; the leader is in the follower's field of view if the angle between the ray and the particles' relative positions is less than the *COV* (Fig. 3.1).

Collisions with the boundaries of both the follower and leader are treated as follows: when the updated particle's position falls outside the boundary the particle is reflected back into the circle. More precisely, we define  $\vec{v}_b$  to be the velocity vector just before collision,  $r_0$  to be the vector joining the center of the circle and the point of intersection of  $\vec{v}_b$  with the boundary, and  $\vec{v}_a$  be the velocity



vector after collision, which is shown to be:

$$\vec{v}_a = \vec{v}_b - 2(\vec{v}_b \cdot \vec{r}_0)\vec{r}_0 \quad (\text{E.1})$$

Then we can write:

$$\phi_a = \arctan\left(\frac{\sin(2\theta_0 - \phi_b)}{\cos(2\theta_0 - \phi_b)}\right), \quad (\text{E.2})$$

where  $\phi_a$ ,  $\phi_b$ , and  $\theta_0$  are the angles the vectors  $\vec{v}_a$ ,  $\vec{v}_b$ , and  $\vec{r}_0$  make with the positive  $x$ -axis respectively. Additionally, to balance out the traveled distance outside the boundary the position is updated as follows:

$$\begin{aligned} x_a &= x_0 + c \cos \phi_a \\ y_a &= y_0 + c \sin \phi_a, \end{aligned}$$

where  $c = x' \cos \phi_b + y' \sin \phi_b - \sqrt{1 - (x' \cos \phi_b - y' \sin \phi_b)^2}$ , and  $(x_a, y_a)$ ,  $(x', y')$  and  $(x_0, y_0)$  are the particle's coordinates before collision, outside the circle and those of  $\vec{r}_0$  respectively. For each value of  $COV$  50 instances with varying initial conditions were followed for  $5 \times 10^7$  iterations. The results, which depend on initial conditions, are then summarized in the phase diagram.

# Bibliography

- [1] E. N. Lorenz (1963) Deterministic non-periodic flow. *Journal of the Atmospheric Sciences* 20(2):130-141.
- [2] N. J. Zabusky, M.D. Kruskal (1965) Interactions of ‘Solitons’ in a collisionless plasma and the recurrence of initial states. *Phys. Rev. Lett.* 15:240-243.
- [3] B. J. Alder, T. E. Wainwright(1967) Velocity autocorrelations for hard spheres. *Phys. rev. lett.* 18:988-990.
- [4] D. Helbing, I.Farkas, and T.Vicsek (2000) Simulating dynamical features of escape panic. *Nature (London)* 407:487.
- [5] D. Helbing (2001) Traffic and related self-driven many-particle systems. *Rev. Mod. Phys.* 73:1067.
- [6] M. Krieger, J. Billeter, and L. Keller (2000) Ant-like task allocation and recruitment in cooperative robots. *Nature (London)* 406: 992.
- [7] Y. Harada, A. Noguchi, A. Kishino, and T. Yanagida (1987) Sliding movement of single actin filaments on one-headed myosin filaments. *Nature (London)* 326:805.
- [8] L. Jelsbak and L. Sogaard-Andersen (2002) Pattern formation by a cell surface-associated morphogen in *Myxococcus xanthus*. *Proc. Natl. Acad. Sci. USA* 99: 2032 .
- [9] J. Parrish and W. Hamner (1997) *Three Dimensional Animals Groups* (Cambridge University Press).
- [10] J.A. Carrillo, M.R. D’Orsogna, V. Panferov (2009) Double milling in self-propelled swarms from kinetic theory *Kinetic and Related Models* 2:363.
- [11] J. A. Canizo, J. A. Carrillo, and J. Rosado (2010) Collective behavior of animals: Swarming and complex patterns *Arbor* 186:1035.
- [12] J. Toner and Y. Tu (1995) Long-Range Order in a Two-Dimensional Dynamical XY Model: How Birds Fly Together. *Phys. Rev. Lett.*75:4326.

- [13] T. Vicsek, A. Czirok, E. BenJacob, I.Cohen and O. Shochet (1995) Novel Type of phase transition in a system of self-driven particles. *Phys, Rev. Lett.* 75: 1226-1229.
- [14] A. Czirok and T. Vicsek (2000) Collective behavior of interacting self-propelled particles *Physica A* 281:17.
- [15] F. Cucker, S Smale (2007) On the mathematics of emmergence. *Jpn. J. Math.* 2:197-227.
- [16] S. Ramaswamy (2010) The Mechanics and Statistics of Active Matter. *Annu. Rev. Condens. Matter Phys* 1:323-345.
- [17] H. Levine, W. Rappel, and I. Cohen (2000) Self-organization in systems of self-propelled particles *Phys. Rev. E* 63:017101.
- [18] J. R. Touma, A. Shreim, and L. I. Klushin (2010) Self-organization in two-dimensional swarms *Phys. Rev. E.* 81:066106.
- [19] M.R. D’Orsogna, Y.L. Chuang, A.L. Bertozzi and L. Chayes (2006) Self-Propelled Particles with Soft-Core Interactions: Patterns, Stability, and Collapse *Phys. Rev. Lett.* 96:104302.
- [20] M.R. D’Orsogna, Y.L. Chuang, D. Marthaler, A.L. Bertozzi and L. Chayes (2007) State Transitions and the Continuum Limit for a 2D Interacting, Self-Propelled Particle System *Physica D* 232:33.
- [21] R. Eftimie (2012) Hyperbolic and kinetic models for self-organized biological aggregations and movement: a brief review *Math. Biol.* 65:35.
- [22] F. Schweitzer, W. Ebeling and B. Tilch (2001) Statistical mechanics of canonical-dissipative systems and applications to swarm dynamics. *Phys. Rev. E* 64:02110.
- [23] D. Ruelle (1969) *Statistical mechanics: rigorous results.* Benjamin, New York.
- [24] F. Vecil, P. Lafitte, J. R. Linares (2013) A numerical study of attraction/repulsion collective behavior models: 3D particle analyses and 1D kinetic simulations. *Physica D* 260:127.
- [25] J. A. Carrillo, Y. Huang, and S. Martin (2014) Nonlinear stability of flock solutions in second-order swarming models. *Nonlinear Analysis: Real World Applications* 17:332.
- [26] I. Prigogine (1955) *Introduction to Thermodynamics of Irreversible Processes.* Springfield.

- [27] T. Vicsek, D. Helbing and A. Czirok (2000) Transitions and optimal self-organization in the collective motion in driven systems. *AIP Conf. Proc.* 501:273.
- [28] H. Ziegler (1983) *An Introduction to Thermomechanics*. North Holland, Amsterdam.
- [29] L. D. Martyushev, V. D. Selesnev (2006) Maximum entropy production principle in physics, chemistry and biology. *Physics Reports* 425:1.
- [30] G. Flierl, D. Grunbaum, S. Levin and D. Olson (1999) From individuals to Aggregations: the interplay between behaviour and physics., *J. theor. Biol.* 196:397-454.
- [31] J. L. England (2013) Statistical physics of self-replication. *J. Chem. Phys.* 139:121923.
- [32] W. Bialek (2012) Statistical mechanics for natural flocks of birds. *PNAS* 109:4786-4791.
- [33] A.E. Parr, Bull. Bingham Oceanogr (1927) A contribution to the theoretical analysis of the schooling behavior of fishes. *Collection* 1:1-32.
- [34] D. V. Radakov (1973) Schooling in the ecology of fish. *New York, NY: John Wiley*.
- [35] E. S. Hobson (1973) Diel feeding migrations in tropical reef fishes *Helgoland Mar. Res.* 24:361-370.
- [36] P. Freon, F. Gerlotto and M. Soria (1992) Changes in school structure according to external stimuli: description and influence on acoustic assessment *Fish. Res.* 15:45-46.
- [37] N. C. Markis et. al. (2009) Critical population density triggers rapid formation of vast oceanic fish shoals *Science* 323:1734-1737.
- [38] S. Jagannathan et al. (2009) Ocean acoustic waveguide remote sensing (OAWRS) of marine ecosystems *Mar. Ecol. Prog. Ser.* 395:137-160.
- [39] N. O. Handegard et al. (2012) The dynamics of coordinated group hunting and collective information transfer among schooling prey *Curr. Biol.* 22:1213-1217.
- [40] D. Helbing, I. Frakas, and T. Vicsek (2000) Simulating dynamical features of escape panic *Nature* (London) **407**, 487.
- [41] Toner J and Tu Y (1998) Flocks, herds, and schools: A quantitative theory of flocking. *Phys. Rev. E* 58:4828-58.

- [42] J. Gautrais et al. (2012) Deciphering Interactions in Moving Animal Groups. *PLOS Computational Biology* 8.
- [43] Y. Katz et al. (2011) Inferring the structure and dynamics of interactions in schooling fish. *PNAS* 108: 18720-18725.
- [44] K. Tunstrom et al. (2013) Collective States, multistability and transitional behavior in schooling fish. *PLOS Comput. Biol.* 9:e1002915.
- [45] S. B. Rosenthal et al. (2015) Revealing the hidden networks of interaction in mobile animal groups allows prediction of complex behavioral contagion. *PNAS* 112,4690-4695.
- [46] J.P. Newman and H. Sayama (2008) The Effect of Sensory Blind Zones on Milling Behavior in a Dynamic Self-Propelled Particle Model *Phy. Rev. E* 78:011913.
- [47] G. Gregoire, H. Chate and Y. Tu (2003) Moving and staying together without a leader *Physica D Nonlinear Phenomena* 181:157-170.
- [48] H. Chate, . Ginelli and F. Raynaud (2008) Collective motion of self-propelled particles interacting without cohesion *Phys Rev. E* 77:046113
- [49] M. Ballerini et al. (2008) Interaction ruling animal collective behavior depends on topological rather than metric distance: Evidence from a field study. *PNAS* 105:1232-1237.
- [50] S. Viscido, J. K. Parrish and D. Grunbaum (2005) The effect of population size and number of influential neighbors on the emergent properties of fish schools *Ecol. Model.* 183:347-363.
- [51] B. H. Lemasson, J. J. Anderson and R. A. Goodwin (2009) Collective motion in animal groups from a neurobiological perspective: The adaptive benefits of dynamic sensory loads and selective attention *J. Theor. Biol.* 261:501-510.
- [52] F. Ginelli and H. Chate (2010) Relevance of Metric-Free Interactions in Flocking Phenomena *Phys. Rev. Lett.* 105:168103.
- [53] A. Strandburg-Peshkin et al. (2013) Visual Sensory Networks and effective information transfer in animal groups. *Current Biology* 23:17.
- [54] B.H. Lemason, J.J. Anderson, R.A. Goodwin (2013) Motion guided attention promotes adaptive communications during social navigation. *Proc. R. Soc. B* 280.
- [55] C. C. Hemmings (1966) Olfaction And Vision in Fish Schooling *J. Exp. Biol.* 45:449-464.

- [56] G. Von der Emde, J. Mogdans and B.V. G. Kapoor (2004) Adaptations for the Reception of Natural Stimuli *Boston, MA:Kluwer*
- [57] A. Jadbabaie, J. Lin, S. Morse (2003) Coordination of groups of mobile autonomous Agents using nearest neighbour rules. *IEE Trans Auto Control* 48:988-1001.
- [58] I. D. Couzin et al. (2005) Effective leadership and decision making in animal groups on the move. *Nature* 433:513-516.
- [59] N. Miller, S. Garnier, A.T. Hartnett and I.D. Couzin (2013) Both information and Social cohesion determine collective decisions in animal groups. *PNAS* 110:5263-5268.
- [60] M.V. Berry (1981) Regularity and chaos in classical mechanics, illustrated by three deformations of a 'circular' billiard. *European Journal of Physics* 2:91-102.
- [61] L. A. Bunimovich (2013) Kinematics, equilibrium, and shape in Hamiltonian systems: The "LAB" effect. *Chaos* 13:903.
- [62] Lancel S, Porter M A and Bunimovich L A (2006) One-particle and few-particle billiards. *Chaos* 16.
- [63] Sinai, Ya. G. (1963) On the foundations of the ergodic hypothesis for a dynamical system of statistical mechanics. *Sov. Math Dokl.* 4:1818-1822.
- [64] A. F. Filippov (1988) Differential Equations with Discontinuous Righthand Sides. Kluwer Academic Publ. Dordrecht.
- [65] O. Makarenkov and J.S.W. Lamb (2012) Dynamics and bifurcations of smooth systems: A survey. *Physica D* 241:1826-1844 .
- [66] F. Colliery and C. Castellano (2015) Interplay between media and social influence in the collective behavior of opinion dynamics. *Physical Review E* 92:042815.
- [67] Stanley Milgram (1967) The Small World Problem. *Psychology Today* 1 (1): 60-67.
- [68] D. J. Watts, and S. H Strogatz (1998) Collective dynamics of 'small-world' networks. *Nature* 393 (6684): 440-442.
- [69] Stanley Milgram (1965) Some Conditions of Obedience and Disobedience to Authority. *Human Relations* 18: 57.
- [70] Erving Goffman (1997) The Goffman reader. Edited by Charles Lemert and Ann Branaman, Blackwell Publishers.

- [71] Nihan, Paul (2007) *Chances and Escapes: The Mathematics of Pursuits and Evasion*, Princeton University Press.
- [72] J. M. Galvez and M. Ordonez (2014) 8-Shaped Trajectory Control for Rugged Rural PV Inverters. *IEEE*.
- [73] A. Naghash, M. Naghshinehy and A. Honari1z (2013) Minimum Time Trajectory Optimization for Flying a Quadrotor in an 8-shaped Path. Proceedings of *IMAV2013*
- [74] Hancock, B. Hawk, G. Roberta (2011) Towards a Philosophy of Containment: Reading Goffman in the 21st Century. *The American Sociologist* 42(4).